ISRAEL ATOMIC ENERGY COMMISSION

ANNUAL REPORT

1996

30 - 22 IA - 1500

CONTENTS

Foreword

Gideon Frank
Director General
Israel AEC

Selecting the research efforts to be highlighted in the Israel Atomic Energy Commission's Annual Report from the large body and broad spectrum of ongoing work is not an easy task. The extensive bibliography of published results attached to the report attests to the scope of this difficulty. Of the many worthwhile projects, four were chosen to represent best the current trends in the continuing R&D program at the research centers of the Israel Atomic Energy Commission.

One of these trends is the growing cooperation with private industry, in an attempt to gear our R&D programs to respond to market demands. Another feature, noted already several years ago, is the extensive collaboration of our scientists and engineers with colleagues at other institutions, in Israel and abroad. Some of the work reported is part of evolving international industrial cooperation projects, illustrating both these trends.

Following a trend common to many nuclear research centers around the world, a substantial part of our research effort is non-nuclear in nature. This is illustrated in the first article, which deals with advances in the application of non-linear optics in diverse fields of science and technology. These include state-of-the-art solid-state lasers, rapid modulation of light signals, development and generation of tunable sources of coherent light, optical data storage and the microscopic probing of biological and inorganic samples. The present work reports on a range of R&D, from the fundamentals of non-linear optical materials to proof-of-principle demonstrations of non-linear subwavelength resolution microscopy, to fabrication of prototype commercial tunable laser systems

The second report considers the microstrain characteristics in some alloys using X-ray diffraction (XRD). The research utilizes XRD line broadening effects to study the characteristics of alloys from especially prepared surfaces. These characteristics include the homogeneity of alloying, hardness and residual thermal stress. Although this work is of a more basic nature, its applications are already in sight.

The third report describes the utilization of passive, dry-air cooling systems for major installations, such as cooling the containment of the Westinghouse AP-600 advanced pressurized water reactor. Good and economic passive dry-air cooling systems would be among the best solutions for containment cooling at inland sites, especially in arid areas.

Noninvasive medical diagnostic methods utilizing radioactive materials have been standard far many years. The most common of these relies on using a gamma camera to determine the distribution of injected or ingested radioisotope-labeled compounds in the human body. The 30-year-old camera technology, although vastly improved over the years, is still handicapped by energy and spatial resolution limitations of the detectors, by the size and bulk of the instrument and other technical problems. The need for further development of an improved, more efficient and compact imaging system is clear. Such a system, based on solid-state detectors, is described in the last report.

I would like to commend the authors of the selected presentations as well as the entire staff of the Israel Atomic Energy Commission for their valuable contributions and achievements and wish them all further success in their continuing fruitful endeavors.

Advances in Nonlinear Optics and Laser R & D

S. Jackel, Z. Kotler, R. Lavi and S. Sternklar

1. Summary

The Nonlinear Optics Group (NLOG) at Soreq NRC is engaged in the development of fundamental and applied technology in the related fields of nonlinear optics and laser development. Our work in nonlinear optics started with the goal of improving laser performance. These efforts were successful and opened the way for R&D in nonlinear optics for other applications. Today we use nonlinear optics to enable continuous tunability of lasers, control the path of light beams, modulate a light signal rapidly, provide optical data storage, and supply new means of microscopically probing biological and inorganic samples. Technology maturation and interaction with users will show which aspects of nonlinear optics will make the most impact.

Activities to be discussed in this report include:

1. Development of flashlamp, diode-laser and laser pumped solid-state lasers.
2. Optical parametric oscillators and sum frequency mixing devices for coherent light generation throughout the visible and infrared portions of the spectrum. These devices are based on the application of commercial single domain crystals and on Soreq fabricated periodically poled bulk and waveguide confined crystals.
3. Nonlinear optical materials development with the goal of designing organic materials which exhibit nonlinear absorption (reverse saturable absorbers), electro-optic polymers, and lasing materials for use in disordered highly scattering media.
4. Development of remote sensing systems based on the technologies developed by the group.
5. Subwavelength nonlinear microscopy effects.

Project sponsors include the Israeli and United States Governments and Israeli private industry. Inter alia, commercial products have been developed.

2. Laser development

2.1 Flashlamp pumped lasers

One of the group's long term goals is the development of high energy compact laser systems. To put this into perspective, the aim is to build shoe-box-size lasers that emit up to 10 Joules, and table-top lasers that produce up to 1000 J. In all cases, generation of a high quality laser beam is a must. High laser output implies even higher pump energies. Flashlamp pumping of high energy solid-state lasers is widely used because of its low cost and easy scaleability to high energy.

We are well on the way to reaching the goal of developing high energy solid-state lasers. To a large extent, our efforts were successful due to the application of unique designs and to the incorporation of nonlinear and adaptive optics devices [Phase Conjugate Mirrors (PCMs) and Variable Radius Mirrors (VRMs)]. These devices allowed use of laser materials with improved storage capacity and high efficiency, such as Nd:Cr:GSGG (Gadolinium Scandium Gallium Garnet) and Nd:glass which, due to poor thermo-optical characteristics, were previously by relegated to curiosity driven research devices or to low average power systems.

To date, 1.7 J pulse energy at 7 W average power and 4 J at 1 W have been obtained in GSGG and glass lasers.(1,2) Higher energies are expected, the limiting factor being damage in polarization rotating Faraday rotators. A test program showed an anomalous pulse duration scaling for Terbium (Tb) doped materials and that switching from Terbium Gallium Garnet (TGG) to Tb:glass increased the damage threshold fivefold (Fig.1).(2) This data is a highly significant for high fluence laser designs.

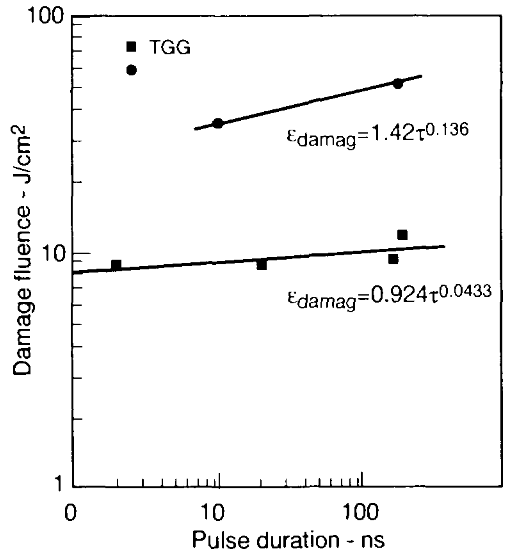

Fig. 1: Faraday rotator damage threshold dependence on pulse duration and material.

The high energy laser design uses a low power oscillator followed by a high power multiple-pass amplifier (MPA). At present, the MPAs are four-pass devices incorporating a VRM and PCM to correct for lowest and higher order thermal lensing aberrations, and Faraday rotators to correct for birefringence and to provide beam path control and isolation (Fig. 2).

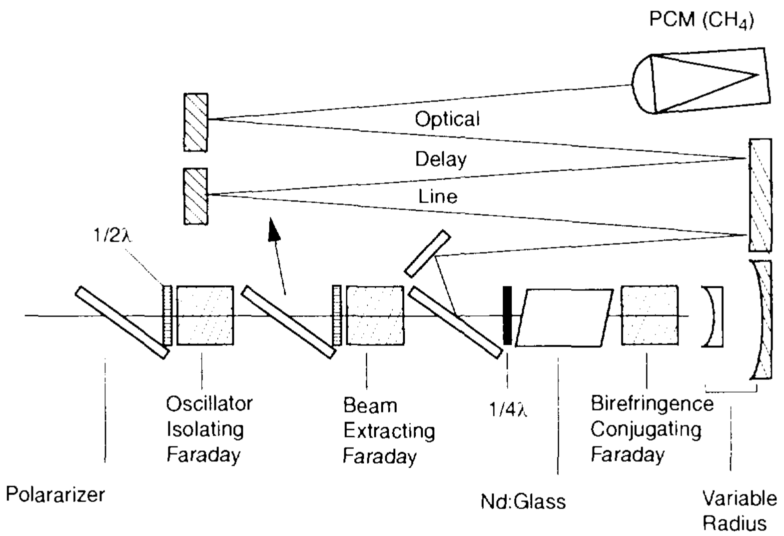

Fig. 2: Schematic design of a high energy quadruple-pass phase and polarization conjugated multiple-pass amplifier.

2.2 Flashlamp pumped oscillator development

Development of Nd:Cr:GSGG and Er:Yb:Cr glass oscillators is motivated by the twofold better efficiency of Nd:Cr:GSGG as compared with Nd:YAG, and by the 1535 nm "eye-safe" wavelength of Er:glass. The thermal aberrations and birefringence encountered in MPAs are even more critical in oscillators, due to the larger number of passes through the distorting medium. We concentrated on the application of VRMs to correct for thermal focusing, since PCMs have not proven effective in oscillator applications. The VRM is an adaptive optic with one degree of freedom, and can be used effectively to compensate for changes in rod thermal focusing for radii of curvature of ∞ to 50 cm simply by changing the spacing between two optical elements. Figure 3 compares the performance of a hemispherical GSGG oscillator with a conventional mirror and with a VRM. The much broader operating range of the laser with the VRM is quite pronounced. Complete microprocessor-controlled feedback makes the VRM an adaptive optic.

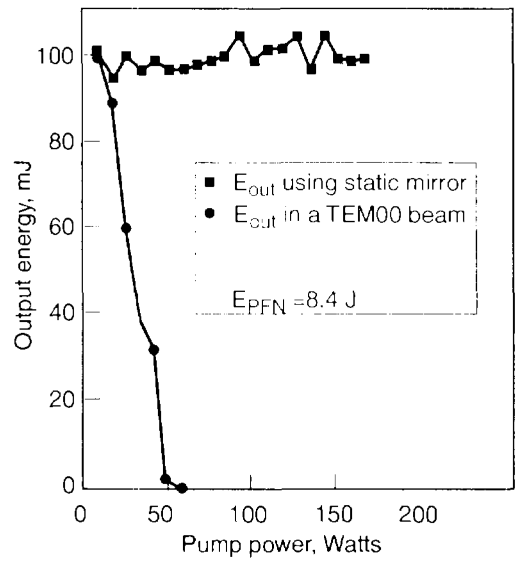

Fig. 3: Comparison of the performance of a hemispherical Nd:Cr:GSGG oscillator with a static mirror and with a variable radius mirror (VRM).

Nd:YAG lasing at 1064 nm has been one of the mainstays of the laser industry. Nd:YAG can, however, lase at other wavelengths. This offers a number of very interesting options for various applications while retaining all of the positive attributes of YAG. A program was undertaken to study the lasing action of Nd:YAG at 1319 nm not only in a single frequency oscillator but also in an oscillator simultaneously lasing at 1064 and 1319 nm. Figure 4 shows a schematic of the dual wavelength laser. Stable simultaneous lasing on two wavelengths using a single lasent with substantially different stimulated emission cross-sections is a unique achievement.

Research into dual wavelength lasers started with the development of a model that allowed optimization of output energies, pulse durations, build-up times, and stable operation. For given output energies, the important parameters were found to be the dual wavelength output coupler reflectivities and the lengths of the lasing cavities. Also of key importance was the suppression of lasing on transitions other than those that gave the desired wavelengths. A design insensitive to changes in pump energy was found. Using this design, an oscillator that produced 100 mJ at 1319 nm in the single wavelength mode, simultaneously produced 60 mJ (1319 nm) and 100 mJ (1064 nm). Timing jitter (a parameter of importance in upconversion applications) was reduced to $< \pm 1$ ns (5% of pulse width).

Fig. 4: Schematic of the dual wavelength ($\lambda 1$=1319 nm, $\lambda 2$=1064 nm) Nd:YAG laser. R1, R2: High reflectivity (HR) mirrors @ $\lambda 2$ & $\lambda 1$; R3: Output coupler with reflectivities ≈ R_a @ $\lambda 2$ & R_b @ $\lambda 1$; R4: HR @ $\lambda 2$ & high transmission @ $\lambda 1$; Q.S.: KD*P Pockels cell Q-switch.

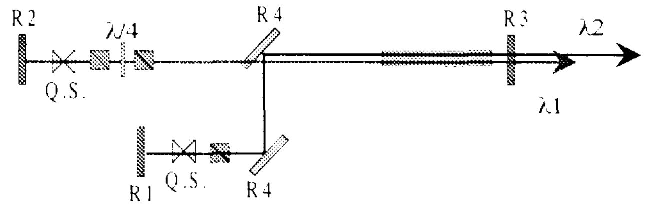

2.3 Diode pumped lasers

Diode pumped solid-state lasers are attractive because: (a) their high average power performance far exceeds that of flashlamp pumped lasers, (b) they are more energy efficient, (c) they are more compact. Worldwide R&D and commercialization efforts in this field are extremely intense. We have chosen to concentrate on the development of high average power, high beam quality, continuously diode pumped lasers. The reasons are twofold: (i), the diode costs ($/watt) are lowest for continuous diodes, and (ii), high average power lasers are the type required in medical and industrial applications.

In general, each generation of laser that we have built has surpassed its predecessor by an order of magnitude.[4,5,6] Our latest laser, the ***Barak 10***, is a 10 W, CW and high repetition rate, short pulse laser with excellent beam quality.[6] It is being exhibited and marketed worldwide. Figure 5 presents typical performance curves for a ***Barak 10***. Figure 6 shows a cross-section of the laser. The four diodes are close-coupled to a specially polished and coated Nd:YAG rod. The cylindrical surface of the rod acts as a focusing lens that concentrates the pump beam in an area that overlaps the low divergence mode of the Nd:YAG laser that we generate. Both the diode and the laser rod are impingement cooled, i.e., water flows in channels that approach but do not directly contact the lasing elements. The YAG rod cooling geometry is restricted to the y direction in order to generate a one-dimensional Cartesian temperature gradient. This reduces birefringence losses in the Brewster face laser rod.

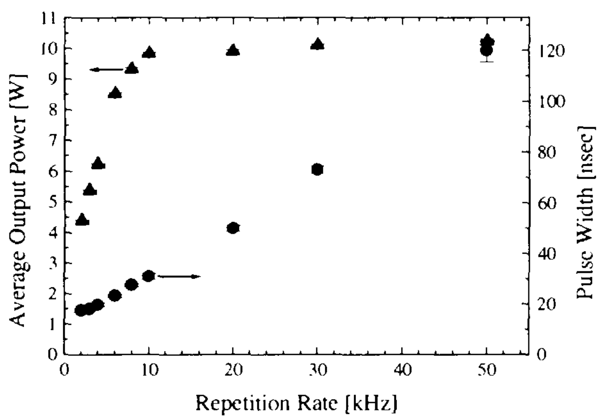

Fig. 5: Performance of the Barak 10 laser. The diode pump is continuous, whereas the Q-switch repetition rate may be varied over a wide range. The Q-switch may be turned off in order to obtain a 10 W CW beam.

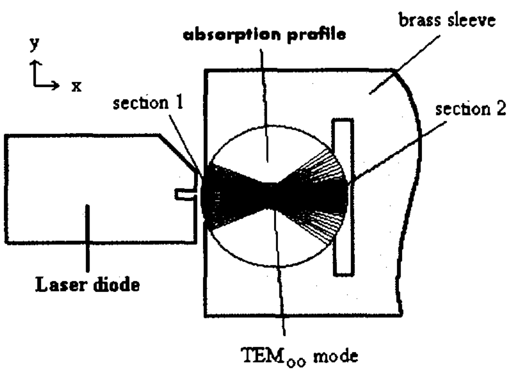

Fig. 6: Cross-section of the Barak 10 laser.

3. Frequency conversion devices

3.1 Periodically poled KTP frequency doubling crystals

During the 1980s and 1990s, the use of potassium titanyl phosphate (KTP) became customary as techniques for growing large crystals (up to 2x2x4 cm) became common and as competition drastically reduced the cost. This crystal is particularly attractive for frequency doubling of 1000 nm light because the angular acceptance minimizes alignment and beam divergence requirements.

The crystal is widely used with pulse pumped (flashlamp and laser diode) Q-switched lasers that produce intensities of tens of MW in the crystal.

CW pumped Q-switched lasers generate lower intensities and therefore efficient frequency doubling is more difficult. Improved efficiency cannot be achieved solely by increasing the length of the crystals because, after a certain laser divergencedictated interaction length, the inverse down-conversion process starts. The onset of the inverse down-conversion is a result of accumulated phase mismatch between the fundamental and harmonic beams. If the phase mismatch could be eliminated, then longer crystal assemblies or more highly focused (higher divergence) beams could be employed.

Quasi-phase matching is a technique for controlling the phase mismatch between the fundamental and harmonic beams. After a certain amount of mismatch is allowed to develop, the crystal is altered so that the polarization matrix is reversed. The phase mismatch in this zone goes to zero, at which point the crystal is returned to its original state. This periodically structured crystal can have vastly superior frequency conversion properties compared with homogeneous bulk crystals.

The first crystal in which quasi-phase matching was attempted was lithium niobate ($LiNiO_3$). Fundamental difficulties with the fabrication technique limited the depth of poling to only 300 μm.

We obtained exceptionally good results by working with Periodically Poled KTP.[7] The Solid-State Physics group at Soreq, in coordination with a group from the

Electrical Engineering Faculty at Tel-Aviv University, successfully periodically poled 1-cm-long KTP crystals of high optical quality and superior nonlinear performance. In these crystals, a periodically varying voltage imprinted a periodic refractive index variation in the crystal. Using the ***Barak 10*** laser, we produced 6 W of green power in a high-repetition-rate Q-switched beam.

Other crystals with different poling periods were used in external cavity optical parametric oscillators to produce tunable mid-IR light.

3.2 Sum frequency mixing

Frequency doubling is the process whereby two photons of the same frequency are combined into one, using the catalytic action of a nonlinear crystal. Over the past decade progress has been steady, with the conversion efficiencies of Q-switched pulse typically reaching 70% in KTP crystals.

Frequency tripling is another well known technique whereby the doubled output of one crystal is combined with the unconverted beam in a second crystal to generate a beam at triple the fundamental frequency. Typical tripling efficiencies in KTP are 40%. In fact, if an appropriate crystal is aligned in the correct orientation, any two photons can be added together to form a higher frequency photon. Sum frequency mixing is of interest to us because we have mastered the technique of locking together in time two short pulse lasers that generate photons at two different frequencies, as well as using Nd:YAG to generate pulses simultaneously at two frequencies. Using Nd:YAG, we can generate photons at 1064 and 1319 nm. Doubling each laser separately generates 532 nm (green) and 660 nm (red). Sum frequency mixing the two fundamental wavelengths yields 589 nm (yellow). Thus, we have generated five separate wavelengths using a single lasing material.

Using two separate Nd:YAG lasers, each lasing at separate wavelengths, we obtained 60 mJ of yellow light at an efficiency of nearly 30% (Fig. 7). Using a single laser emitting two wavelengths, we obtained 20 mJ of yellow light at an efficiency of 15%. Performance was limited by available input energy at 1319 nm.

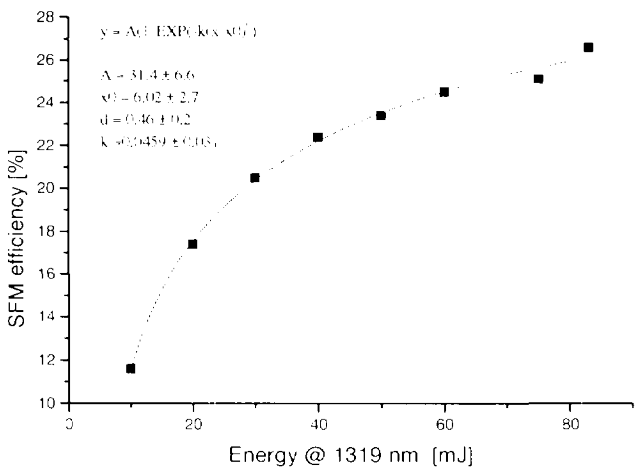

Fig. 7: Upconversion efficiency for the sum frequency mixing (SFM) of 1064 and 1319 nm synchronized pulses.

3.3 Optical parametric oscillators

Lasers are excellent sources of coherent light. They are, however, limited to emitting at specific frequencies or to confined spectral bands. Optical Parametric Oscillators (OPOs) use difference frequency mixing to obtain continuously tunable coherent light over extremely broad spectral ranges. For instance, one of our first OPOs used frequency tripled light from a Nd:YAG laser and was continuously tunable throughout the entire visible portion of the spectrum and well into the near infrared.[8]

Difference frequency mixing (the inverse of sum frequency mixing) is the process by which a single photon is split into two lower frequency photons. The efficiency of this process is enhanced, when the build-up starts from noise, by building a resonator (two mirrors that reflect one or both of the difference frequency photons) around the nonlinear mixing crystal. The resulting device is an optical parametric oscillator (OPO).

Because of the importance of 3-5μm tunable light sources for applications such as remote sensing, we have devoted considerable effort to the development of mid-IR OPOs. Prior to the invention of periodically poled crystals, we built extra cavity OPOs for attachment to high energy lasers and intra-cavity OPOs for incorporation into lower power, high repetition rate Q-switched oscillators.(9) Figure 8a and 8b shows an example of the intracavity laser and its mid-IR performance.

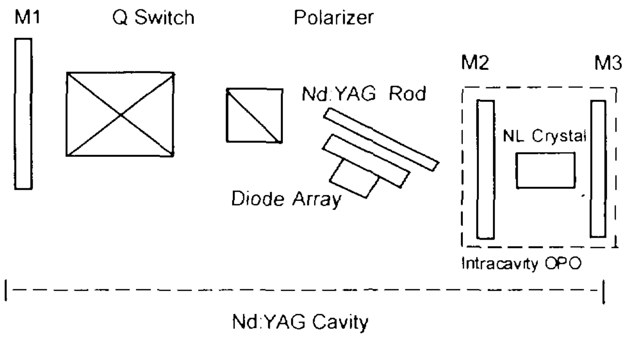

Fig. 8a: MID-IR intracavity optical parametric oscillator (OPO) imbedded in a diode-pumped laser.

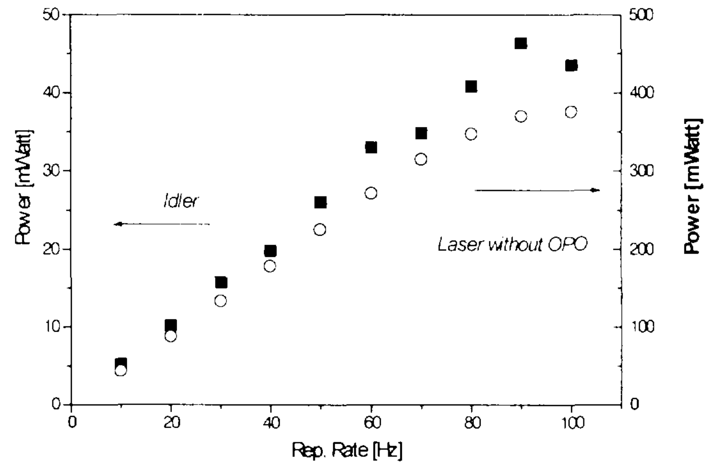

Fig. 8b: Intracavity optical parametric oscillator (OPO) output compared to standard laser output

3.4 Narrow linewidth OPOs

Narrow line width infrared OPOs are required for remote sensing lidar systems. Linewidth can be narrowed by injection locking the OPO, i.e., injecting a narrow bandwidth seed pulse or by inserting a linewidth narrowing grating into the OPO cavity and tuning it to the appropriate wavelength. One problem of the first approach is the need to find a laser source that emits at the proper infrared wavelength; the second approach has the disadvantage of increasing the losses within the OPO and substantially reducing the OPO output.

We have devised a hybrid solution that takes advantage of the OPO's properties.[10,11] The pump laser is narrow bandwidth; therefore, if one of the two OPO frequencies is narrow linewidth, then the second frequency will also be narrow linewidth. If a dye laser is tuned to the short wavelength OPO frequency (signal), then the infrared output (idler) will also have the desired bandwidth. The dye laser and the OPO can be combined into a single coupled cavity. Narrowing the linewidth of a dye laser is easy because the high gain of standard dye lasents compensates for the extra losses of the spectral grating. The end result is a compact, efficient, and robust narrow-linewidth (0.2 cm^{-1}) source (Fig. 9).

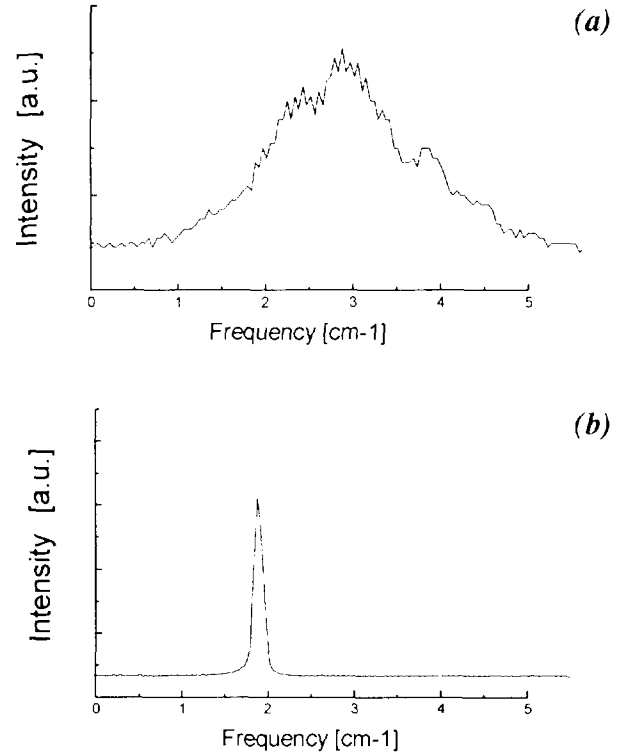

Fig. 9: Bandwidth of unseeded (a) and seeded (b) optical parametric oscillator

4. Nonlinear optical materials development

4.1 Second order nonlinear chromophores and polymers

Our activities are aimed at the development of new, thermally stable and highly efficient nonlinear optical (NLO) chromophores, as well as electro-optic (EO) and photorefractive (PR) polymers. These materials could be used in electro-optic integrated optical devices for ultra-fast light modulation (EO polymers) and dynamic memories (PR polymers). Various promising chromophores with 1,3-indandione-2-ylidene moiety as an efficient electron accepting group within donor-acceptor push-pull polyenes, have been synthesized and studied.

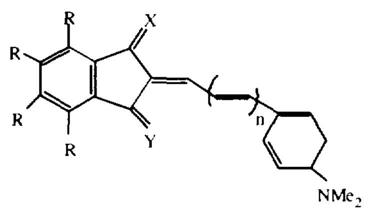

The electronic structure of these 1,3-diketone derivatives can be tuned easily by the further chemical modifications that makes these compounds attractive for detailed investigations of 'structure - properties' relationships. Second-order nonlinear properties of the chromophores are studied by EFISH (electric-field-induced SHG), and by Hyper Rayleigh Scattering (HRS) at 1.06μm and 1.54μm. The results of $\mu\beta$ obtained by EFISH for various new chromophores are presented below.[12]

Table 1 - Results of the electric field induced second harmonic measurements.

Compound	λ_{max} (nm)	$\mu\beta_0 \times 10^{-48}$ esu	
1	534	230*	1)R=H,X=Y=O,n=1
1(NEt_2 derivative)	552	399*	
2	570	500*	2) R=F,X=Y=0,n=1
3	592	966* ; 460 **	3) R=H,X=C(CN)$_2$,Y=0,n=1
4	670	>1000*	4) R=H,X=Y=C(CN)$_2$,n=1
5	604	280**	5) R=H,X=Y=C(CN)$_2$,n=0

* In Chloroform;
** In Toluene

Electro-optic polymers were prepared from the new chromophores as guest-host and sidegroups in optical polymers. Corona poling techniques have been used and thoroughly studied (high temperature poling under inert conditions for PVK polymers). Evaluation of the EO polymer properties is carried out by SHG from thin poled films.

We have also studied a unique photochromic dye with large second-order nonlinearity. The transition is based on a reversible formation - cleavage of a C-C bond. The bicyclic di-indandione derivative (λ_{max}=480nm in toluene) undergoes a reversible photochemical ring opening to form an isomer (λ_{max}=640nm in toluene). This isomer constitutes a conjugated donor-acceptor system and exhibits considerable second-order optical nonlinearity as found by electric field induced SHG (EFISHG) measurements. The photochromic conversion is observed also in the crystalline form indicated visually by crystal color change from red to green.

Nonlinear asymmetric zeolites, which were doped with chromophores within the pores but which maintained their polar ordering, were studied using the Kurtz powder technique and two-photon absorption. High frequency doubling efficiencies were observed (> x10 quartz). New organic salt crystals (quinoline derivatives) which possess polar order were also studied and found to show large NLO activity (>2x urea) in powder tests. These crystals are UV-transparent.

4.2 Optical properties of microspheres

The microsphere activity has developed around several different aspects, corresponding to different physical effects and microsphere sizes. Typically, the activity can be divided into two main subjects: (i) micromanipulation and testing of nonlinear optical microspheres, and (ii) laser action in diffusive media.

4.2.1 Nonlinear optical microspheres

This project is devoted to the development, study and manipulation of microspheres with giant nonlinear optical properties. These properties are due to degenerate spherical optical modes of the microspheres giving rise to giant optical resonance (morphology dependent resonance

MDRs). Most of the study has been dedicated to the microlaser.

Microlasers consist of polystyrene microspheres filled with DCM laser dye. After a careful choice of high sphericity microspheres (~40μm diameter), we obtained lasing from the microspheres by pumping directly with green, pulsed laser light focused by a microscope. A typical magnified image of a lasing microsphere is shown in Figure 10. Because the MDRs are circular modes propagating near the surface, one obtains a strong light enhancement near the surface.

In order to study the coupling of lasing microspheres with different micro-optical components, we have built an optical tweezers system which allows precise 3D manipulation of the microspheres. The next stage is thus to study the coupling efficiency of a lasing microsphere with an optical waveguide and maximize this coupling for future micrometer-sized electro-optical devices.

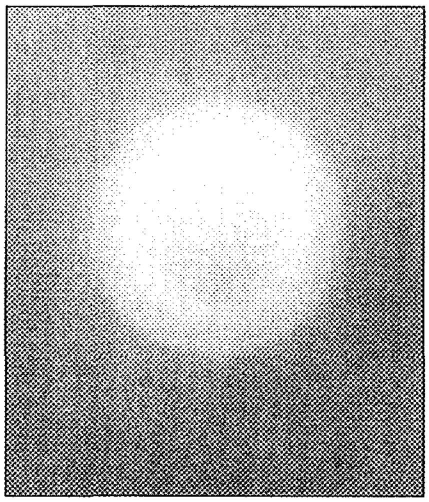

Fig. 10: Magnified image of a lasing microsphere.

4.2.2 Laser action in diffusive media

Following the recent discovery of laser action from diffusive media containing laser dyes, we initiated a series of experiments aimed at characterizing and optimizing these effects. The applications of such inexpensive lasing media cover the range from medical applications (especially skin treatments) to product identification (in warehouse and supermarket inventories).

Dye-methanol solutions containing suspensions of 32 nm diameter TiO_2 (titanate) particles exhibited lasing action when excited with a pulsed, frequency doubled Nd:YAG laser (532 nm). When the solution did not contain scatterers, increases in pump power resulted only in an increase in the dye luminescence (limited by dye saturation). However, when the concentration of the scatterers increased, the emission did not saturate with increasing pump power, as occurred with luminescence, but increased linearly. Moreover, one could observe a measurable reduction of the emission linewidth, from tens of nanometers down to less than 5 nm, as well as an increase in the light emission efficiency. Similar results have been obtained in dye-doped plastic films, showing the flexibility of this class of materials.(13)

After obtaining the preliminary results that showed lasing-like action in dispersions of titanate nanospheres in laser-dye solution, and the experimental evidence of optimum conditions for lasing, our efforts were concentrated on elucidation of the mechanisms which caused the effect, in order to further optimize such lasing. Therefore, several experimental techniques as well as a simple theoretical model were devoloped.

4.2.2.1 Mapping techniques

A series of systematic experiments were conducted in which the dye concentration and the scatterer density were varied independently, and we investigated how these parameters affected the lasing process. It was discovered experimentally that there exist completely isolated lasing regimes. Figure 11 (experimental data for high pump energy) depicts these regions. Typically, one can see three lasing zones, one at very high dye (rhodamine 6B) concentration, and two around 10^{-3} M dye concentration. The high dye concentration lasing zone is not relevant to the problem at hand and corresponds to strong chemical interaction between titanate particles negatively charged and rhodamine ions. However, two different regimes appear clearly at low and at high titanate densities for roughly the same dye concentration. The low-TiO_2-density enhancement is due to weak scattering of amplified spontaneous emission towards the detector, whereas the high-TiO_2-density enhancement is due to trapping of photons inside the highly scattering gain medium.

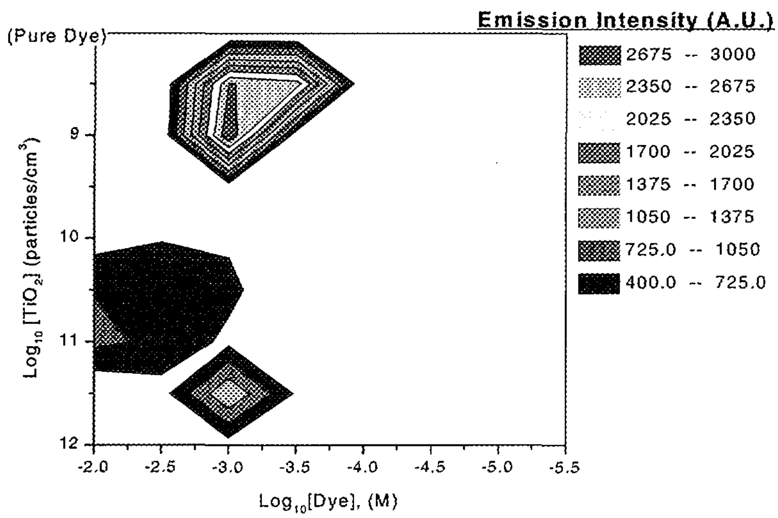

Fig. 11: Parametric mapping of diffuse media lasing

4.2.2.2 Spot size dependence threshold

Once it was established that a lasing effect can result from photon trapping due to high scattering, it seemed clear that the threshold for lasing had to depend on the pump spot size. Experiments with thin dyed polymeric films filled with titanate nanospheres showed directly that the sample macroscopic size influenced the lasing threshold.(14) Three different samples with thicknesses varying between 1 and 10μm were used in deriving the results presented in Figure 12. It can be seen that the thereshold is independent of the thickness. However, the threshold appears to vary with $L^{-3/2}$ (where L is the focal spot diameter).

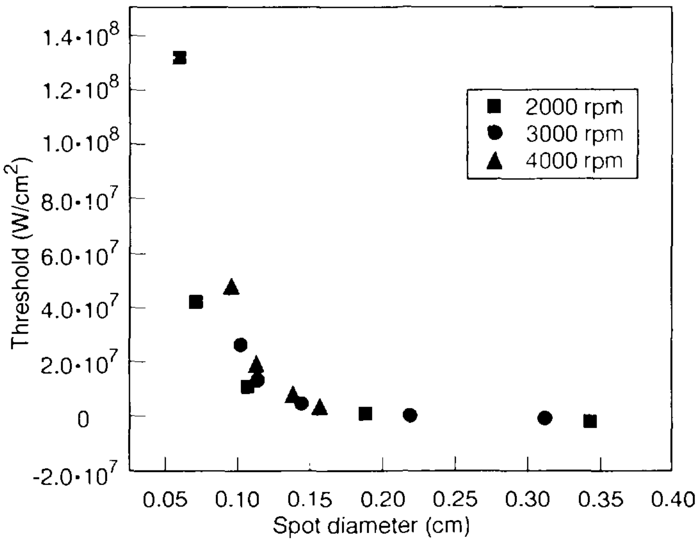

Fig. 12: Dependence of threshold on pump focal spot size for lasing in the trapped photon mode.

4.2.2.3 Photon diffusion model

With our system the lasing threshold (P_{th}) can be determined directly and precisely. Since the lasing threshold is a basic parameter in lasing theory, investigation of the effect of various parameters on the threshold enables comparison between experiment and theory and can be expected, therefore, to lead to further understanding of the lasing phenomena in diffusive media.

Using a combination of laser and photon diffusion theory, we were able to derive analytical expressions for critical parameters such as the threshold. Thus for the lasing threshold as a function of pump fluence the following expression was derived:

$$P_{th} = 4\pi h\nu\, l^* \;/\; L\sigma\tau_f\eta_Q \qquad (1)$$

where $h\nu$ is the photon energy, l^* is the photon transport length, and $\sigma\tau_f\ \eta_Q$ are specific parameters of the lasing material (dye in our case). Although reasonable agreement was obtained between the model and the experimental result both the experiment and the theory still need improvement in order to better understand the physical mechanisms.

4.3 Materials with efficient nonlinear absorption

We have studied materials which possess optical limiting capabilities due to their nonlinear absorption properties. Such mechanisms are known to be fast (subnanosecond response time) and do not exhibit increased scattering (unlike suspensions of absorbing particles). Since two photon absorption is an intensity dependent process, and since known materials typically have high intensity threshold, we have directed our attention to another class of materials: those which exhibit reverse saturable absorption (RSA) properties. This optical limiting mechanism is fluence dependent and rapid (on a picosecond time scale). Strong limiting effects based on RSA have already been demonstrated in several organic molecules. The RSA mechanism results from excited state absorption with a stronger absorption cross-section than the ground state (at certain desirable frequencies). The excited state is either an excited singlet (S_1) state or a triplet (T_1) state populated by an efficient intersystem crossing mechanism. The S $\rightarrow$ T transition is the main mechanism responsible for RSA in metallo-phthalocyanines (M-Pc) and metallo-porphyrines (M-Por). We have studied the RSA properties of heavy metal phthalocyanines, starting with commercial products. Commercial Pb-Pc was purified to yield two fractions: Pb^{+4}-Pc and Pb^{+2}-Pc. The former fraction exhibited a much stronger nonlinear effect than the latter. It was also found out that oxygen in the solution induces strong quenching effects. The quenching almost eliminates the nonlinear effect unless special care is taken during solution preparation. This is particularly true for the highly efficient RSA material Pb-Pc, whereas it was found to play no role for Zn-Pc. Z-scan measurements carried out in toluene solution with a 10ns pulsed laser at 532nm yielded the absorption cross-sections shown in Table 2 (fit based on a model assuming efficient and fast S$\rightarrow$T transition, and long-lived T state).

M-Pc	σ_{01}	σ_{34}	$\sigma_{34} / \sigma_{01}$
Pb^{+4}-Pc	2.75	188	68
Pb^{+2}-Pc	4.75	18	3.8
Zn^{+2}-Pc		98	

Table 2 - Absorption cross-sections measured for reverse saturable absorbers (RSA).

As can be seen from Table 2, the reduced fraction of Pb-Pc has a much lower nonlinearity. The sensitivity to oxidation state of the molecule led us to investigate of the effect of oxidation. For this purpose we recently initiated electrochemical studies of Zn-Pc which is not sensitive to the presence of oxygen. A specially designed cell, suitable for electrophotochemical investigation, is in preparation and will enable investigation of oxygen-sensitive compounds such as Pb-Pc. Solid samples of sol-gel containing Zn-Pc have also been prepared. Specially designed metallo-Pc compounds are currently being synthesized. These new materials will enable us to elucidate the role of side groups in RSA activity as we change from strong donors to strong acceptors.

5. Remote sensing

Laser-based remote sensing systems are ideal for detection and analysis of air, water, and land-surface borne chemicals, because there is no need for close physical contact between the sensor / operator and the unknown agents, and because the range and field of view of the detection system may be large. We have concentrated on the development of Differential absorption lidar (DIAL) techniques. In this technique, one looks at the absorption spectra of the target molecules. By analyzing two frequencies per absorption feature, one at the absorption peak and one just beyond the absorption line (looking at the background), signal variations due to extraneous sources can be factored out and the system sensitivity can be increased substantially.

Many chemicals have strong absorption features in the infrared. For this reason our IR OPO development has found an ideal application. A DIAL OPO must not only be tunable to the right frequency, but must also be frequency stable and must produce photons on and off the absorption line. Our work has shown that narrow linewidth OPOs are not suited to the requirements of DIAL systems. Instead, it was found that OPOs with a spectral width that extended several times beyond the width of the targeted absorption line had the required characteristics of frequency stability and on / off line photon production, as well as simplicity of design.

To use this wide bandwidth DIAL transmitter required the development of a special detection technique.[15] Soreq is the first to utilize this gas-correlation receiver (GCR) in an active DIAL system. Simply put, the GCR splits the return signal into two branches: one part goes directly to a detector and gives a measure of the total return signal; the other part goes through a cell containing a sample of the chemical being sought, and then to a second detector. If there were traces of the chemical in the atmosphere, then the absorption feature would have reduced the on-line light intensity even before the gas cell was reached. The extra absorption of the gas cell would have a relatively small effect. If there were no traces of the chemical in the atmosphere, then the gas cell would have a relatively greter effect This procedure can increase the sensitivity one hundred fold over that obtained with conventional DIAL systems.

6. Nonlinear optics and light-matter interaction in the near-field regime

Optics is usually considered as useful for devices larger than the wavelength of the light. This is due to the fact that the interaction of light with sub-wavelength features, in any medium, leads to energy loss through decay in the form of evanescent waves. However, in recent years great strides have been made in the development of microscopes (near-field scanning optical microscope, or NSOM) which break this diffraction barrier. Light which is forced through sub-wavelength apertures can sample and acquire information concerning sub-wavelength spatial features in media which are in the 'near-field' of the light, i.e., at distances smaller than the aperture's diameter. In this fashion, images are acquired with a resolution much higher than the diffraction limit would normally allow.

The Nano-Optics Laboratory at Soreq NRC is dedicated to the theoretical and experimental study of nonlinear and other types of light-matter interactions in the sub-wavelength spatial regime. Applications to be developed include high-density optical memories, nano-sized optical devices for integrated optics, and improvement of the NSOM technology for imaging.

A theoretical study of the interaction of light exiting a sub-wavelength aperture with Kerr medium (where the refractive index n depends on the light intensity I via $n=n_o + n_2 \cdot I$), leads to new and unexpected predictions concerning the light's response.(16) Due to the strong spatial gradients in the light intensity, it is possible to induce convergence of the light through interaction with a negative Kerr medium. Figure 13 displays this 'light-bunching' effect. We are currently studying other configurations in order to optimize and possibly create self-channeling of the sub-wavelength light. This would have important applications, for example in forming sub-wavelength wave guides and in guiding light through sub-wavelength apertures with improved efficiency.

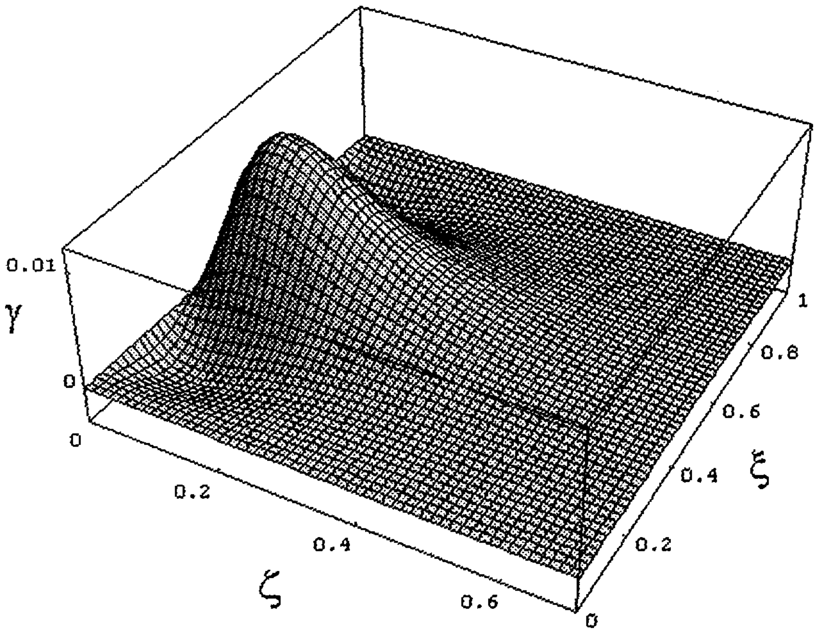

Fig. 13: Self-convergence of light with sub-wavelength spatial dimensions.

7. References

1. S. Jackel, I. Moshe, A. Kaufman, R. Lavi, and R. Lallouz, "High energy Nd:Cr:GSGG lasers based on phase and polarization conjugated multiple-pass amplifiers," Opt. Eng. 36, 2031(1997)

2. S. Jackel, I. Moshe, A. Kaufman, R. Lavi, R. Lallouz, and Z. Jackel, "Faraday rotators for use in multijoule Nd:Cr:GSGG and Nd:Glass phase and polarization conjugated multiple-pass amplifier," in *Proceedings of the 10th Meeting on Optical Engineering in Israel*, Proc. SPIE 3110(1997)

3. I. Moshe, S. Jackel, R. Lallouz, and Y. Tzuk, "Dynamic compensation of thermal lensing and birefringence in high brightness Nd:Cr:GSGG oscillators," in *Proceedings of the 10th Meeting on Optical Engineering in Israel*, Proc. SPIE 3110(1997)

4. R. Lavi, S. Jackel, S. Zdaka, O. Levi, and R. Lallouz, "Comparison between Nd:YAG and Nd:YLF Laser Oscillators, End Pumped by High Brightness Diode Laser Arrays," in *Proceedings of the 8th Meeting on Optical Engineering in Israel*, Proc. SPIE 1971 326, (1993)

5. R. Lavi, S. Tsadka, S. Jackel, and R. Lallouz, "Chromatic coupling of multiple laser diode pumps to laser materials," Opt. Comm. 114, 435 (1995)

6. E. Lebiush, R. Lavi, I. Tzuk, S. Jackel, R. Lallouz, and S. Tsadka, "Efficient high power high repetition rate diode side-pumped Q-switched Nd:YAG rod lasers", in *Proceedings of the 1997 Advance Solid-Sate Lasers Conference*, Proc. OSA, (1997)

7. A. Englander, R. Lavi, M. Katz, M. Oron, D. Eger, E. Lebiush, G. Rosenman, A. Skilar, and A. Arie, "Efficient second harmonic generation of a high repetition rate diode pumped laser with bulk periodically poled KTP," in *Proceedings of the 1997 Advance Solid-Sate Lasers Conference*, Proc. OSA, (1997)

8. R. Lavi, S. Fastig, A. Englander, S. Jackel, and R. Lallouz, "A high efficiency visible OPO pumped by the third harmonic of a multi-mode Nd:YAG laser," Nonlinear Optics 11, 153 (1995).

9. R. Lavi, A. Englander, and R. Lallouz, "Highly efficient low-threshold tunable all-solid-state intracavity optical parametric oscillator in the mid infrared," Opt. Lett. 21, 800 (1996)

10. I. Paiss, S. Festig, and R. Lavi, "Narrow linewidth optical parametric oscillator with an intracavity laser gain element," Opt. Lett. 21, 1652 (1996)

11. S. Paiss, S. Festig, and R. Lavi, "Design of low threshold narrow linewidth optical parametric oscillators," in *Proceedings of the 10th Meeting on Optical Engineering in Israel*, Proc. SPIE 3110(1997)

12. T. Khodorkovsky, L. Shapiro, O. Neilands, I. Ledoux, J. Zyss, B. Zinger, P. Shaeir, and Z. Kotler, "New, efficient NLO chromophores based on 1,3-indandione derivatives", French-Israeli Meeting on Nonlinear Optics, Les-Arcs, France, Jan. 96.

13. B. Sfez and Z. Kotler, "Lasing action from random media with gain", accepted for publication in Advanced Materials (1997)

14. B. Sfez, Z. Kotler, S. Margel, and B. Nitzan," Lasing without cavity," in *Proceedings of the 10th Meeting on Optical Engineering in Israel*, Proc. SPIE 3110(1997)

15. S. Fastig, I. Paiss, and M. Kleinman, "Wide bandwidth DIAL system - analysis and sensitivity studies," in *Advances in Atmospheric Remote Sensing with Lidar*, Springer-Verlag Press, Berlin, 459 pp. (1996)

16. S. Sternklar, E. Granot, and Y. Ishbi "Sub-wavelength gradient optics," Fourth International Conference on Near-Field Optics, Jerusalem, Israel (1997)

X-Ray Diffraction (XRD) Characterization of Microstrain in Some Iron and Uranium Alloys

G. Kimmel, D. Dayan, G. A. Frank and A. Landau

1. Summary

The high linear attenuation coefficient of steel, uranium and uranium based alloys is associated with the small penetration depth of X-rays with the usual wavelength used for diffraction. Nevertheless, by using the proper surface preparation technique, it is possible of obtaining surfaces with bulk properties (free of residual mechanical microstrain). Taking advantage of the feasibility to obtain well prepared surfaces, extensive work has been conducted in studying XRD line broadening effects from flat polycrystalline samples of steel, uranium and uranium alloys.

The XRD line broadening analysis has been used as a semi- quantitative method for measuring nonhomogeneity of alloying, hardness, Izod notch toughness, fracture toughness and residual thermal stresses. Good correlation between the microstrain and properties such as hardness and toughness was found after heat treatments and cold work. Comparable correlation was found between the microstrain in the supersaturated α-uranium phase quenched from the γ region, and the concentration of the alloying elements. The measured microstrain in the supersaturated α-uranium phase was used as a quantitative indicator for determination of the solubility limit of Ta and W in γ-uranium.

2. *Introduction*

X-ray diffraction (XRD) is a valuable technique that can yield considerable information on structure and properties of crystalline materials. This technique not only identifies the phases present in a sample but can provide more information from the peak profiles, allowing determination of crystallite size and microstrain, on the structure of crystalline phases.

For perfectly periodic ideal crystals the intensity profile can be described as shock spikes placed at the solutions of Bragg's equation:

$$\lambda=2d\sin\theta \qquad (1)$$

Where λ is the X-ray wave length , d is the interplanar spacing (d-spacing) and θ is the scattering angle (Bragg's angle).

For *real* polycrystalline materials the intensity profile tends to be broader due to two main imperfections: Scattering from small coherent domains (Scherrer, 1918), and internal microstrain associated with variations in the d-spacing of the scattering crystals (Stokes and Wilson, 1944).

The experimental intensity profile can be regarded as a convolution of two profiles. The first is from a *real* polycrystalline sample and the latter is due to non-ideal experimental conditions. The letter is known as the *instrumental profile* and its broadening arises from factors such as, axial divergence, flatness, transparency and surface roughness of the sample (Wilson, 1962).

In order to extract the *real* crystal profile from the total broadening, it is necessary to deconvolute the instrumental broadening from the experimental profile. The full width at half maximum (FWHM) is used as a measure of the total broadening in this work. By performing *line profile fitting* to the experimental diffraction results, the FWHM is evaluated for every diffraction peak . Fitting the best polynomials (in this case second order) to the sample's and to a reference samples FWHMs as a function of θ gives a continuous representation of the experimental $B(\theta)$ and instrumental $b(\theta)$ broadening, respectively. The deconvolution of $b(\theta)$ from $B(\theta)$, i.e., the calculation of the broadening coming from the real crystals $\beta(\theta)$, can be obtained by one of the following equations:

$$\beta(\theta)^2=B(\theta)^2-b(\theta)^2 \quad (2a)$$

$$\beta(\theta)=B(\theta)-b(\theta) \quad (2b)$$

Equations 2a and 2b assume Gaussian and Lorentzian forms of diffraction peaks, respectively. This assumption is rarely true and has to be regarded as an approximation. In cases where most of the experimental broadening arises from the sample, i.e., $B(\theta)^2 >> b(\theta)^2$ both equations give good approximation for $\beta(\theta)$ (Klug and Alexander,1974). Only such cases will be considered in this work.

The strain ε and the coherent domain size L can be obtained by Klug-Alexander dependence:

$$\beta^2 cos^2(\theta)=(\lambda/L)^2+16\varepsilon^2 sin^2(\theta) \quad (3a)$$

$$\beta cos(\theta)=(\lambda/L)+4\varepsilon sin(\theta) \quad (3b)$$

This expression can be derived from Bragg's equation by assuming Gaussian or Lorentzian broadening functions for both strain and size. Although this assumption does not agree with the opinion that Gaussian and Lorentzian broadening arises from strain and size effects respectively (Halder and Wagner, 1966; Gupta and Anantharaman, 1971; Nandi and Sen Gupta, 1978), we used this dependence for two reasons: (i) in this work the strain effect is more dominant; and (ii) the strain and size are evaluated by linear regression of $\beta^2 cos(\theta)$ *vs* $sin^2(\theta)$ termed Williamson-Hall plot (Williamson and Hall, 1953; Langford, 1992). Therefore, if Klug-Alexander dependence is not a good approximation for the systems analyzed in this work these will be, poor linear correlation.

Due to the high attenuation factor of uranium and steels, the X-ray penetration depth is relatively small (2-5μm). Hence, the information obtained by XRD broadening analysis is relevant only to the surface. Thus, gaining information about the bulk by this method depends upon surface treatments that will erase surface damage resulting from polishing and grinding. Because mechanical polishing can introduce strains into the surface, other methods for peeling of damaged surface layers have to be used, leaving only the effects in the bulk material.

An enormous number of steels with different compositions and properties is used as one of the principal structural materials. The proper process needed to achieve the desired assets is well documented. The preferred commercial materials is those which tolerate deviation in process conditions without damaging the final quality.

However, the ability to maintain small tolerance of some characteristics with a wide range of production conditions is not always clear and the desired quality is not easy to attain, due to the poor sensitivity of the characteristic. For example, the density and the composition will not change significantly within a wide range of tempering conditions for certain steel. The correlation between XRD line width and the condition of steels is well known. In residual stress measurements the broadened diffraction lines of some steels are inconvenient and special care must be taken for the determination of line position (Kurita, 1991). Line broadening analysis is currently studied in plastically deformed metals and in ball milled iron powders (Wagner and Aqua, 1963; Ungár, 1995) in order to investigate unisotropical distribution of internal stresses. In the present work we studied XRD broadening effects in steels, in samples with different mechanical properties, in order to determine whether mechanical properties and XRD broadening are correlated.

Iron exhibits three solid phases before melting at ≈1540°C. The solid phases consist of the following crystallographic structures: δ(1400-1540°C) is cI2, i.e., tungsten type; γ(910-1400°C) is cF4, i.e., copper type; and α(below 910°C) is cI2 also, but with smaller lattice parameter.

Rapid cooling of steel from the γ-phase to the α can produce a highly distorted supersaturated phase with a *tI2* (body centered tetragonal) structure designated by α'. This phase is created by athermal martensitic transformation and gives rise to a hard and brittle product.

Uranium with a melting point of approximately 1132°C has three phases: γ (775-1132°C) is cubic-*cI2*; β(668-to 775°C) is complex *tP30*, i.e., primitive tetragonal with 30 atoms per unit cell and α (below 668°C) is orthorhombic-*cO4* (Burke & al., 1976). As determined by X-ray measurements, the γ→β and β→α transitions are accompanied by volume decreases of 0.70% and 1.12% respectively (Chiotti et al., 1959). Studies with pure uranium have shown that neither of the high temperature phases, γ or β could be retained by quenching. The addition of various solutes to uranium enables one to obtain the isothermal martensitic transformation β→α or the athermal transformation γ→α. The final product is generally supersaturated with the solute and slightly distorted. Those phenomena are related to the cooling rate and composition of the uranium base alloys. The U-Ta, U-W and U-V alloys belong to binary systems with low solubility in the γ-uranium; (Saller and Rough,1952). Schramm et al., 1950; Dayan et al., 1994; Kimmel and Dayan, 1995; Dayan and Kimmel, 1996. Rapid cooling from the γ-phase is accompanied by the formation of α'-phase. The high strength and hardness of the quenched samples and the nature of the broad diffraction patterns, indicate that a state of non-uniform microstress exists in the alloys (Douglas, 1961). After prolonged annealing at high α range, the broadening effects of γ quenched uranium alloys are suppressed due to complete segregation of the solute and other impurities.

In the present paper we report on XRD line broadening effects in pure uranium and in various uranium alloys caused by different heat treatments, alloying, cold work, and surface preparation techniques. We also show that line broadening analysis may become a sensitive tool for evaluation of Izod notch and fracture toughness in steels and in uranium alloys, respectively.

3. *Experimental Techniques*

3.1 *General methodology*

The XRD analysis was performed with a Philips diffractometer using monochromatic Cu-radiation (λ=0.15406 nm for the $K_{\alpha 1}$ characteristic line). The K_{β} was removed by a reflected beam graphite monochromator. X-ray data were taken from 20 to 150° 2θ, while scanning in steps of 0.02° (2θ) with counting intervals ranging from 0.5 to 8 sec per step. The multiline integral breadth method (Williamson and Hall, 1963) has been adopted for evaluation of the mean coherent cell size and the average microstrain. The Williamson-Hall procedure has the advantage of speed and convenience (Guillou et al., 1995), and it has been utilized in other recent studies such as Langford et al. (1993) and Louër (1994). A similar method was presented by Langford et al. (1986). Utilization of the more powerful Fourier (Warren-Averbach), variance and related methods was abandoned at this stage because most of the diffraction lines in uranium are not well resolved, due to the low symmetry of U-α structure. Moreover, in case we find an isolated line in the lower Bragg angles, such as *020* or *111*, the higher orders of these reflections are indistinct and too close to other lines. This limitation of the Warren-Averbach method has been mentioned in earlier work (Langford et al., 1988). Nevertheless, utilization of the Fourier (WA) methods is investigated now.

The followings procedure have been used for the line profile analysis:

1. Selecting a range of the analyzed diffractograms with some diffraction peaks.
2. Performing line profile fitting for each peak that results in *FWHM of profile*, area, and height values for each Bragg line. This procedure is done with Philips PC-APD software, and gives a fixed *FWHM* to integral breadth ratio. In our software version the fitting is made in steps including no more than eight Bragg reflections at a time. A typical example of profile fitting results is shown in Fig. 1.

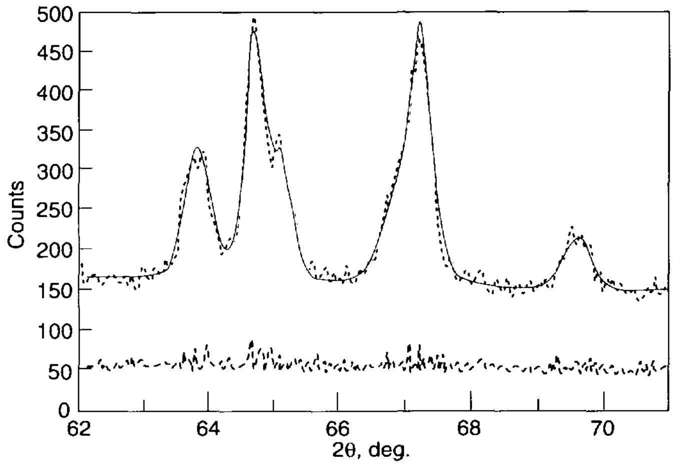

Fig. 1: An example of profile fitting for a selected XRD spectrum.

3. Finding the best fitted polynomial function $B(\theta)=a_0+a_1\theta+a_2\theta^2$ for the *FWHM* of the sample.
4. Finding the best fitted polynomial function $b(\theta)=a_0+a_1\theta+a_2\theta^2$ for the *FWHM* of the corundum plate standard (NIST, 1976), simulating the instrumental broadening.
5. The extent of the broadening effect can be examined visually just by looking at the vertical displacement of the B line, from the b line as seen in Fig.2 Then, by using equation 2a or 2b, the *real* sample broadening $b(\theta)$ can be extracted.

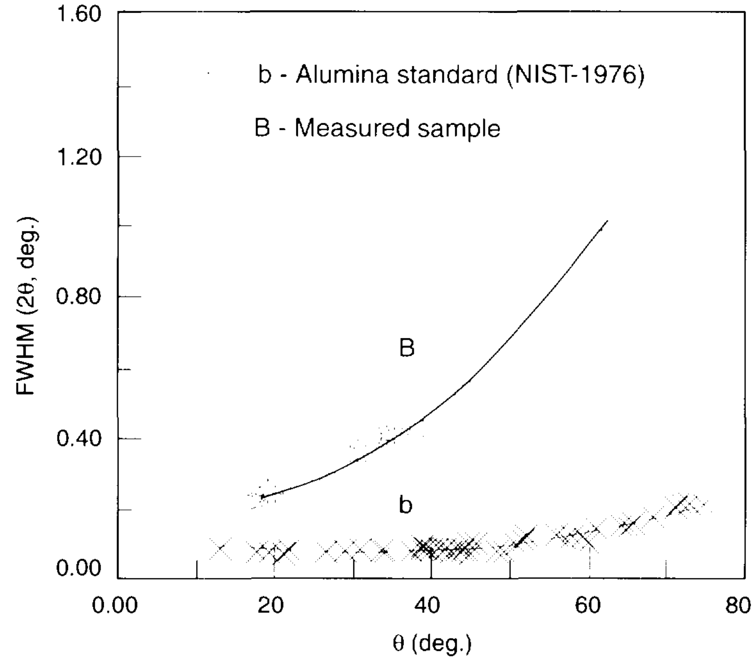

Fig. 2: Broadening effect: a comparison between B and b plots vs 2q. The function B(θ) is measured from the uranium spectrum and b(q) as obtained from corundum plate (NIST1976).

6. Strain and size data derived from the Williamson-Hall plot using eq. 3 for our application are shown in Fig.3 for uranium after cold work (forging).

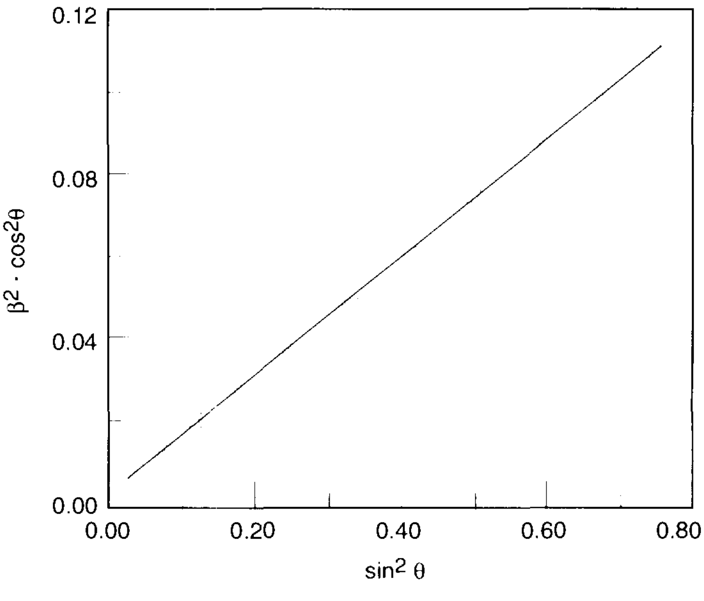

Fig. 3: Williamson-Hall plot for the case shown in Figure 2.

3.2 Samples preparation

Steels - The samples were prepared from several types of steels such as carbon-based alloyed steel, plain carbon steels and high-speed steel (HSS). All elemental concentrations are given in weight-percent. Different toughness and hardness were obtained by different thermal treatment, which included quenching from the γ-phase and tempering. Most samples sliced from Izod test specimens were polished mechanically and then electrolytically to remove the surface damage.

Uranium and uranium alloys - Small ingots of pure uranium U- 0.2 wt% (0.93at.%)V, U-0.75wt%Ti, and dilute uranium tantalum and tungsten alloys were prepared in an arc melting furnace under an atmosphere of purified argon. The various cast samples were remelted several times and the alloys were heat-treated in a vacuum furnace at 1040°C for 24 h. to ensure reasonable homogeneity. Chemical analysis, microscopy (light and SEM-EDAX) and surface hardness were used for the structural, morphological and mechanical characterization. The characterization of the microstrain and coherent domain size in the different samples was evaluated from a line profile analysis of XRD spectra.

Several U-Ti samples were prepared for fracture toughness measurement. These samples were water-quenched from γ treatment (20 min. at 850°C), followed by aging at 370°C for 6 h. The fracture toughness test took place at -40°C.

Surface preparation - In order to establish whether it is possible to obtain reliable surfaces for XRD of steel, uranium and uranium alloys, we performed some measurements on mechanically and electrolytically polished surfaces of pure uranium and low alloyed steel. After each preparation stage, an XRD analysis was performed and the breadths of the different peaks were measured and then plotted against theta in degrees.

Figure 4 shows diffractograms of tempered steel fully annealed after mechanical polishing. (3000 mesh diamond) and electrolytic polishing. The effect of the latter was marked; in all lines $K\alpha_1$- $K\alpha_2$ are split and the carbides lines are detected. Without electropolishing, $K\alpha_1$- $K\alpha_2$ are always overlapped and the carbides lines are hidden.

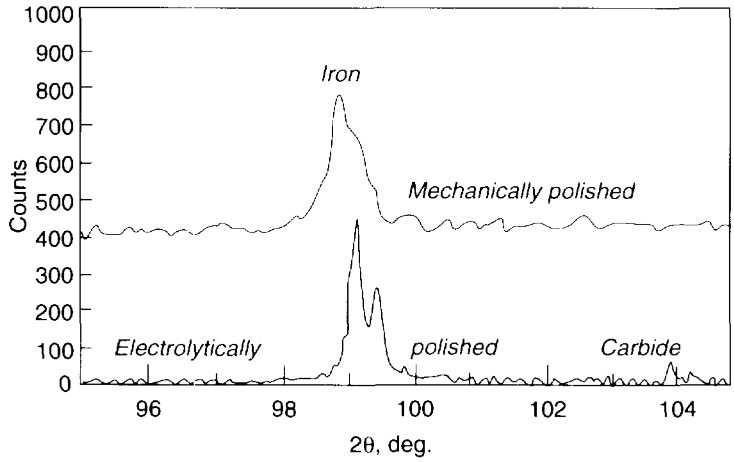

Fig. 4: Diffractograms of tempered steel as mechanically (top) and electrolytically (down) polished surface.

Figure 5 shows the FWHM versus θ plots for these two cases, in both of which there is uniform broadening. Williamson-Hall treatment results in a low level of microstrain (0.07%) and no size effect in the electropolished surface; and in microstrain of 0.165% and a domain size of 63 nm for the mechanically polished surface.

A flat surface of an annealed pure uranium sample was selected for the examination of surface treatment. The flat surface was examined by XRD after mechanical grinding with emery papers, polishing with diamond cloths, and finally after electropolishing in a bath containing 50 g of chromic acid, 420 cc of acetic acid and 60 cc of distilled water.

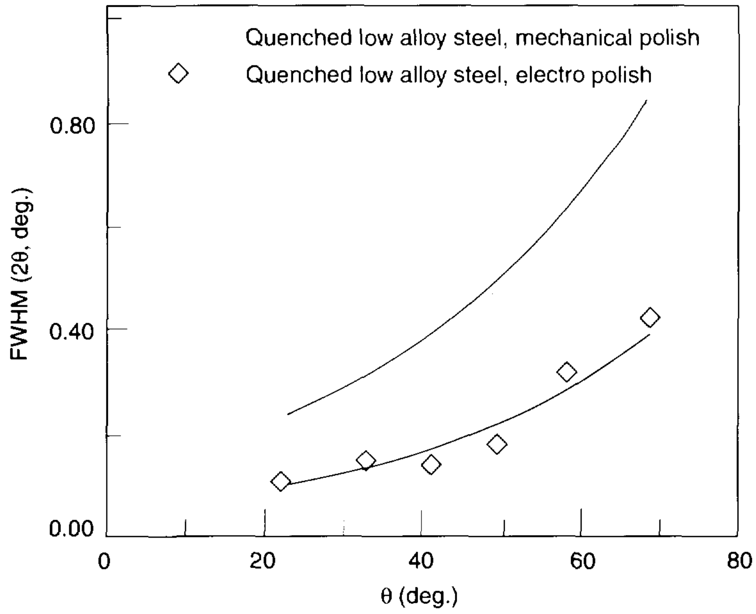

Fig. 5: ***Line breadth (FWHM) of quenched low alloy steel as mechanically (top) and electrolytically polished surface (down).***

Figure 6 shows five plots of *FWHM* of XRD lines vs Bragg angle θ. The sample with mechanical grinding on 180 grit paper exhibited the broadest diffraction lines. Finer paper (1000 grit) resulted in similar broad XRD lines. Diamond polishing reduced the broadening effect, and electropolishing removed most broadening effects.

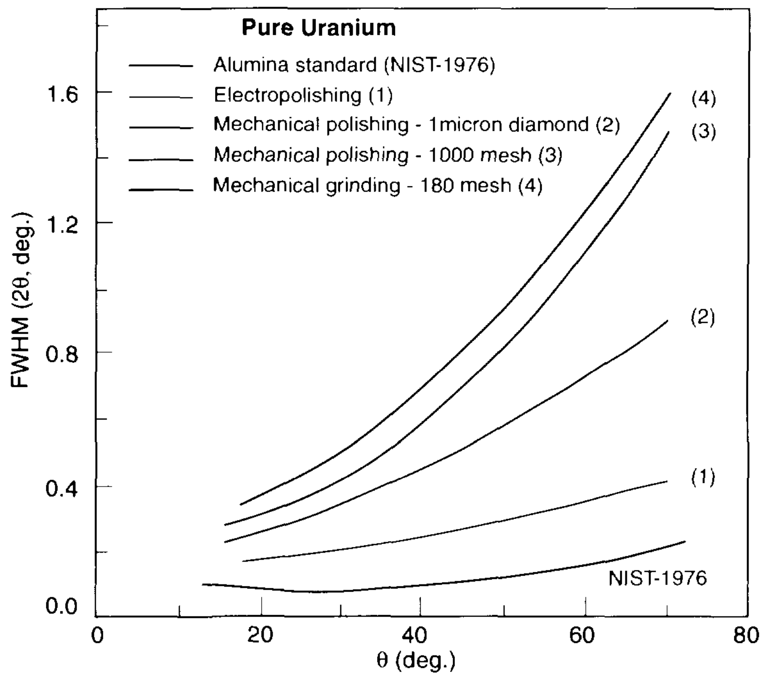

Fig. 6: ***Broadening effects in pure uranium with several degrees of surface damage.***

Similar behaviors were obtained for U-0.2wt.%V after the same surface treatment. The results are illustrated via Williamson-Hall plots in Figure 7.

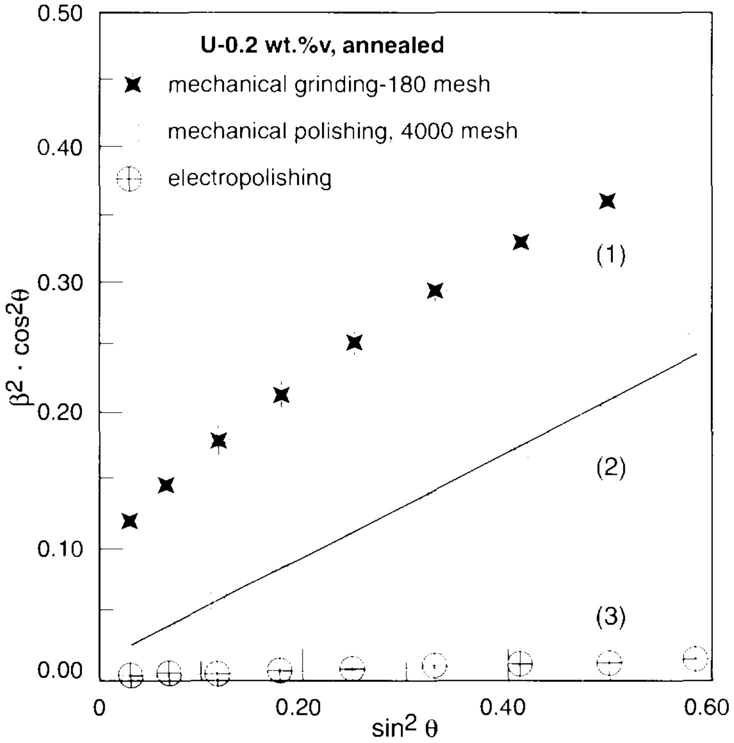

***Fig. 7:** Williamson-Hall plots for U - 0.2%wt V, after several degrees of surface damage (see also Table 1).*

***Table 1:** Strain and size data for uranium surfaces*

Sample	Surface treatment	Microstrain %	Mean coherent cell size nm
pure uranium	grinding, 180 mesh	0.331	31
pure uranium	polishing 4000 mesh	0.253	155
pure uranium	electropolishing	0.043	-
U - 0.2 wt.% V	grinding 180 mesh	0.312	26
U - 0.2 wt.% V	polishing 4000 mesh	0.260	150
U - 0.2 wt.% V	electropolishing	0.063	-

4. Results

4.1 Medium alloyed steel

We received from the industry several samples of 0.4% C, 3% Cr 1% Mo steel which were gamma-quenched and tempered by the supplier according to established procedures of the manufacturer (oil quench from gamma followed by tempering at 550°C). The treatments were made in the factory with the typical tolerance of an industrial process. The results of the mechanical tests were within an acceptable range without significant variations among samples. However, the Izod notch toughness (impact test) was not uniform, showing scattered data (20-43 J).

Typical plots of FWHM vs θ are shown in Figure 8 for steels with different Izod notch toughness. A clear gap between the total line breadth functions is evident. From the line broadening analysis it was deduced that the size effect was approximately the same in all samples. STM observations support this finding. Thus, the microstrain was the main reason for the differences in the broadening effect.

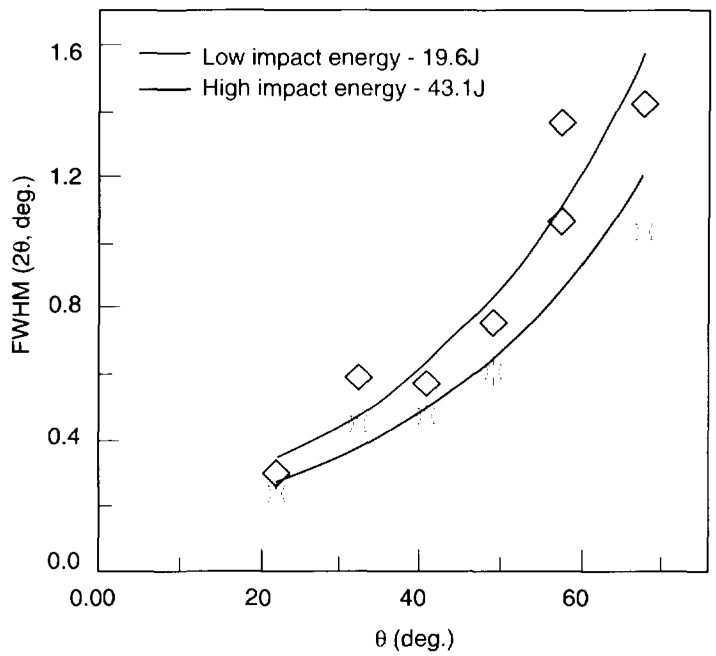

***Fig. 8:** Line breadth (FWHM) of steels with two different Izod notch toughness.*

Figure 9 shows that the microstrain was correlated with the Izod notch toughness, exhibiting linear relation.

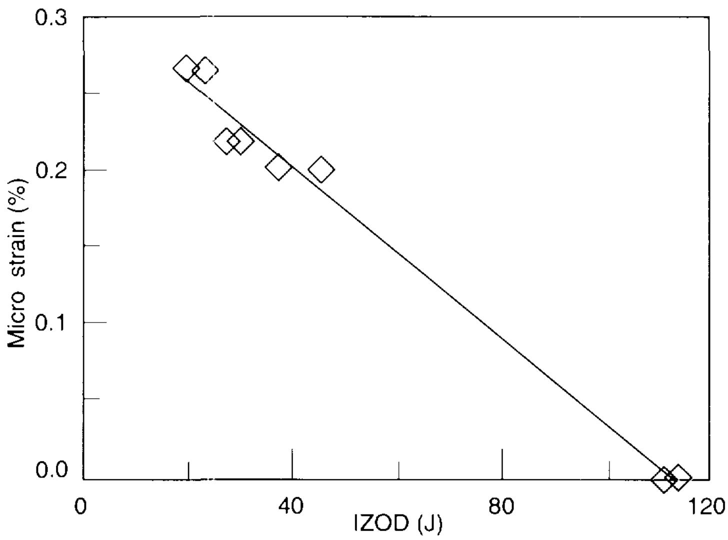

Fig. 9: Correlation between microstrain and Izod impact data for heat resisting steels.

4.2 Heavily alloyed steel

The high speed steel M10 is heavily alloyed (0.9% C, 0.3% Mn, 0.3% Si, 4.2% Cr, 8.2% Mo, 2% V, the balance being Fe). The alloy is heterogeneous with two kinds of carbides. An X-ray diffractogram (Fig. 10) shows sharp lines of carbides and broad lines of alpha- Fe. The difference in broadening effects between the metallic phase and carbides is displayed in Figure11.

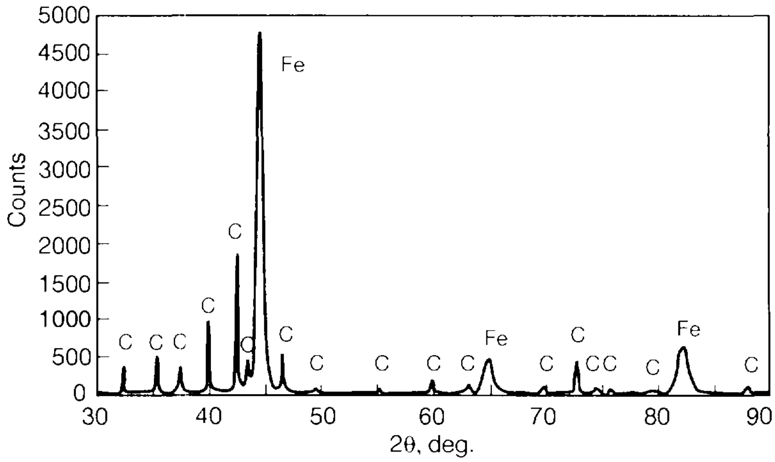

Fig. 10: Diffractograms of high speed steel (M10) after electropolishing (sharp lines for carbides and broad lines for iron base a phase).

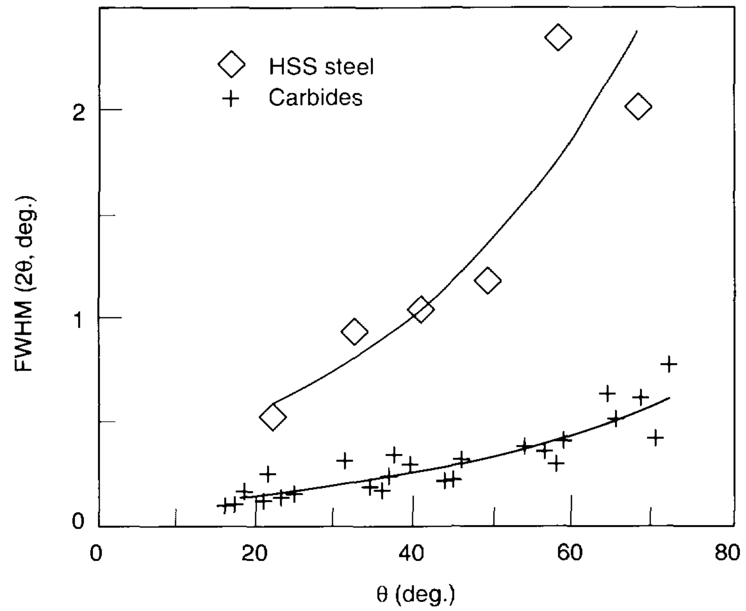

Fig. 11: Line breadth (FWHM) versus Bragg angles for tempered steel: comparison between carbides and iron base a phase

Broadening analysis of the carbides does not show size effect and indicates only a small strain (0.06 %). The broadening effects in the metallic structure are caused by the size of the cells (20 nm) and by the microstrain (0.4%). This value of microstrain exceeds the known elastic/plastic limit. Thus, it is suspected to be a structural broadening effect, like overlapping diffraction lines of two phases with close lattice parameters (like two alpha-like structures of different composition). To check this hypothesis, additional studies using TEM, STM, etc. are needed. The scattering of steel broadening is typical to other steels.

Nonuniform broadening effect in steels

The scattering of FWHM values around the polynomial function (see Fig. 11) is systematic and not random. It may be attributed to tetragonal distortion because the FWHM of *200* and *310* reflections were always higher than the average trend. When the tempering of medium carbon low alloy steel is completed, and all carbon has been segregated, the broadening becomes uniform and the tetragonality distortion disappears (Fig. 12). However, in the HSS (Fig. 11), in spite of the fact that the alpha Fe phase is mixed with carbides, it still exhibits "tetragonal distortion".

Nonuniform broadening effects were found also in ball-milled iron (Ungár, 1995) and are attributed to the effect of dislocation contrast (Ungár and Borbély, 1996).

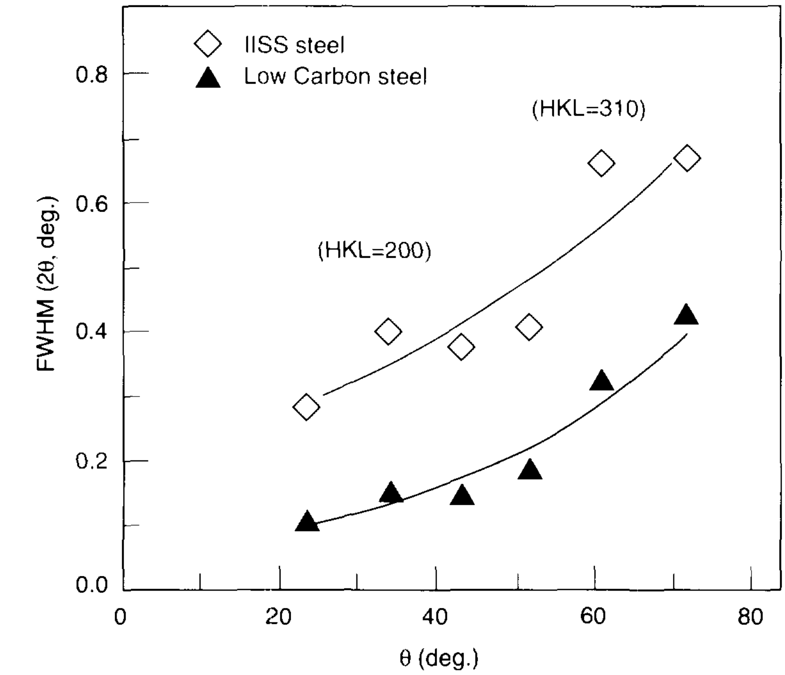

Fig. 12: Line breadth (FWHM) vs Bragg angles for tempered steel: nonuniform broadening effect.

4.3 *Alloying and heat treatments*

Heat treatment of pure uranium- A pure uranium sample containing less than 500 ppm impurities was heat treated at 800°C for 6 hours and quenched in water. Other samples were held at 800°C for 2 h and cooled slowly at the furnace cooling rate. One of these samples was annealed at 200°C for 24 h and cooled slowly. The diffraction patterns of these samples showed that, even in pure uranium, there is a distinguishable line broadening effect after quenching from high temperature (Fig. 13). The sample that was furnace-cooled gave the sharpest diffraction spectrum available for uranium.

The Williamson-Hall analysis resulted in a rather small microstrain of 0.065% in the water-quenched sample and 0.049% in the slowly cooled sample (see Table 2), both from the same temperature (800°C). Considering the variation between thermal expansion coefficients in different directions in uranium as 15 ppm/K, thermal strain due to of anisotropic contraction can be built up by cooling from 320 to 440°C. According to Collot and Reisse (1971), it is reasonable to assume that only above 420°C plastic deformation relax all thermal stresses instantly. Thus, it is concluded that uranium samples quenched from high temperatures should include residual microstrain up to 0.065%, probably due to thermal stresses.

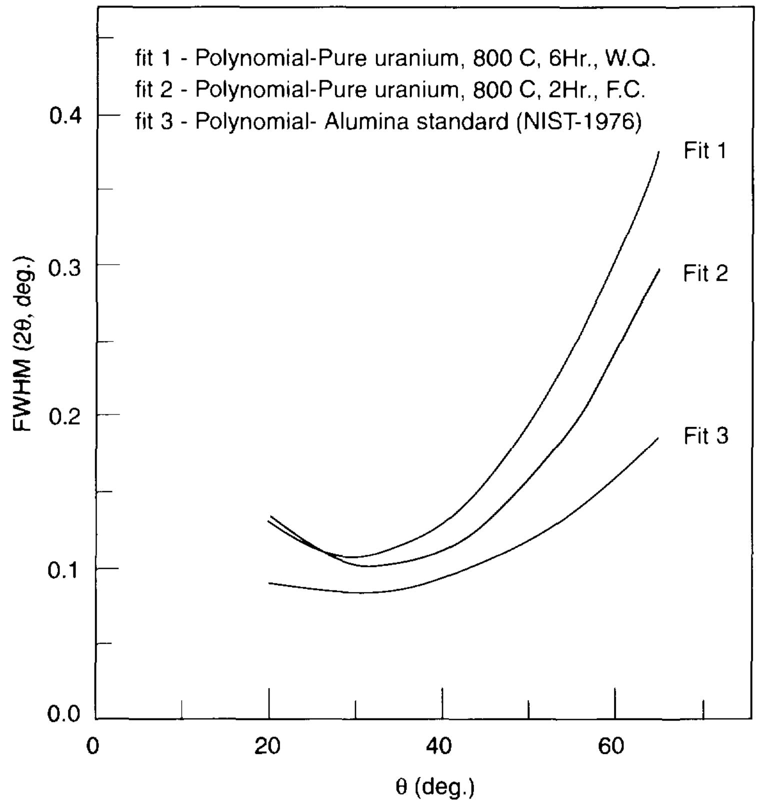

***Fig. 13:** Broadening effects in pure U after heat treatment at 800°C for 6 h and water quench (Fit 1) and, after slowly cooling from 800°C to room temperature at the furnace cooling rate (Fit 2). (Both samples were polished electrolytically).*

Table 2: Microstrain after several heat treatments

Sample	Heat treatment	Microstrain (%)
pure uranium	800°C, 2h, F.C.	0.049
pure uranium	800°C, 6h, W.Q.	0.064
U - 0.2 wt.% V	850°C, 2h, F.C.	0.063
U - 0.2 wt.% V	850°C, 2h, W.Q.	0.171

FC - Furnace Cooling
WQ - Water Guenching

Microstrain in heat-treated dilute uranium-Ta and W alloys - Tungsten and tantalum were reported to be immiscible in α uranium and to have small solubility in γ uranium. We observed that quenching of uranium with small amounts of Ta and W from temperatures in the γ range produces very small lattice distortion; however, severe broadening effects occur (Fig. 14). Williamson-Hall analysis resulted in a pure strain effect (no small domains), which increases with the concentration of the supersaturated alloy.

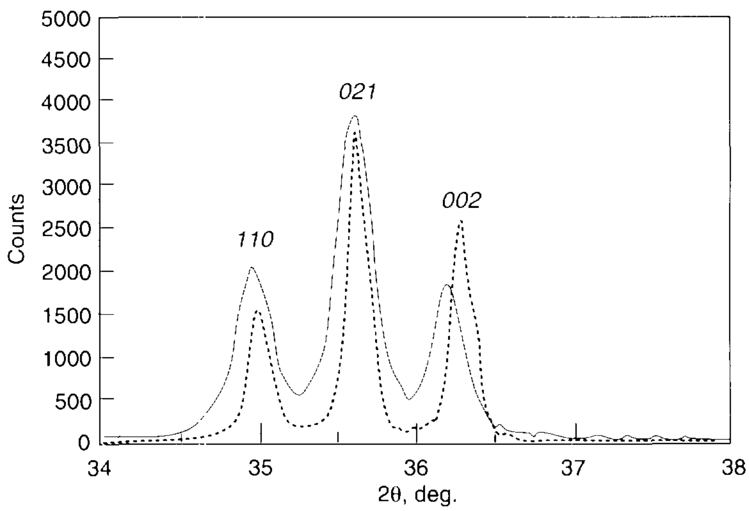

Fig. 14: Part of the U-Ta spectrum after water- quenching( ) and after slow cooling (---) from 1040°C, showing severe broadening effect in the sample after γ quenching.

A plot of microstrain vs concentration is presended in Figure 15 for both alloying elements W and Ta. It should be noted that the solubility limit was defined by the appearance of the *cI2* structure diffraction lines for W and Ta, as well as by SEM observations. We found that the solubility limits for the alloys are 2.6 and 2.00 at.% for Ta and W, respectively. These values are above the reported data for the solubility limits in γ uranium (Schramm et al., 1950), but are beyond the solubility limit of these elements in α-uranium. Therefore, in both cases the supersaturated state should be assumed.

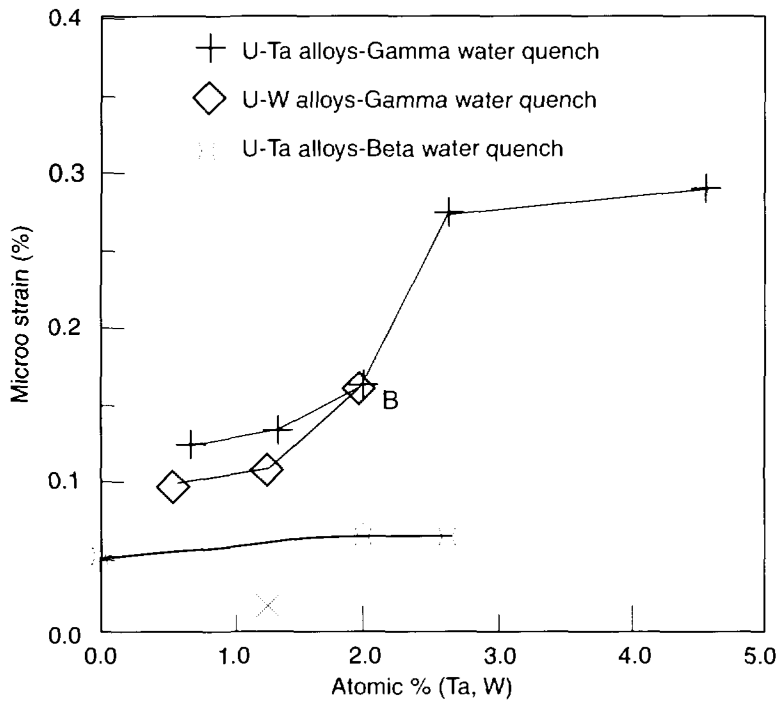

Fig. 15: Microstrain vs concentration in quenched samples of U with Ta and W after g quenching, and with Ta after b quenching.

Quenching from the β phase resulted in different behavior of W and Ta. Tungsten was found to be a β stabilizer. The characteristic of the room temperature β structure of U dilute W is reported elsewhere (Dayan et al., 1994). On the other hand, all samples with Ta quenched from β showed diffraction of free tantalum, without any broadening effect (Dayan and Kimmel, 1996). The microstrain of β-quenched samples is displayed in Figure15, which shws that the strain in β–quenched samples is in the range of thermal stress and independent of Ta concentration.

4.4 Microstrain and mechanical properties

Effects of cold work - Cold work of uranium (U-0.2% V) results in increased hardness. The hardness increases sharply until 10% reduction and continues to rise moderately but steadily. XRD studies of forged samples showed a broadening effect which can be removed by thermal annealing. After data processing by the Williamson-Hall method, the strain component was found to increase with the percent reduction in the same manner as the hardness. The simultaneous increase of both characteristics, the microstrain and the hardness, is illustrated in Figure 16. The correlation between degree of cold work and XRD line broadening has been reported in other alloys, for example in carbon steel (Kurita, 1991) and in Al-Mg (Ji et al., 1993).

Fig. 16: Simultaneous increase of microstrain and hardness in forged U 0.2 wt.% V.

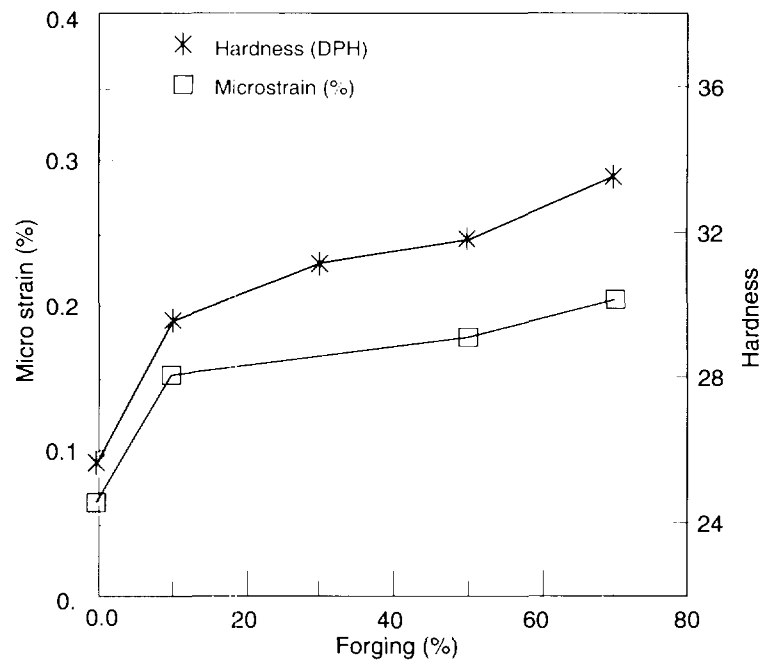

Fracture toughness - The correlation between XRD line width and fracture toughness of U-0.75wt.% Ti samples was evaluated. The samples underwent the same heat treatments, solution treatment at 850°C for 20 min and water quench, following aging at 370°C for 6 h, and displayed almost the same mechanical properties such as tensile strength, elongation and hardness, within an acceptable range of tolerance. However, the fracture toughness (FT) results were scattered within a wide range of values. After performing XRD line broadening analysis, it was found that the domain size was the same for all samples, but the microstrain was fluctuating. Figure 17 shows that microstrain and fracture toughness are linearly dependent.

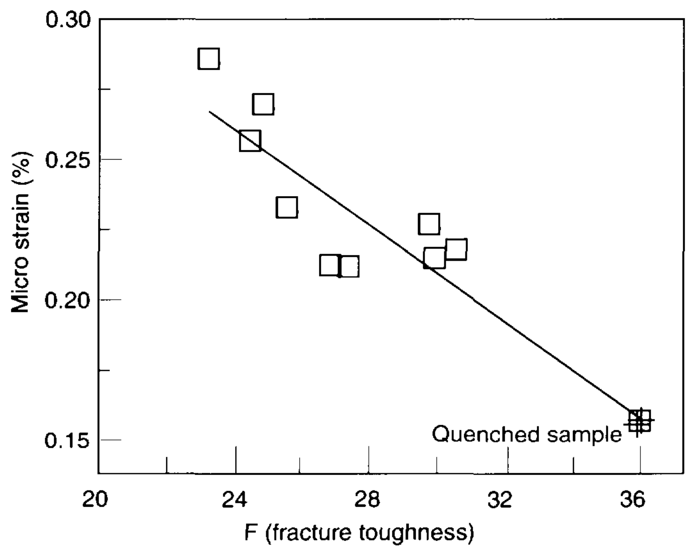

Fig. 17: Correlation between microstrain and fracture toughness (stress intensity factor), expressed in KSI√in.

Effect of solubility - Since a correlation was found between solid solution and microstrain, we deemed, it worthwhile to check the hardness of each sample with a metastable solid solution. The results show a simultaneous increase of hardness with microstrain for U-Ta alloys (Fig. 18).

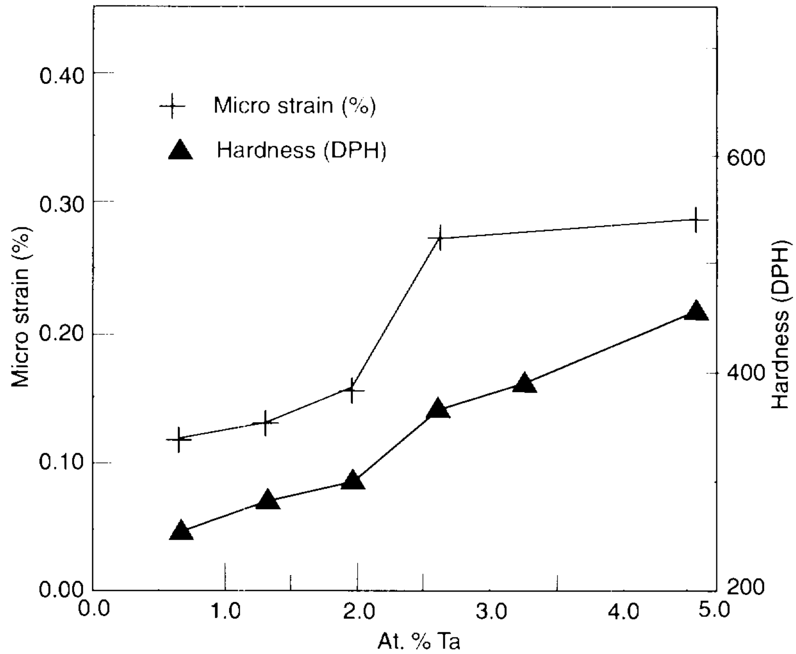

Fig. 18: Simultaneous increase of microstrain and hardness in alloyed U-Ta as a tool for determining solubility limit.

5. *Summary and Discussion*

The observations made in the two different system studied were similar.

1. A surface free of polishing damage is required and electropolishing is an efficient way to remove surface damage in uranium alloys and in steels.

2. The strain is the main probe for a physical process in the metallic systems. Metastable solid solutions in metallic alloys increase the microstrain.

3. The microstrain is probably correlated with fracture toughness as indicated in Figure 17. Such correlation may be of scientific significance because it provides a convenient way to study the empirical connection between these two properties. Furthermore, it is readily seen from Figure 8 that if the microstrain is really a linear function of the Izod notch toughness, one can evaluate the upper limit of Izod notch toughness for the heat-resisting steels (by extrapolation to the point with zero microstrain). The value of 114 J which was derived by such a procedure is in agreement with the high values of Izod notch toughness in steels (Wyatt and Dew-Huges, 1974). If this correlation will be established with more data and also with fracture toughness tests, it could become an excellent characterization tool for both quality

control and research.

4. The correlation between microstrain and hardness or strength is not absolutely clear. In several cases, for example U-Ta dilute alloys, aging raised the hardness and relaxed the microstrain. In heat-resisting steels the variations in hardness and strength were equal for some samples, but the microsrain differed. This point is important because there is also no general rule which correlates hardness with toughness. Broadening analysis can be used as an additional tool to clarify this point.

This work showed that a considerable amount of information relevant to the tested materials structure can be obtained from an analysis of the broadening effects. In spite of the fact that X-rays are mainly a near-surface probe, in particular for uranium, most artifacts caused by improper surface preparation can be eliminated.

Two different types of broadening effects were found: those caused by cold work and those observed in metastable solid solutions. In both cases the broadening effect could be quantified using in, microstrain as the parameter in the analysis. A correlation we found between the strain, the amount of cold work, and the amount of an added element

For materials belonging to a similar family and when the effect of concentration was eliminated, we were able to obtain a general experimental dependence between the microstrain and the hardness of the samples. In cases of softening or hardening (by thermal annealing, aging or cold work) we could replace the hardness test could be replaced by measurement of microstrain. Nevertheless, we do not claim that this dependence is a general rule; it should be utilized only after making a calibration curve.

It is possible that the microstrain following cold work has a different origin from that which is induced by metastable supersaturated solid solution. Whereas in the case of cold work we obtained both strain and size effects, in the supersaturated state we found mostly microstrain. We tend to attribute this microstrain to fluctuations in concentration of the added alloying element. These fluctuations in concentration result in an enhanced hardening.

The main effect of adding new elements into solid solution is the lattice parameter distortion, which results in shifts of the XRD line positions. In uranium the solubility limit of most elements is less than 1% at., with almost no change in lattice parameters. However, metastable supersaturated α' uranium alloys with solubility up to 5 at.%. are known in uranium with added γ-stabilizing lements, titanium, niobium, zirconium, molybdenum, ruthenium and rhenium. (Douglas 1961; Tangri, K. and Williams 1961; Virot 1962, Hills et al., 1963; 1965; Jackson et al., 1963; Anagnostides et al., 1964; Tangri, et al., 1965; Jackson and Larsen, 1967; Yakel 1976). Continuous change of lattice parameters of α' uranium alloys was reported by many workers. Together with peaks shifts, severe line broadening was also reported (Douglas, 1961), but without quantitative data. TEM studies of γ water quenched uranium with additions Ti and Ti+V exhibited nonhomogeneous structures within the nano-scale (Landau et al., 1986, 1993). Therefore, it is reasonable to attribute the microstrain found by XRD to local fluctuations in the concentrations of the alloying elements.

Whereas the stability range of the γ stabilizer elements (Nb, Zr, Ti, Mo etc.) is very large in the γ phase, in U-Ta and U-W the solubility in γ is limited to less than 3 at.%. Consequently, the α structure lattice parameters in γ quenched samples with Ta and W are almost unmodified (Dayan et al., 1994; Dayan and Kimmel, 1996). However, broadening effects in the α structure in γ quenched samples were quite obvious, and line broadening analysis was the most sensitive method for the characterization of alloys which are not defined as γ stabilizers, such as U-Ta , U-W and U-V. The correlation between microstrain and concentration of the dissolved element can be used to measure the solubility limit in the high-temperature phase. In the range where the microstrain was increasing continuously with concentration after quenching from the high-temperature phase, it is implied that during the solution treatment at the higher temperature, the equilibrium state was a solid solution. The solubility limit of Ta in γ - U is indicated by the "saturation" of the broadening effect as a function of (see Fig. 18). The minor difference in the microstrain values of pure U in comparison with U-0.2%wt. V after complete annealing (see Table 1), may be attributed to an excess of vanadium which could not be removed completely.

6. References

Anagnostidis, M., Colombie, M. and Monti, H. (1964) J. Nucl. Mat. 11:67-76.

Burke, J.J., Colling, D.A., Gorum, A.E. and Greenspan, J. Physical Metallurgy of Uranium Alloys., Brook Hill Co., Chestnut Hill, Massachusetts, in cooperation with the Metals and Ceramics Information Center, Columbus, Ohio, 1976.

Chiotti, P., Klepfer, H.H. and White, R.W. (1959) Trans. Am. Soc. Metals 51: 772.

Collot, C. and Reisse, R. (1971) Mem. Sci. Rev. Met. 6:419-434.

Dayan, D., Beeri, O., Herrmann, B., Landau, A., Zahavi, A. Livne, Z. And Kimmel, G. (1994) J. Alloys Compounds 226:89-93.

Dayan, D. and Kimmel, G.(1996) J. Alloys Compounds 243:161-166.

Douglas, D. L. (1961) Trans. ASM 53:307-319.

Guillou, N., Auffredic, J.P. and Louer, D. (1995) Powd. Diffr. 10:236-240.

Gupta, R.K. and Anantharaman, T.R. (1971) Z. Metallkd. 62:732-735.

Halder, N.C. and Wagner, C.N.J. (1996) Adv. X-Ray Anal. 9:91-102.

Jackson, R. L., and Larsen, W. L. (1967) J. Nucl. Mat. 21: 263-276.

Jackson, R. J., Williams, D. E. and Larsen, W. L (1963) J. Less Comm. Met. 5:443-461.

Ji, N., Lebrun, J.L. and Sainfort, P.(1993) Mater. Sci. Forum 133-136:537-542.

Hills, R. F.,Howlett B. W., and Butcher, B. R. (1965) J. Nucl. Mat. 16:109-128.

Kimmel, G. and Dayan, D. (1995) Proceeding International Conference, X-Ray Powder Diffraction, Analysis of Real Structure of Matter, Size and Strain, 95 21-25 Aug. 1995, Liptovsky Mikulás, Slovakia, I20, p. 23.

Klug, H. P. and Alexander L. E. (1974) X-Ray Diffraction Procedures 2nd. ed. John Wiley and Sons, New York.

Kurita, M. (1991) Adv. in X-ray Anal. 34:633-642.

Landau, A., Kimmel, G. and Talianker, M. (1986) Script. Met. 20:1313-1316.

Landau, A. Talianker, M. and Kimmel, G. (1993) J. Nucl. Mat. 207:274-279.

Langford J.I. (1992) Accuracy in Powder Diffraction II, E. Prince and J.K. Stalick (eds) NIST 846, 110-126.

Langford, J.I, Boultif, A., Auffrédic, J.P. and Louër, D.(1993) J. Appl. Cryst. 26:22-33.

Langford, J.I., Delhez, R., de Keijser, Th. H. and Mittemeijer, E.J.(1988) Aust. J. Phys. 41:173-187.

Langford, J.I, Louër, D., Sonnenveld, E.J. and Visser, J.W.(1986) Powder Diffraction 1:211-221.

Louër, D. (1994) Adv. X-ray Anal. 37: 27-35.

Nandi, R. K. and Sen Gupta, S. P. (1978) J. Appl. Cryst. 11: 6-9.

Saller, H.A. and Rough, F. A. (1952) U. S. A.E.C. publ., AECD-3323 and BMI-716.

Scherrer, P. (1918) Goettingen. Nach. 2:98.

Schramm, F. G., Gordon, R. and Kaufman, A. R. (1950) J. Metals 188:195.

Stokes, A.R. and Wilson, A.J.C. (1944) Proc. Pys. Soc. Lond. 56:174-181.

Tangri, K. and Williams, G. I. (1961) J. Nucl. Mat. 4:226-233.

Tangri, K., Chaudhuri, D. K. and Rao, C. N. (1965) J. Nucl. Mat. 15:228-287.

Ungár, T. (1995) Proceeding International Conference, X-Ray Powder Diffraction, Analysis of Real Structure of Matter, Size and Strain, 95 21-25 Aug. 1995, Liptovsky Mikulás, Slovakia, I12, p. 23.

Ungár, T. and Borbély, A. (1996) Appl. Phys. Lett. 69:3173-3175.

Virot, A. (1962) J. Nucl. Mat. 5: 109-119.

Wagner, C.N.J. and Aqua, E.N. (1963) Adv. X-ray Anal. 7:46-64.

Williamson, G.K. and Hall, W.M. (1953) Acta Met. 1:22-31.

Wilson, A.J.W. (1962) X-Ray Optics, Methuen, London.

Wyatt O.H., and Dew-Huges, D. (1974) Metals, Ceramic and Polymers, Cambridge University Press, London.

Yakel, H. L. (1976) "Review of X-ray Diffraction Studies in Uranium Alloys. Physical Metallurgy of Uranium Alloys. Burke, J.B. Colling, D.A. Gorum A.E., and Greenspan, J. [Eds.]Chapt 7. Pp. 259-308 Brook Hill Publishing Company, Chestnut Hill, MA, U.S.A.

Passive Cooling Systems in Power Reactors

J. Aharon, R. Harari, M. Haim, Y. Weiss, Y. Barnea, M. Katz and M. Szanto

1. *Summary*

This paper reviews several R&D activities associated with the subject of passive cooling systems, conducted by the N.R.C.Negev thermohydraulic group. A short introduction considering different types of thermosyphons and their applications is followed by a detailed description of the experimental work, its results and conclusions. An ongoing research project is focused on the evaluation of the external dry air passive containment cooling system (PCCS) in the AP-600 (Westinghouse advanced pressurized water reactor). In this context some preliminary theoretical results and planned experimental research are for the fature described.

2. *Introduction*

The basic design requirement of novel cooling systems in nuclear applications inherent safety. Self-operating cooling systems are needed during all stages of the fuel life cycle. These Passive Cooling Systems (PCS) are used in the nuclear industry in order to act upon the overheated reactor facilities in the wake of any possible event of emergency scenarios, as well as to cool spent fuel in various storage configurations.

The main characteristic of the PCS is that they do not rely on blowers or pumps for fluid circulation. Rather, the flow is circulated by the buoyancy forces resulting from density gradients due to heat transfer processes from fission products. The circular flow patterns and the resulting heat transfer mechanisms, are termed Induced Mixed Convection

(IMC)[1]. In this phenomenon, defined within a confined space, a buoyancy driven flow adjacent to the surface, caused by the heat transfer, induces a secondary flow in the fluid core. The secondary flow can be of the aiding or "opposed" type, depending on the external flow direction.

These thermally derived systems are often called thermosyphons and are used in many engineering applications with various configurations. There are two major types of thermosyphons: one in which the working fluid is simply contained in a closed or partially closed container, forming a cooling cycle along its boundaries (Fig. 1); and another in which the flow is thermally induced through channels, forming an open or closed loop (Fig. 2). In systems classified as the first type, the heat and momentum transfer process is driven by utilizing buoyancy forces on a fluid contained in a vessel. Therefore, a net heat transfer, at suitable points, is required for continuous operation and mechanical inputs are excluded. Figure 1 shows two types of thermosyphons which were investigated.

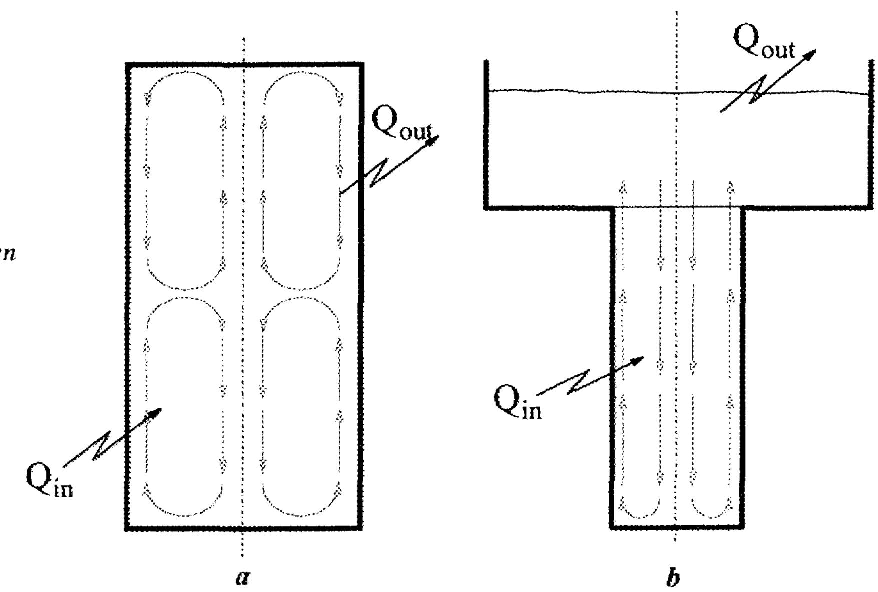

Fig.1: The closed (a) and an open (b) thermosyphon.

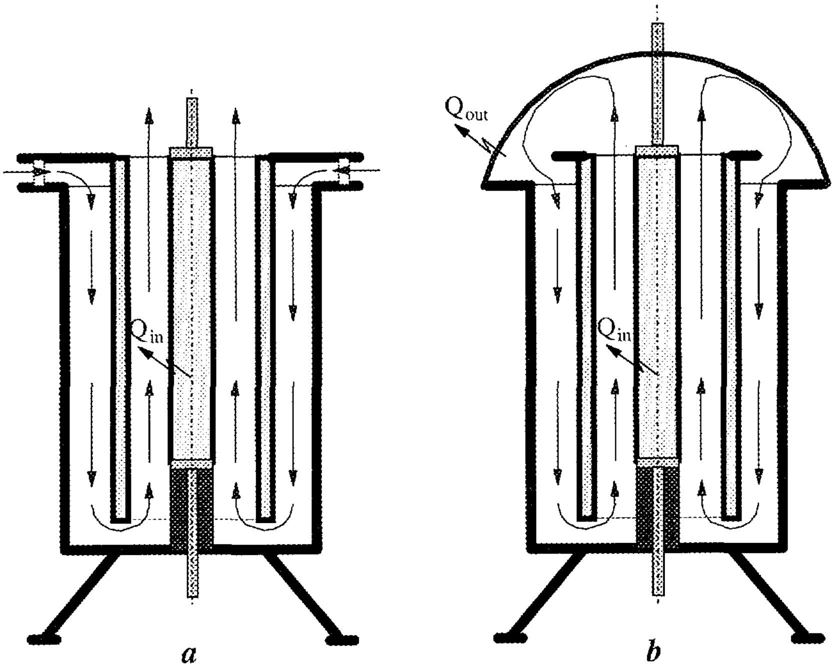

Fig.2: An open (a) and a closed (b) loop thermosyphon

The thermosyphons are purely free convection devices, being either open or closed. The open system is basically more efficient, since it is capable of removing higher heat transfer rates. For example, in the case of an emergency loss of cooling event in a nuclear reactor, it is necessary to remove large amounts of heat as quickly as possible. Thus, cooling the reactor by using an open thermosyphon connected to a common industrial water supply located on the building's roof seems to be quite feasible. The water supply would form a natural reservoir for an open thermosyphon and would allow the discharge of a large amount of energy in it.

Similarly, passive heat removal from gas-cooled nuclear reactors (HTGR and HTR), during a postulated Loss of Cooling Accident, requires various engineering solutions such as a Hot Gas Duct (HGD). The HGD is a preheated cylindrical duct, located higher than the nuclear reactor core to enable the removal of the decay heat by a process of natural thermosyphon cycle. During normal operating conditions the lower plenum is heated to compensate for external heat losses and to maintain along the HGD, a constant temperature necessary to direct the flow in the passive cooling cycle. A buoyancy-driven downward flow adjacent to the inner surface, caused by the external heat transfer to the surroundings, may induce an opposed upper flow in the duct's core. That possible flow generates an overall Opposed Induced Mixed Convection (OIMC) effect and, consequently, the undesired axial temperature gradient.

The open thermosyphon is another system, in which a similar heat transfer process takes place. There an OIMC flow field is developed by heating circumferencially a vertical tube closed at its bottom and open at the top to a large reservoir.

Understanding the interaction between the flow adjacent to the tube's wall and the opposed induced flow at the core, was a challenging subject for many researchers. Referring to a similar heat transfer process, Lighthill[2] solved analytically the problem of cooling turbine blades, as convective flow in narrow vertical tubes, with constant outside wall temperature. The author employed an integral momentum boundary layer analysis to describe various laminar and turbulent flow regimes. Evans et al.[3] reported a similar analytical and experimental study, of transient natural convection in a vertical cylinder. An analytical model was developed by dividing the system into three regions: a thin boundary layer rising along the heated walls;

a mixing region at the top where the boundary layer discharges and mixes with the fluid at the upper core; and a main core region which slowly falls as plug flow. Japikse and Winter[4] reported a theoretical and experimental study of the boundary layer heat transfer in an open thermosyphon, recommending some practical correlations to determine the laminar and turbulent flow regimes as well as the transition zone. Ostrach[5] reviewed the natural convection phenomenon in enclosures, pointing out that the interactions between the boundary layer and the core remain an unsolved problem, inherent to all confined convection configurations. Recently, Weiss et al.[6] analyzed the OIMC phenomenon by a theoretical model, assuming boundary layer type of flow in the turbulent regime, and found that such a model is defined only over a certain domain. Additionally, further downstream, different heat transfer regimes are anticipated. In order to characterize all possible existing flow regimes, an advanced numerical simulation in the turbulent flow regime was carried out[1], providing a good fit to the experimental results [1,7,8].

Systems related to the second type of thermosyphon (Fig.2), use natural convection to generate flow within the system channels, forming an overall Aiding Induced Mixed Convection (AIMC) or OIMC effect. For example, in the open loop thermosyphon (Fig. 2a), the inner channel is clearly dominated by natural convection phenomena. The flow within the channels is a combination of forced and free convection. The forced convection flow component is the result of the fluid being drawn through the external channel by the buoyancy forces in the inner channel. Based on this phenomenon, the Westinghouse AP-600 reactor design uses such a type of passive containment cooling system. The air flow path designed between the steel reactor containment hot shell and the concrete shield building, creates an open loop thermosyphon. External cold air is introduced through specially designed shutters located at the upper level of the concrete shield building, while cooling the hot steel containment generates an induced upward air flow.

Various studies of different types of natural circulation loops were reviewed by Mertol and Greif [9]. For this type of system, work related to natural convection on vertical plates, vertical cylinders, between vertical parallel plates and in vertical tubes was considered. These configurations represent the basic mechanisms associated with natural or induced mixed convection in the system.

Understanding the influence of boundary conditions on natural convection along the containing walls is very important. In a large number of these applications the surface heating conditions are non-uniform i.e., the natural convection on one side of the wall is coupled with another heat transfer mechanism on the other side. Aharon and co-workers[10,11] measured the heat transfer coefficient for free convection on a vertical plate with general boundary conditions (neither constant temperature nor constant heat flux). In these experiments coupling between free convection and other heat transfer processes, taking place on the other side of the plate, was investigated.

Referring to natural circulating loops, the commonly used basic assumption is that the induced flow is fully developed. However, it must be recognized that full development cannot be expected at all elevations in the channel but only above a certain distance from the channel entrance. Considering the developing flow region higher heat transfer coefficient are obtained.

Bodoia and Osterle[12], Bar-Cohen and Rohsenow[13], Burch et al.[14] and Webb and Hill[15] analyzed the development of the induced flow between vertical parallel plates. Davis and Perona[16] analyzed numerically the development of the induced flow in a heated vertical open tube. From the velocity and temperature profiles obtained for various stages of the flow development, a graphical correlation between volumetric flowrate and heat transfer rates was found.

Clarksean[17] analyzed experimentally the characteristics of a thermosyphon designed to cool cylindrical spent fuel heat sources passively. The analysis is based on recognizing the physics of the flow within different regions of the thermosyphon in order to develop empirical heat transfer correlations. Considering the external dry air passive containment cooling of the AP-600 reactor, Barnea et. al[18] and Harari et. al.[19] developed a theoretical model to predict pressure drop, mass flowrate, hot surface temperature and heat transfer coefficient behavior in an open loop thermosyphon configuration. This theoretical model served to optimize the design of an experimental system in order to verify the calculated parameters.

Buoyancy induced flows are complex because of the essential coupling between the flow and energy transport phenomena. These flow fields can be classified as either external (free convection) or internal (natural convection). The PCS are basically natural convection problems, that is classed as an internal problem. Internal problems are considerably more complex than external ones, because the region external to the boundary layer is affected by the boundary layer itself. The interaction between the boundary layer and the external flow field constitutes a central problem in determining the heat transfer coefficient. Furthermore, the flow pattern and the resulting heat transfer mechanism cannot be predicted a priori from the given boundary conditions and geometry.

Experimental measurements in this complex flow and heat transfer field are very difficult. Using conventional measuring probes may introduce disturbances, which can cause cardinal changes in the entire flow field. most complicated parameters to measure are the velocity profiles, which are an essential tool for determining different types of flow regimes. Therefore, the best way to overcome the mentioned difficulties is to combine temperature profile measurements, flow visualization and advanced numerical simulation results.

Some of the experimental systems that were built to evaluate the feasibility of these passive cooling systems are presented herein, along with, describing the experimental apparatus buildup, highlighting some measurement difficulties, and reporting the typical results. Some of these experimental systems are still part of an ongoing research program carried out in the Thermohydraulics Laboratory at NRC-Negev.

3. Experimental systems and results

3.1 The effect of boundary conditions on free convection

Considering a vertical flat plate that on one side transfers heat by natural convection to a fluid at temperature T_∞ at a general boundary condition, namely, the other side of the plate is exposed to an environment of a constant temperature, T_a, with which heat is exchanged with an effective heat transfer coefficient (h_{eq}). In engineering solutions for heat transfer problems, the effective heat transfer coefficient could be the result of a forced convection or one-dimensional conduction in the wall.

The apparatus used in the experiments is shown schematically in Figure 3. The experimental plate consists of three layers: the exposed stainless steel plate, the aluminum isothermal plate and an insulation layer between the two plates. The exposed plate, which is the heat transferring surface, is 600 mm wide x1020 mm high and x0.5 mm thick; it dissipates the heat to the surroundings. The isothermal plate is 600 mm wide x1020 mm high x 6 mm thick. The high thermal conductivity of the aluminum and the fact that the aluminum plate is 6 mm thick, make it possible to maintain the plate at uniform temperature. Eight pairs of heating strips are bonded to the back side of the isothermal plate. Each pair had a temperature controller to keep all the heating zones at a uniform temperature.

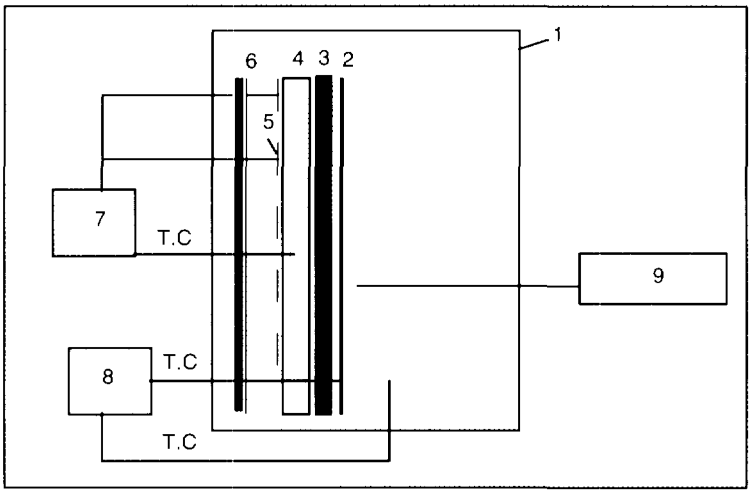

Fig. 3: Schematic diagram of the experimental apparatus: (1) Perspex test chamber, (2) stainless steel plate, (3) insulation layer - h_{eq}, (4) isothermal plate, (5) heaters, (6) backup rock wool insulation, (7) temperature controller, (8) temperature measuring instrument, (9) hot wire anemometer.

The constant temperature of the aluminum plate represents the hot temperature- T_a. A couple of ceramic paper layers, each 3 mm thick with a thermal conductivity of ~0.08 W/m-°C, was inserted between the aluminum and the stainless steel plates. These insulation layers have an effective heat transfer coefficient, h_{eq}, the value of which can be altered by changing the number of the insulating layers.

In order to measure the surface temperature of the stainless steel plate (the exposed surface), 20 chromel alumel thermocouples of ~1 mm diam. were brazed on the surface. The junctions of these thermocouples were placed in the vertical direction along the center line of the plate. In order to measure and control the temperature of the aluminum plate, eight thermocouples were connected to the plate covering the entire controlled heating zone. To reduce heat loss from the rear of the plate, two 50mm layers of rock wool insulation were installed on the back side of the heaters and the isothermal plate. Temperature stratification in the test chamber was measured by the use of K- type thermocouples,(see Fig. 3).

Experiments were carried out in the closed Perspex chamber to avoid any air currents; the chamber and the measuring instruments are shown in Figure 4.

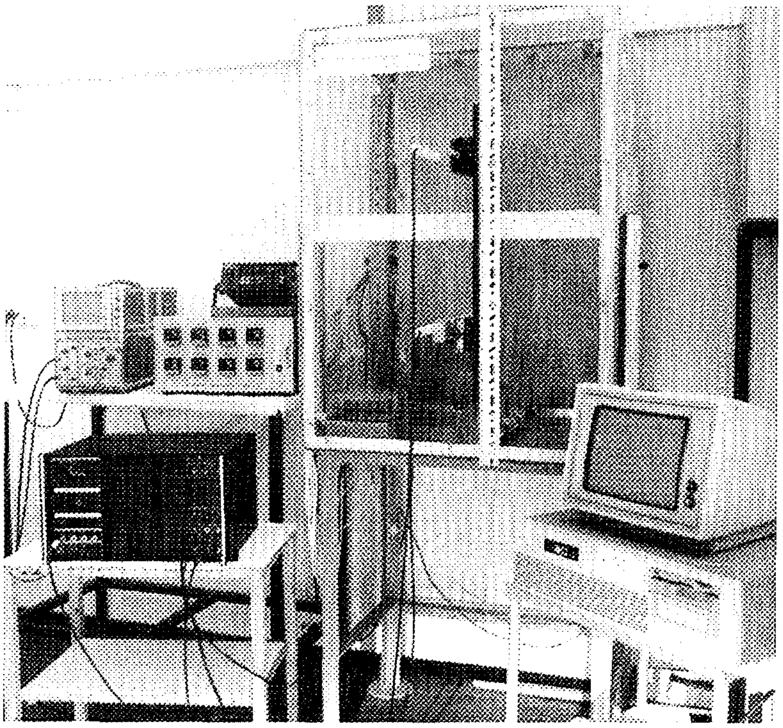

Fig. 4: The test chamber and measuring instruments

The figure shows a plot of the experimental data for the three values of, h_{eq} in which the results are plotted as log Nu vs. log Ra*, where:

$$Ra^* = \frac{h_{eq}}{h(x)+h_{eq}} \cdot \frac{g\beta(T_a - T_\infty)x^3}{\nu^2} \cdot \Pr \qquad (1)$$

Figure 5 covers a range of local Rayleigh numbers between 1.3×10^5 and 2.46×10^8 and the results for various - h_{eq} values are denoted by different symbols.

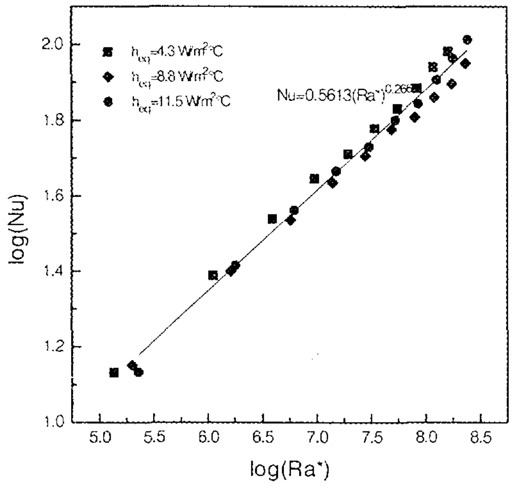

Fig. 5: Free-convection heat-transfer correlation for heat transfer from a heated vertical plate.

The linear least squares fit of log (Nu) or a function of (Ra*) yields the following correlation

$$Nu = 0.5613 \cdot (Ra\,*)^{0.266} \qquad (2)$$

for which the deviation of a single experimental value from the fitted value did not exceed 12%.

3.2 Flow and heat transfer characteristics of the OIMC phenomenon

The research was focused on the OIMC phenomenon, i.e. the flow field structure in a vertical cylinder, closed at the bottom and open at the top, and being heated circumferentially. To achieve a better understanding of the flow field and the related heat-transfer process, two different experimental systems were built. The first was a flow visualization system, with water as the working fluid, whereas the second system enabled quantitative measurements of the temperature field in air. Experiments were performed in the turbulent flow regime. In order to learn about all possible flow regimes, the visualization tests were conducted at three different length-to-diameter ratios

(L/D=1, 5, 10). Quantitative measurements of the cylindrical wall temperature, as well as of the radial and axial temperature profiles in the flow field, were taken in the air system.

The apparatus used, shown schematically in Figure 6, consists of a heated vertical cylinder closed at the bottom and open at the top to the surroundings. The test section was a stainless-steel cylinder, 25cm I.D, x 125cm high x 4mm thick. Along the cylinder's wall, in the vertical direction, 16 2mm-diam. holes were drilled at intervals of 10 and 5cm in the lower and upper halves, respectively;. one type-K thermocouple was soldered at each of these holes. An additional 16 type-K thermocouples were inserted at the same intervals along the centerline. They were attached to a vertically mounted thin rod, 5mm in diameter. Radial temperature distribution was obtained at three different vertical levels by additional moveable thermocouples, attached to a mechanical traversing system. The thermocouples were guided radially, through the wall of the cylinder, by special tubes welded opposite each soldered thermocouple. Temperatures were measured simultaneously at three different levels.

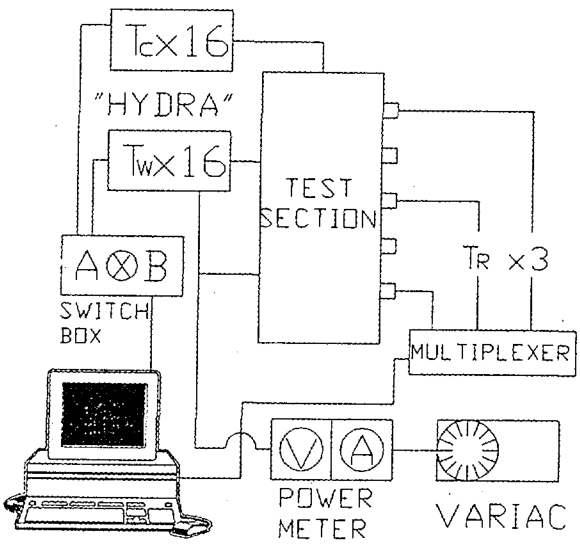

***Fig. 6:** The experimental apparatus for quantitative measurements in air*

Six identical electrical heating blankets were used to create constant heat flux at the wall. They were connected through a power measuring device to a Variac transformer. A 5cm thick blanket of glass wool was used to insulate the test section in the radial direction. The cylindrical test section was based on a 10cm thick plate of wood, sealing the bottom and serving as a thermal insulator.

The wall and centerline thermocouples were connected to two multichannel measuring devices (Hydra, Fluke) and, through a switch box, to the computer. The three radial probes were connected through a multiplexed box to a DAQ card (both National Instrument products) on the same computer. The data were collected simultaneously from the probes by a DAQ software Lab VIEW™. The software enabled us to control the scan rate as well as to average values measured at each point. Calibration experiments to estimate the system's heat loss had been carried out previously.

The net input heat flux (q″) was obtained by subtracting the external heat loss from the gross heat electrical input. The initial procedure for each test involved heating the cylinder until steady-state conditions were established.

Three radial temperature probes were moved simultaneously in the radial direction, starting from the wall and going backward toward the centerline. During the radial temperature measurements, wall and centerline temperature profiles were sampled simultaneously by the computer at fixed time intervals.

In order to study the possible flow regimes, a visualization apparatus (Fig. 7) was built. It consists of a thin glass tube, 40mm I.D. sealed by a rubber plug at the bottom. The open end was connected to the base of a cold reservoir fabricated from Perspex. The cold reservoir, with its glass tube extension, was mounted on top of a hot water reservoir. Steady state was achieved in the hot water reservoir by circulating the water through an electrically heated bath. Three different glass tubes were used to form three length to diameter ratios (L/D=1, 5, 10). To trace the developed patterns of flow, $KMnO_4$ crystals were dropped to the bottom of the tube. The experiments were carried out while heat was transferred between the two reservoirs, through the thin glass tube.

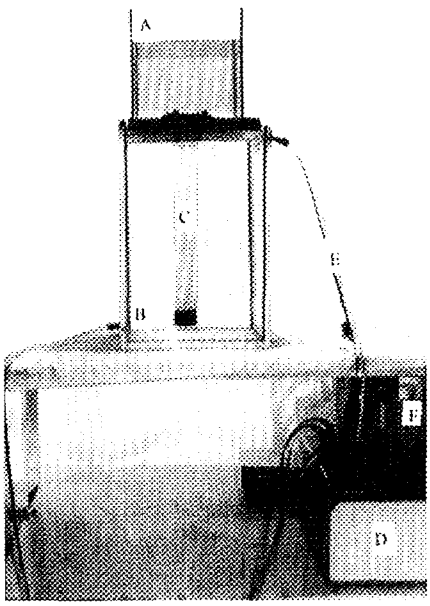

Fig. 7: The flow visualization apparatus

In the cold air system the measured temperature profiles were normalized as:

$$T^* = \frac{T - T_0}{q''d/k} \qquad (3)$$

where T_0 is the temperature measured at the tube entry region and q"d/k is a characteristic temperature difference for the constant heat flux case. This characteristic temperature difference is determined from (a) the net heat flux transferred by convection (q″), (b) the tube diameter, and (c) the air thermal conductivity taken at the entry condition. Two typical radial temperature profiles at two levels along the tube are presented in Figures 8 and 9, respectively, for $Ra_d^*=5\times10^8$. From these temperature profiles it is understood that a radial temperature profile typical to a boundary layer exists at lower levels of the tube, whereas near the entry levels, radial gradients were observed up to the centerline. Wall temperature profiles for three different heat fluxes are presented in Figure10. Referring to the measured wall temperature profile, three different regimes of heat transfer are observed. The wall temperature increases from the bottom of the tube, until a maximum is reached at approximately x/d=1 (zone 1). At this zone a better heat transfer mechanism takes place, and the temperature decreases in a moderate slope (zone 2). The third regime is determined between x/d≅3 and x/d=5 and is characterized by a sharper decrease in wall temperature. Based on numerical simulation results, visualization and the measured temperature profiles, it was found that the OIMC can be characterized by three main regimes.

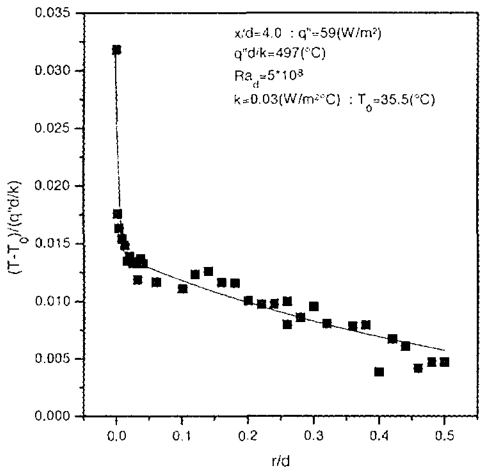

Fig. 8: Radial temperature profile at x/d=4.0

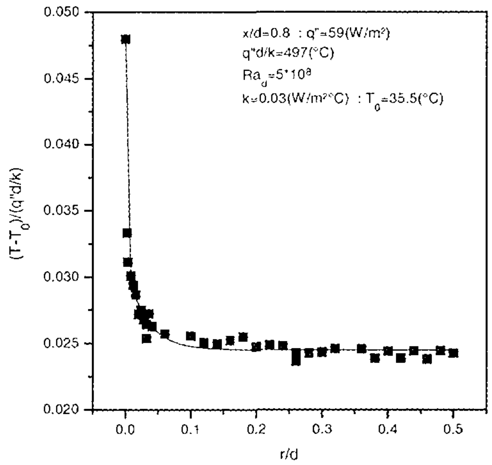

Fig. 9: Radial temperature profile at x/d=0.8

The first regime, at the bottom, constitutes a boundary layer type of flow adjacent to the heated wall. The second regime, above the first, behaves like a direct contact counter flow heat exchanger. This regime is characterized by a similar velocity and temperature profiles at each section of the cylinder. The third is a mixing regime at the entry region of the cylinder.

Under certain conditions the cold fluid from the reservoir did not penetrate into the cylinder's core. Actually, an enhanced mixing heat transfer process takes place at the boundary between the cylinder and the reservoir, forming a "separation interface". The mixing causes the upcoming hot fluid to cool down, and return downward along the centerline of the cylinder, whereas the cold fluid in the reservoir is heated and rises upward at the reservoir centerline. Such behavior of the inlet flow field affects the efficiency of the cylinder as a passive cooling device. These findings are at odds with the basic assumption in the literature that the heated fluid adjacent to the wall is discharged from the open end into the cold reservoir, whereas a central core of cold fluid is continuously replacing the hot fluid, entering at the temperature of the reservoir.

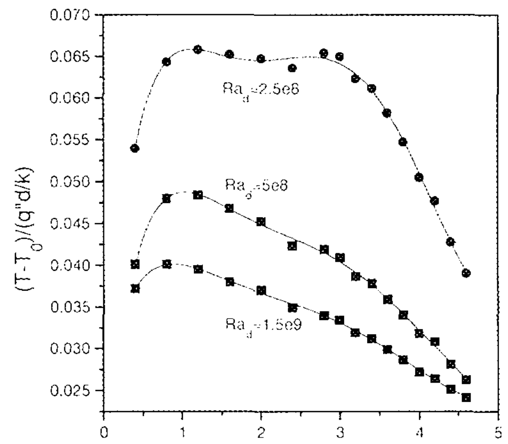

Fig.10: Wall temperature profile at three different heat fluxes.

3.3 *Flow and heat transfer characteristics of an open loop thermosyphon*

An additional subject of interest and R&D activity is the gravity-driven passive safety systems type of the AP600 (Westinghouse advanced pressurized water reactor). An ongoing research is focused on the evaluation of the external dry air (PCCS). Primary theoretical models[18,19] were developed and used to calculate the mass flow rate of the natural circulating air and the resultant heat transfer processes were proposed and evaluated. Based on these calculations, an experimental test was designed. The schematic description of the experimental apparatus assembled is presented in Fig. 11. The test section consists of an inner electrical heated metal pipe (Fig.12a) and an outer metal envelope (Figure 12b), simulating the containment and shield building respectively and creating a typical U-shape annular air flow path. The following parameters will be measured: (a) air inlet and outlet temperatures; (b) axial distribution of air mean velocity and temperature; (c) axial pressure drop; and (d) axial distribution of the temperature on the heated surface.

This planned research for the future is concerned with evaluating experimentally the calculated parametric trends and testing the fully developed flow assumption. The parameters trends are related to two items of interest: (i) Scaling-up the hydraulic diameter of both the hot and the cold channel by increasing the external diameter (D) by an order of magnitude (up to actual reactor containment size) and maintaining a constant hydraulic diameter along the flow path. (ii) Different ratios between the hot and cold channels' diameters ($D_{h1}/D_{h2}\neq1$) and a possible optimal design. Referring to the hydraulic and thermal parameters (assuming fully developed flow in the channels), the mass flowrate and the overall pressure drop indicate maximum and minimum values, respectively, for $D_{h1}/D_{h2}\approx0.5$ (Figs. 13,14), while a minimum value of the maximum temperature is obtained for $D_{h1}/D_{h2}\approx2$ (Fig.15). The behavior of the heat transfer coefficient, taking into account the possibility that the flow is in either the laminar or turbulent regime, is presented in Figure 16.

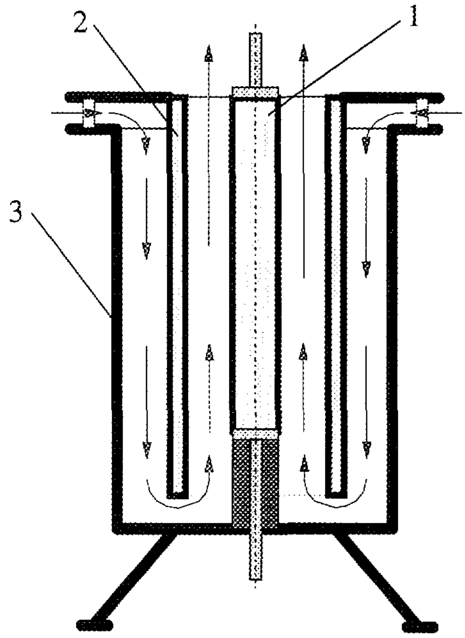

Fig. 11: Schematic description of the test section: (1) electrical heating pipe, (2) shield, (3) envelope

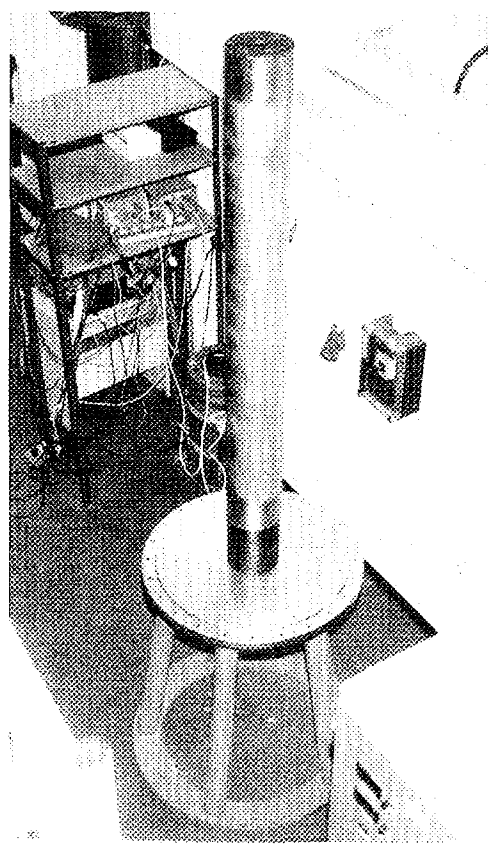

a

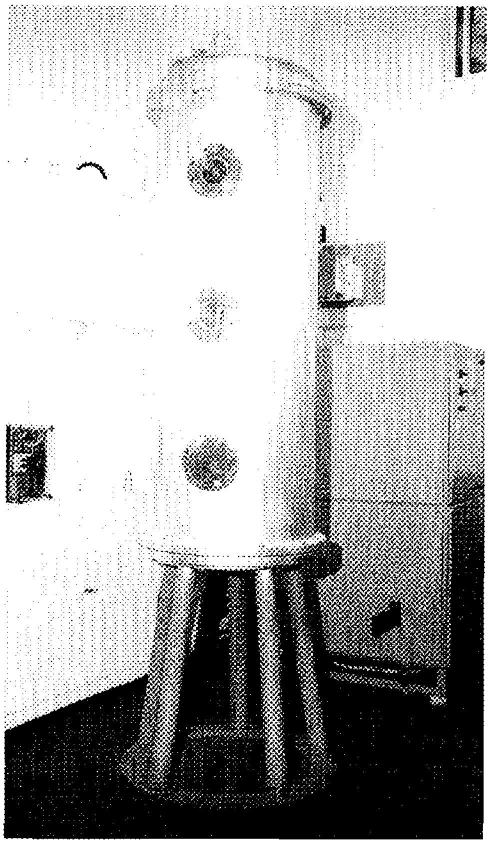

b

Fig.12 a) The electrical heating metal pipe; b) The outer metal envelope simulating the containment and shield building.

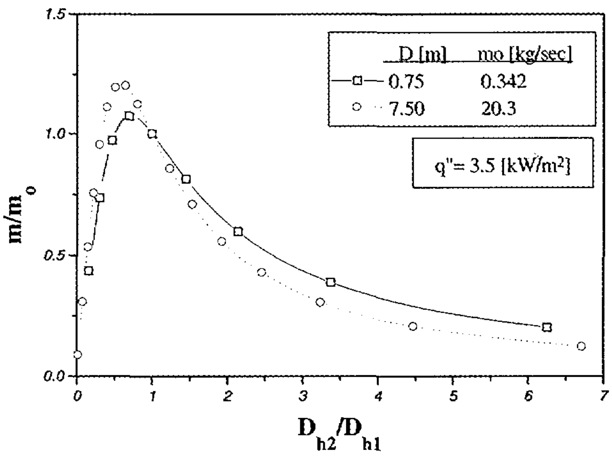

Fig. 13: Coolant mass flowrate vs. hydraulic diameter ratio.

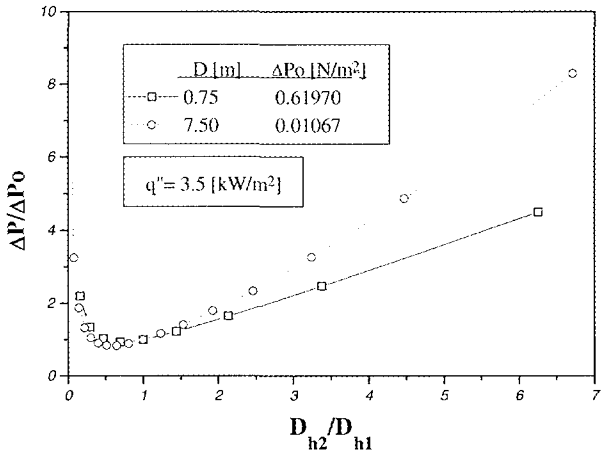

***Fig. 14:** Pressure drop vs. hydraulic diameter ratio.*

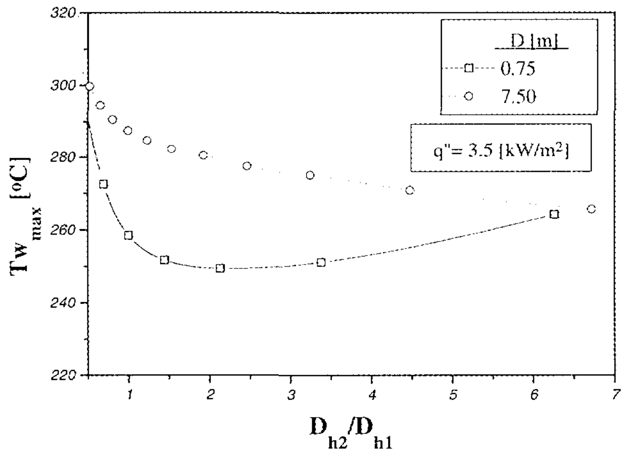

***Fig. 15:** Maximum surface temperature vs. hydraulic diameter ratio.*

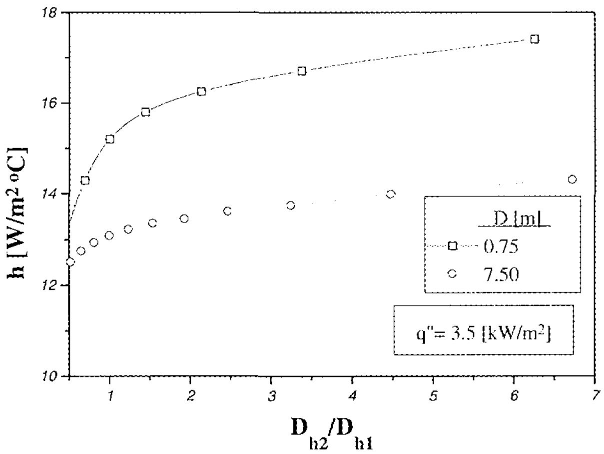

***Fig. 16:** Convective heat transfer coefficient in the hot channel vs. hydraulic diameter ratio.*

4. Nomenclature and subscripts

d - diameter
D - external diameter
g - gravity acceleration
h - convection heat transfer coefficient
L - length
m - mass
Nu_x - Nusselt number (hx/k)
P - pressure
Pr - Prandtl number (ν/α)
k - thermal conductivity
q″ - heat flux
r - radial distance
x - axial distance
Ra_d^* - $g\beta q'' d^4/\nu\alpha\kappa$
T - temperature
α - thermal diffusivity
β - volumetric coefficient of thermal expansion.
ν - kinematic viscosity
a - hot side
eq - equivalent
o - nominal (exp. test conditions)
h1 - hydraulic diameter of hot channel
h2 - hydraulic diameter of cold channel
w - wall condition
∞ - ambient, cold side

5. *References*

1. Y .Weiss, Analysis of Buoyancy-Induced Mixed Convection, Ph.D. Thesis, Ben-Gurion University of the Negev, Beer Sheva, Israel, October 1996.

2. M.J. Lighthill, Theoretical Considerations on Free Convection in Tubes, Q. J. Mech. Appl. Math. 4, 398-439 (1953).

3. L.B. Evans, R.C. Reid, and E.M. Drake, Transient Natural Convection in a Vertical Cylinder, AIChE 14, 251-259 (1968).

4. D. Japikse, and E.R.F. Winter, Single - Phase Transport Processes in the Open Thermosyphon, Int .J. Heat Mass Transfer, 14, 427-441 (1971).

5. S. Ostrach, Natural Convection in Enclosures, ASME, Heat Transfer, 110, 1175-1190, (1988).

6. Y. Weiss, Y. Barnea, and I. Shai, Induced Mixed Convection in a Hot Gas Duct, 25th Israel Conference on Mechanical Engineering, Haifa Israel, pp. 527-529, 1994.

7. Y. Weiss., M. Szanto., I. Shai., and G. Ben-Dor., Characteristics of the Entry Flow Field in an Open Thermosyphon, The 4th Int. Conf. "Heat Transfer 96", Udine, Italy, July, pp. 83-93, 1996.

8. Y. Weiss, C. Lahav, M. Szanto and I. Shai, Heat Transfer Characteristics of Induced Mixed Convection (IMC), 26th Israel Conf. on Mechanical Engineering, Haifa Israel, pp. 300-302, 1994.

9. A. Mertol, and R. Greif, A Review of Natural Circulation Loops, in: Natural Convection Fundamentals and Applications, edited by C. Kakac., W. Aung., and R. Viskanta., Hemisphere Publishing Corporation, Washington, D.C. 1985.

10. Y. Weiss., Y. Aharon, and I. Shai, Natural Convection on a Vertical Flat Plate at General Boundary Condition, 10th Int. Heat Transfer Conf., pp. 16-NC-32, 1994.

11. J. Aharon, C. Lahav, H. Kalman, and I. Shai., An Experimental Investigation of Laminar Free Convection from a Vertical Flat Plate at General Boundary Condition, 26th Israel Conf. on Mechanical Engineering, Haifa, Israel, 1996.

12. J.R. Bodoia, and J.F. Osterle, The Development of Free Convection Between Heated Vertical Plates, Trans. ASME J. Heat Transfer, 10, 40-44 (1962).

13. A. Bar-Cohen, and W.M. Rohsemow, Thermally Optimum Spacing of Vertical, Natural Convection Cooled, Parallel Plates, Trans. ASME, J. Heat Transfer, 106, 116-123 (1984).

14. T. Burch, T. Rhodes, and S. Acharya, Laminar Natural Convection between Finitely Conducting Vertical Plates, Int. J. Heat Mass Transfer, 28, No. 6, 1173-1186, (1985).

15. B.W. Webb, and D.P. Hill, High Rayleigh Number Laminar Natural Convection in an Asymmetrically Heated Vertical Channel, Transfer, 111, 649-656 (1989).

16. L.P. Davis, and J.J. Perona, Development of Free Convection Flow of a Gas in a Heated Vertical Open Tube, Int. J. Heat Mass Transfer, 14, 889-903 (1971).

17. R. Clarksean, Experimental Analysis of Natural Convection within a Thermosyphon, Proc. Experimental Heat Transfer, Fluid Mechanics and Thermodynamics, Honolulu, Hawaii, USA, pp. 17, (1993).

18. Y. Barnea, Y. Weiss, M. Haim, and Y. Aharon, Evaluating the Dry Passive Containment Cooling of the Westinghouse AP-600 Reactor, 25th Israel Conf. on Mechanical Engineering, Haifa, Israel, pp. 518-520, 1994.

19. R. Harari, Y. Weiss, Y. Barnea, Thermohydraulic Modeling of the Dry Air PCCS Process in the Westinghouse AP-600 ALWR. The 25th Israel Conf. on Nuclear Engineering, Herzelia, Israel, pp. 7.2, 1996.

A New Generation of Gamma Cameras Based on Solid State Detectors

Y. Eisen, C. Gilath, G. Cohen, A. Shor, E. Polak, H. Cohen, Z. Baum, E. Izsac

1. Summary

The development of a new generation of gamma cameras, utilizing advanced CdTe and CdZnTe solid state detectors and offering several advantages over the present conventional cameras which employ NaI(Tl) scintillators, is described.

Nuclear Medicine is a medical imaging modality which demonstrates the organ function. It is based on administering radioisotope-labelled compounds (radio-pharmaceuticals) to the patient and then mapping distributionin space (and occasionally also in time) with gamma cameras.

The technology of present gamma cameras is based on a scheme developed by Anger some 30 years ago. The main components of a conventional gamma camera are illustrated in Figure 1. The radiation emanating from the patient is transmitted through a collimator and detected by a large NaI(Tl) scintillation crystal, which converts the incident radiation into light scintillations which are detected by a two-dimensional array of photomultipliers tubes (PMTs). The location of a scintillation in the crystal is determined by the relative signals in the adjacent PMTs. Thus an image of the radiation is obtained.

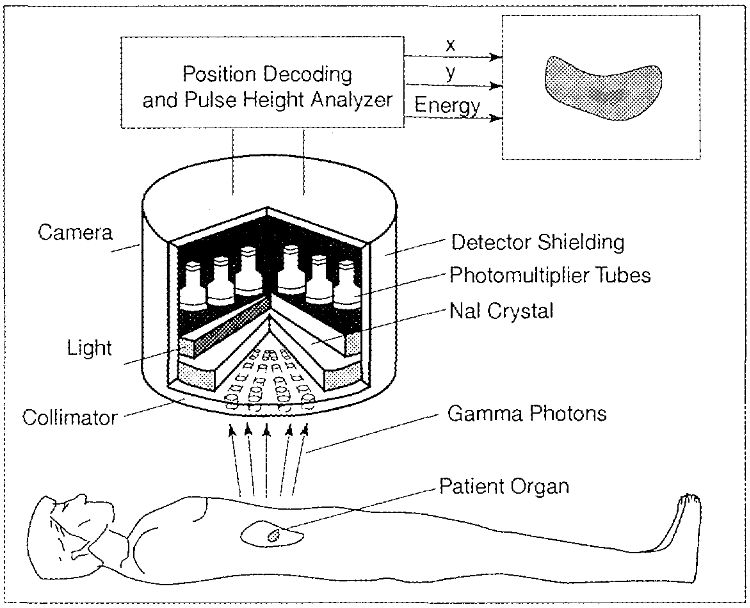

Fig. 1: Main components of a conventional gamma camera

Over the past three decades there has been a steady improvement in the original Anger camera. Image resolution and uniformity have increased and the advent of digital electronics has enabled better image correction and manipulation. However, the technology has reached a level of maturity where any real improvement can be achieved only from a radical change, as done with solid state detectors.

Scintillation type (Anger) cameras have some inherent shortcomings:

- The energy of the incident gamma radiation photon absorbed in the scintillator is transformed to light with relatively low efficiency. This implies a relatively poor energy resolution, which prevents efficient scatter rejection and thus causes deterioration in the contrast resolution. Typical energy resolution in NaI(Tl) scintillators, at the most commonly used energy in nuclear medicine, 140 Kev, is approximately 10% FWHM (full width at half maximum). It has taken present technology 30 years to get from 12% to 10%.

- Current intrinsic spatial resolution is limited by the scintillator thickness, the incident photon energy and the size and packaging ratio of the PMTs.
- Anger cameras present some image distortions (pincushion and barrel) inherent to the use of PMTs.
- At high count rates (above 100,000 counts/sec) Anger cameras suffer from pile-up distortions.

  The need for shielding both the scintillating crystal and the PMTs, which occupy a relatively large volume, results in a large, heavy and cumbersome gamma camera head. Mobile Anger gamma cameras are heavy and not practical; portable cameras are not feasible. Positioning of the camera head becomes difficult or even impossible under certain circumstances. Also tomographic gamma cameras (SPECT-single photon emission computed tomography) in which the head rotates around the patient, demand large and heavy gantries.

2. *THE NEW GAMMA CAMERA TECHNOLOGY AND ACHIEVEMENTS*

When X-rays or gamma photons impinge on room temperature spectroscopy grade detectors, electron - hole pairs are generated. These result in an electrical pulse carrying information on the energy of the incoming radiation. Thus, the conversion from radiation into an electrical pulse takes place in the detector itself. Solid state detectors perform the combined function of the scintillator and the PMTs in an Anger camera. CdTe and CdZnTe are more advanced solid state detectors that can be used in the new generation gamma cameras.

The use of solid state detectors in gamma cameras offers several advantages over currently used Anger scintillation cameras:

- Better (5% or even less) energy resolution, with resulting superior scatter rejection and better contrast resolution in the resulting image. The lower the energy resolution, the better the image quality. This attribute becomes important with large-size patients (who already provide increased radiation absorption between the organ of interest and the camera head) and many newer nuclear medicine procedures in which the target organ to background ratio is relatively low (e.g. scintimammography and the use of labelled monoclonal antibodies or peptides for imaging of malignant lesions). Improved contrast resolution leads to improved detectability of lesions.

- Better intrinsic spatial resolution can be achieved. Spatial resolution is dependent neither on the detector thickness nor on the incident photon energy, but only on the detector element area size. This attribute manifests itself in improved image quality and better spatial resolution and therefore contributes to improved detectability.
- The use of solid state detectors removes the need for the photon interaction position decoding (as necessary in Anger cameras). The position of the interaction is defined by the detector element in which the interaction takes place. Perfectly linear and homogeneous images are obtained, without any geometric distortions (barrel and cushion).
- Solid state detectors are-count-rate tolerant and for all practical purposes no pile-up distortions are observed.
- Much lighter camera heads become feasible. The heads are very thin compared with conventional ones, since no long PMTs are used.
- Mobile and portable gamma camera systems become practicable. They enable bringing the imaging to the patient rather than transporting a critically ill patient to the camera and taking unacceptable risks. Furthermore, patients can be diagnosed at any location in the hospital, office or even their home.
- Planar and tomographic (SPECT) cameras can be built with much simpler mechanics than conventional cameras. This leads to cost reduction and a decrease in the system footprint, a practical aspect that should not be ignored.
- The area of the camera head face is nearly equal to the useful field of view. This enables imaging of locations

on the body at much closer proximity than with an Anger camera head, a feature very important in breast, thyroid, parathyroid and other imaging protocols.

- The thermal stabilization of the camera head is very rapid. (Present Anger cameras are kept constantly under power and heavy battery backups are used when attempting mobile configurations).
- Current technology still relies on vacuum tubes. Replacing the PMTs with solid state devices improves system stability and reliability.

Soreq NRC has amassed 15 years of experience with room temperature solid state CdTe and lately also with CdZnTe detectors. Various detectors were designed and characterized, and applications were developed for security inspections of cargo and passenger luggage. One of these applications culminates in the Aisys 370 automatic luggage inspection and bomb detection system (protected by several patents), the manufacture of which was licensed to Magal Security Systems Ltd. From the early 1990s various medical applications of these detectors were considered and explored. It was decided to focus on the development of gamma cameras. The practical and business values of this application were recognized by the Chief Scientist of the Israel Ministry of Trade and Industry, who provided partial financial support for this development effort.

At a later stage, the United States Israel - Science and Technology Commission undertook to fund the development of a new generation of gamma cameras based on solid state detectors. A collaboration among Isorad Ltd. (the commercial arm of Soreq NRC), General Electric Medical Systems and eV Products, Inc. (a developer and manufacturer of solid state detectors) was set up. The objective of this project is to develop, engineer, manufacture and market the new gamma cameras in a cost effective way. CdZnTe detectors were chosen for this development.

Two camera prototypes were developed. One of them, in a mobile planar configuration with a head having a field of view of 16 cm x 16 cm, is shown in Figure 2. Figure 3 illustrates the prototype camera ready for use in a hospital emergency room. Soreq NRC's efforts were concentrated on the development of the new head, which is central to the performance of the camera and represents the most innovative part of the system. In addition, emphasis was placed on the development of the necessary acquisition, processing and display software. Soreq's developments are protected by several patents.

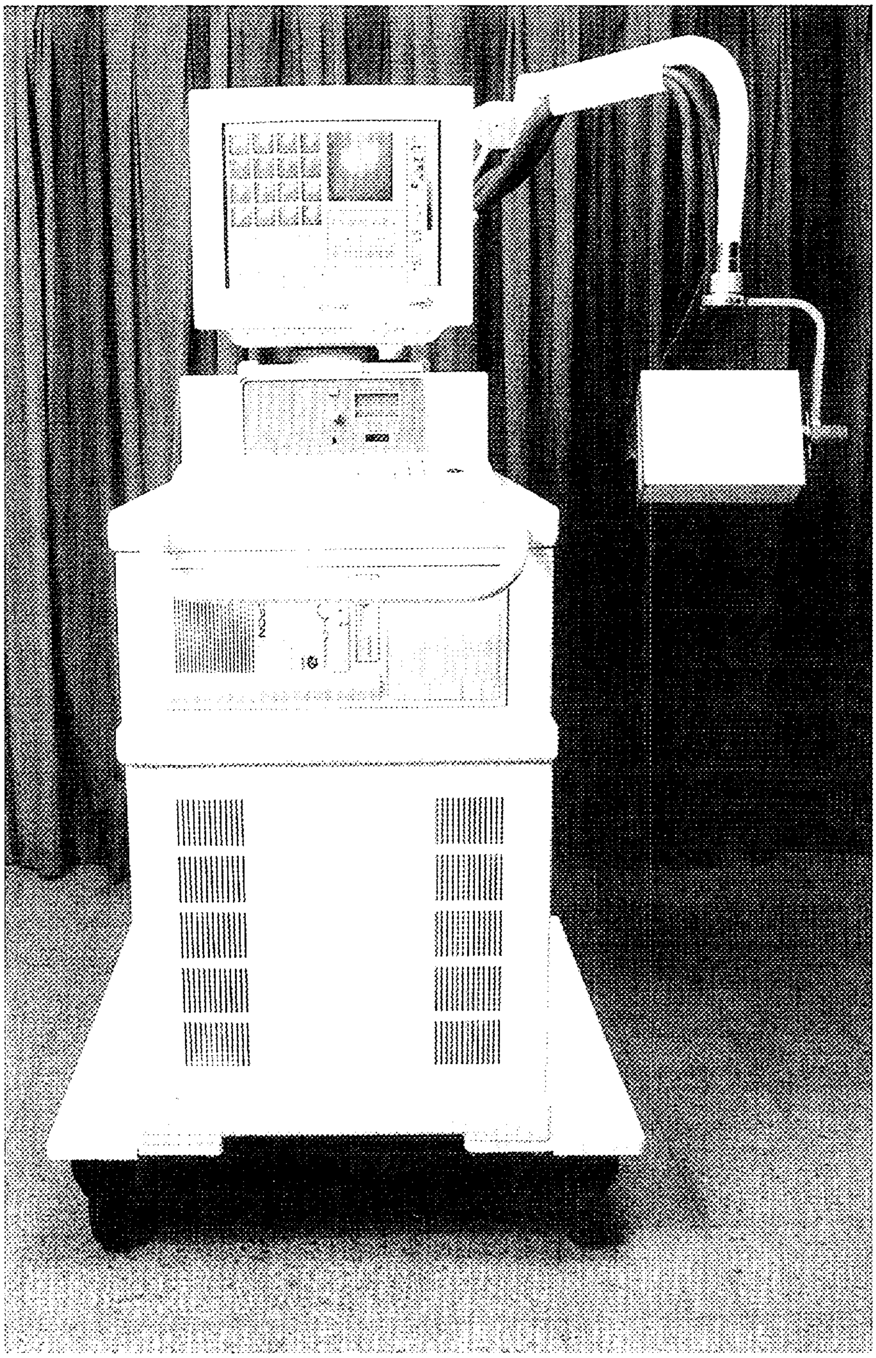

Fig. 2: The prototype for a new generation gamma camera based on solid state detectors.

Fig. 3: The prototype camera in the emergency room of a major US hospital.

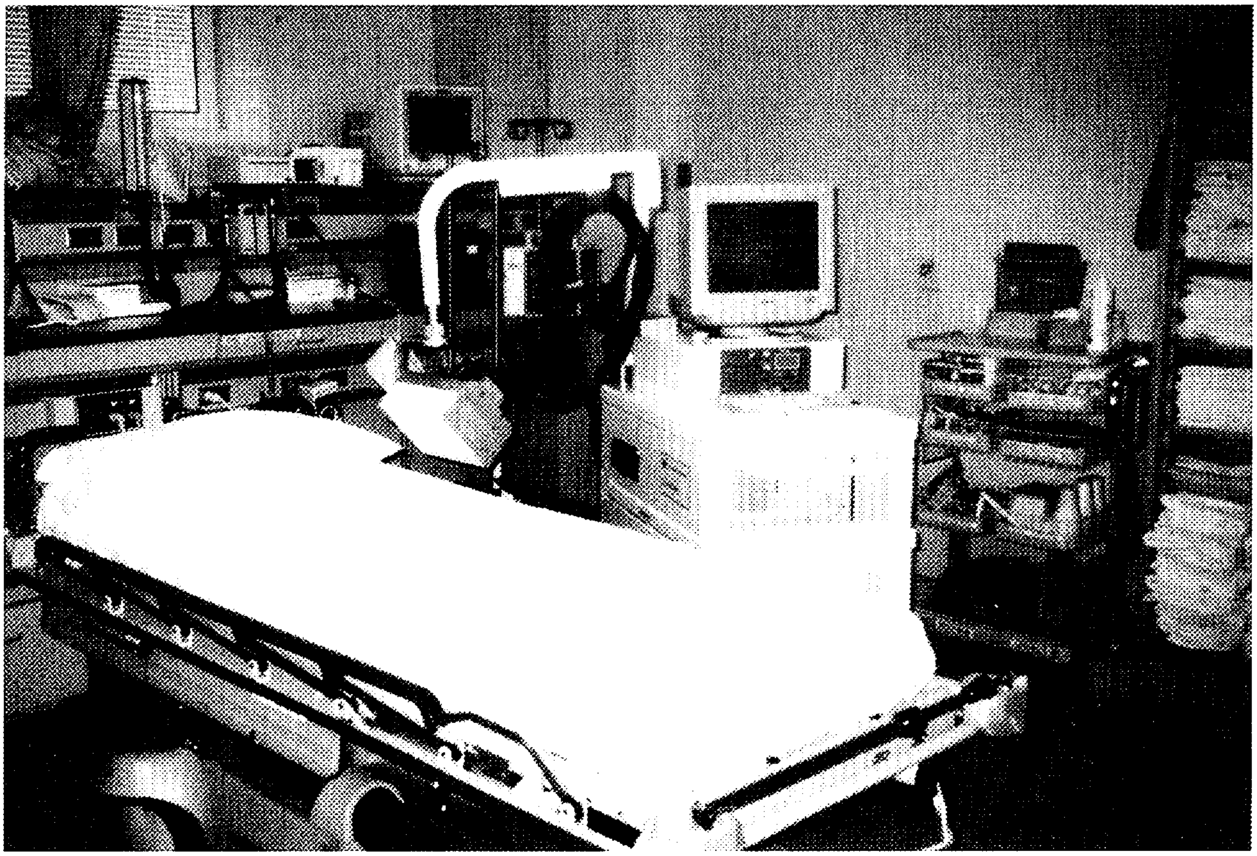

The prototype was evaluated in various clinical environments, first in Israel and then in the USA and Canada. Some typical images obtained with this prototype are shown here. Common nuclear cardiology procedures, such as MUGA (multiple gated angiography) which implies ECG gating (see Fig. 4) and myocardial perfusion imaging (see Fig. 5), were performed. Various other nuclear medicine procedures, such as thyroid (see Fig. 6), parathyroid, breast, and kidney imaging, etc., were also performed.

The diagnostic capability of the prototype camera was found to be similar or superior to that of conventional cameras. The mobility of the camera and the ease of positioning its head on the patient were greatly appreciated by both physicians and technical personnel. The potential of solid state-detector-sbased gamma cameras was proven.

Work on the United States-Israel Science and Technology Commission project continues towards the achievement of its technological and commercial objectives.

Fig. 4: Results of a MUGA (multiple gated angiography) procedure performed with the prototype camera and compared with a conventional camera.

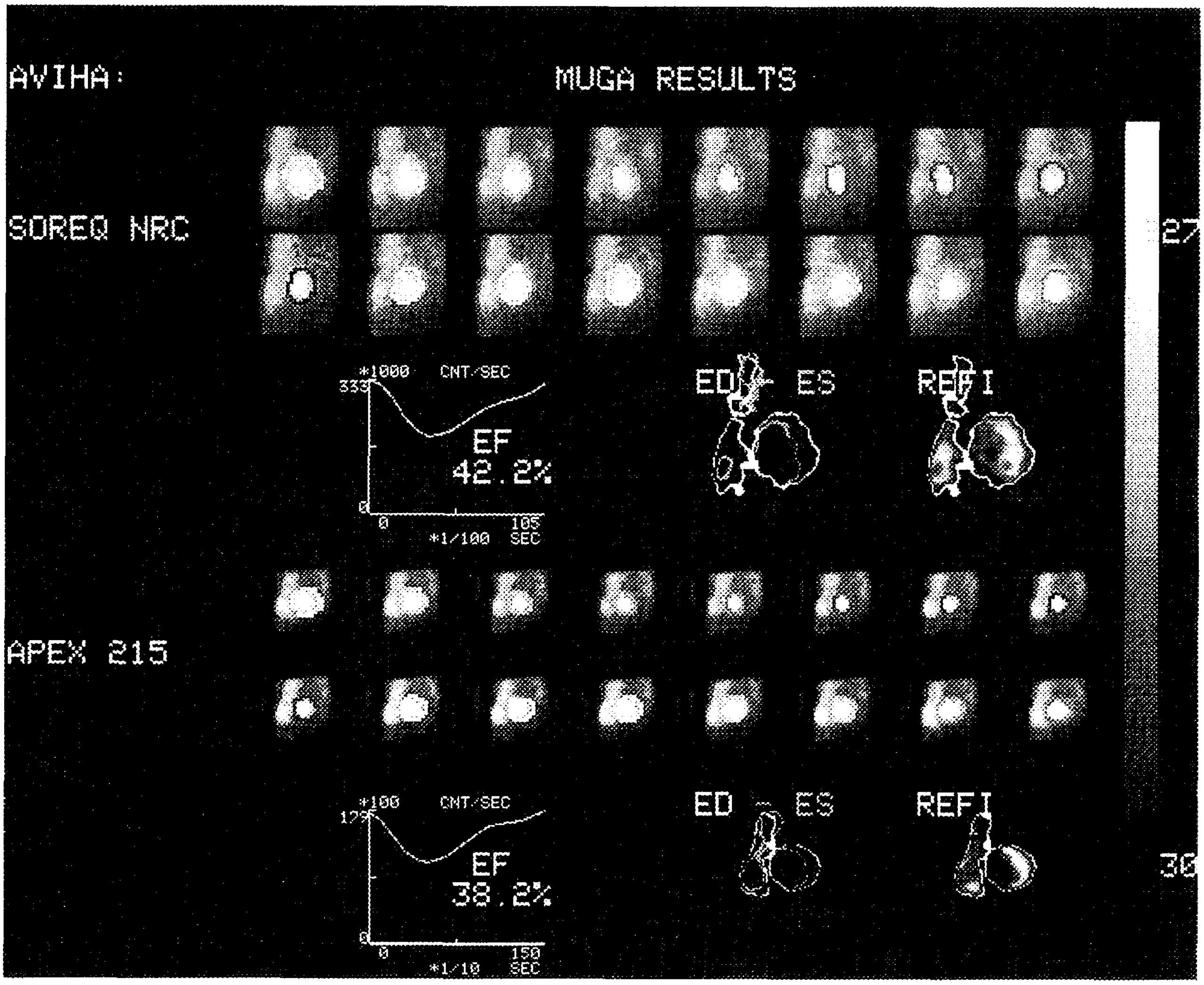

Fig. 5: Results of a myocardial perfusion procedure performed with the prototype camera.

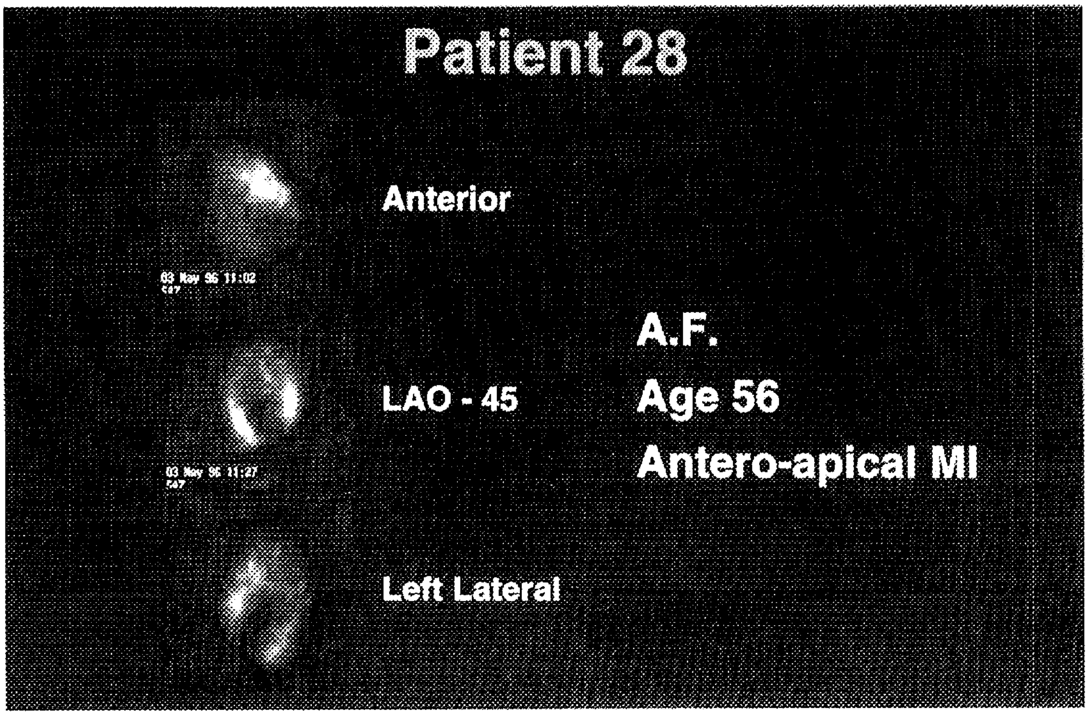

Fig. 6: Results of thyroid imaging performed with the prototype camera.

Bibliography

AHARON J., LAHAV Y., SHAI I. and KALMAN, H.
An experimental investigation of laminar free convection from a vertical flat plate at general boundary conditions.
In: 26th Israel Conference on Mechanical Engineering, (Haifa, Israel, May 1996,) Proceedings, p. 319-321 (1996).

AHARON J., LAHAV Y., KALMAN H. and SHAI, I.
Coupling conduction with laminar free convection vertical flat plate - an experimental study.
In: 19th Conference of the Israel Nuclear Societies (Herzlia, Israel 9-10 Dec., 1996) Proceedings, 7.5 p. 1-4 (1996).

ALADJEM, A.
Zirconium-hydrogen.
Diffus. Defect Data, Part B, 49-50, 281-329 (1996).

AKKERMAN, A., BOUTBOUL, T., BRESKIN, A., CHECKIK., R., GIBREKHTERMAN, A. and LIFSHITZ, Y.
Inelastic electron interactions in the energy range 50 eV to 10 keV in insulators : Alkali halides and metal oxides.
Physica Status Solidi B, 198, 769-784 (1996).

AKKERMAN, A., BARAK, J., LEVINSON, J. and LIFSHITZ, Y.
Modeling of proton induced SEUs.
Radiat. Phys. Chem. 48, 11-22 (1996).

ALIMI, R., GOLDENBERG, C. and ONN, U.
The effect of boost injection on the performances of the SPETC gun.
In: 16th International Symposium on Ballistics (San Francisco, CA, USA, Sept. 1996) Proceedings, Vol. 1, p. 353-362 (1996).

ALIMI, R., PERELMUTTER, L. and ONN, U.
Modeling an internal injection process for the SPETC gun.
In: 16th International Symposium on Ballistics (San Francisco, CA, USA, Sept., 1996) Proceedings, Vol. 1, p. 409-418 (1996).

AMIT, M.
Measurement of "hot spots" in copper vapour lasers.
In: Pulsed Metal Vapour Lasers. NATO Advanced Research Workshop on Pulsed Metal Vapour Lasers - Physics and Emerging Applications in Industry, Medicine and Science (St. Andrews, UK, 6-10 Aug., 1995) Proceedings, p.195-9 (1996).

ARAD, B., ELIEZER, S., GILATH, I., MOSHE, E. and SIMON, C.G.
Laser simulation of hypervelocity impacts in space.
In: 3rd International Conference Dynamics and Control of Structures in Space (London, UK, 27-31 May, 1996) Proceedings, p. 431-440 (1996).

ARKUSH, R., VENKERT, A., AIZENSHTEIN, M., ZALKIND, S., MORENO, D., BRILL, M., MINTZ, M.H. and SHAMIR, N.
Site related nucleation and growth of hydrides on uranium surfaces.
J. Alloys Compd. 244, 197-205 (1996).

ASHKENAZY, J., RAITSES, Y., APPELBAUM, G. and GUELMAN, M.
Study and diagnostics of the effect of length variation in Hall thrusters.
In: IEPC '95 - 24th International Electric Power Conference, (Moscow, Russia, 19-23 Sept., 1995) Proceedings, Vol. 1, p. 238-245 (1996).

BAER, A., ELIEZER, S., HENIS, Z. and SCHWOB, J.L.
X-ray laser scheme driven by two laser pulses.
Laser Part. Beams 14 (4), 625-630 (1996).

BAER, A., SCHWOB, J.L., ZIGLER, A., ELIEZER S. and HENIS, Z.
High-gain Ni-like x-ray laser driven by two laser pulses.
Kvantovaya Elektron. 23, 393-398 (1996).

BAER, R. , CHARUTZ, D.M., KOSLOFF, R. and BAER, M.
A study of conical intersection effects on scattering processes: The validity of adiabatic single-surface approximations within a Quasi-Jahn-Teller model.
J. Chem. Phys., 105, 9141-9152 (1996).

BAER, R., ZEIRI, Y. and KOSLOFF, R.
Influence of dimensionality on deep tunneling rates: A study based on the hydrogen-nickel system.
Phys. Rev. B, Condens. Matter 54, R5287-R5290 (1996).

BAHIR, G. , ARIEL, V. , GARBER, V. , ROSENFELD, D. and SHER, A.
Response to "Comment on electrical properties of epitaxially grown CdTe passivation for long-wavelength HgCdTe photodiodes"
Appl. Phys. Lett., 68, 2453-2455 (1996).

BAR-NOY, T., HARELL, A. and KAGANOVICH, A.
Use of computer simulations in physics teaching.
In: 2nd International Conference Teacher Education: Stability, Evolution and Revolution (Israel, Jul., 1996) Proceedings, p. 57 (1996).

BAR-NOY, T.
Use of computer simulations in physics teaching in Israel.
In: American Association of Physics Teachers Summer Meeting (College Park, MD, USA, 5-10 Aug., 1996) Proceedings, p. 106 (1996).

BAR-SHALOM, A., KLAPISCH, M. and OREG, J.
Phase-amplitude algorithms for atomic continuum orbitals and radial integrals.
Comput. Phys. Commun. 93, 21-32 (1996).

BARAK, J., LEVINSON, J., VICTORIA, M. and HAJDAS, W.
Direct processes in the energy deposition of protons in silicon.
In: IEEE Nuclear and Space Radiation Effects Conference (Indian Wells, CA, USA, 15-19 July, 1996) Proceedings.
IEEE Trans. Nucl. Sci. 43, 2820-6 (1996).

BARAK, J., LEVINSON, J., AKKERMAN, A., LIFSHITZ, Y. and VICTORIA, M.
A simple model for calculating proton induced SEU.
In: RADECS 95. 3rd European Conference on Radiation and its Effects on Components and Systems (Arcachon, France, 18-22 Sept. 1995) Proceedings, p.431-436 (1996).

BARAK, J., LEVINSON, J., AKKERMAN, A., HASS, M., VICTORIA, M., ZENTNER, A., DAVID, D., EVEN, O. and LIFSHITZ, Y.
A new approach to the analysis of SEU and SEL data to obtain the sensitive volume thickness [ICs].
In: RADECS 95. 3rd European Conference on Radiation and its Effects on Components and Systems (Arcachon, France, 18-22 Sept. 1995) Proceedings, p.321-325 (1996).

BARAM, A.
The universal repulsive-core singularity - a temperature-dependent exam pie.
J. Chem. Phys.105, 2129 (1996).

BEHAR, E., MANDELBAUM, P., SCHWOB, J. L., BAR-SHALOM, A., OREG, J. and GOLDSTEIN, W.H.
Dielectronic recombination rate coefficients for highly ionized Ni-like atoms.
Phys. Rev. A, 54, 3070-3077 (1996).

BELAISH, I., LEVINSON, S., GERMAN, U., PELLED, O., LAICHTER, Y., WANGROVITZ, U., TIROSH, D. and BARAK, D.
ASIA a radioactive in air monitoring system.
In: 19th Conference of the Israel Nuclear Societies (Herzlia, Israel, 9-10 Dec., 1996) Proceedings, 8.3 p.1-4(1996).

BELAISH, I., LEVINSON, S., GERMAN, U., PELLED, O., LAICHTER, Y., WANGROVITZ, U., TIROSH, D. and BARAK, D.
R.I.S. - 125 125I air monitor system.
In: 19th Conference of the Israel Nuclear Societies (Herzlia, Israel, 9-10 Dec., 1996) Proceedings, 8.1 p. 1-4 (1996).

BEMIS, R.A., SHILOH, K. and ELLINGSON, W.A.
Nondestructive evaluation of thermally shocked silicon-carbide by impact acoustic-resonance.
Trans. ASME, J. Eng. Gas Turbines Power 118 (N), 491-494 (1996).

BEN-SHACHAR, B., WEINSTEIN, M. and GHERMAN, U.
The minimum measurable dose (MMD) of CaF2:Dy measured via glow curve deconvolution with the automatic 6600 thermoluminescent detector.
In: 19th Conference of the Israel Nuclear Societies (Herzlia, Israel, 9-10 Dec., 1996) Proceedings, 10.5 p. 1-4 (1996).

BEN-SHACHAR, B., WEINSTEIN, M. and GHERMAN, U.
Some dosimetric properties of the Lif:Mg,Ti evaluated by the automatic 6600 thermoluminescent reader.
In: 19th Conference of the Israel Nuclear Societies (Herzlia, Israel, 9-10 Dec., 1996) Proceedings, 8.2 p.1-3 (1996).

BEN SHLOMO, A., SCHLESINGER, T. and KUSHILEVSKY, A.
Radiation dose to the patient in several diagnostic x-ray examinations performed with conventional radiography equipment in three major medical centers in Israel; a comparative study.
In: 19th Conference of the Israel Nuclear Societies (Herzlia, Israel, 9-10 Dec., 1996) Proceedings, 4.1 p. 1-4(1996).

BIDERMAN, S., HOROWITZ, A., EINAV, Y., BEN-AMAR, G., GAZIT, D. and KIMMEL, G.
Production of oriented sapphire components.
In: 1996 Annual Conference of the Israeli Association for Crystal Growth (Jerusalem, Israel, 3 Dec., 1996) Proceedings, p. 13 (1996).

BLAU, P.
Impedance matching and electric field penetration in metal vapour lasers
In: Pulsed Metal Vapour Lasers. NATO Advanced Research Workshop on Pulsed Metal Vapour Lasers - Physics and Emerging Applications in Industry, Medicine and Science (St. Andrews, UK, 6-10 Aug., 1995) Proceedings, p. 215-220 (1996).

BLOCH, J. and MINTZ, M. H.
The hydriding kinetics of beta-quenched uranium-0.1wt.% chromium.
J. Alloys Compd. 241, 224-231 (1996).

BOUTBOUL, T., AKKERMAN, A., BRESKIN, A. and CHECHIK, R.
Electron inelastic mean free-path and stopping power modeling in alkali-halides in the 50ev-10kev energy-range.
J. Appl. Phys. 79, 6714-6721 (1996).

BRANDON, S., GAZIT, D. and HOROWITZ, A.
Interface shapes and thermal fields during the gradient solidification method growth of sapphire single crystals.
J. Cryst. Growth 167, 190-207 (1996).

BREZENITSKY, M., MOREH, R., DAYAN, D. and KIMMEL, G.
The use of STM as a novel characterization tool for metallic alloys.
In: 1st Conference of the Israel Materials Union (Natania, Israel, 29-30 Apr., 1996), Proceedings, p. 3.12 (1996).

BROWN, D., OLSHER, R.H., EISEN, Y. and RODRIGUEZ, J.F.
A real-time pulsed photon dosimeter.
Nucl. Instrum. Methods Phys. Res. A, 373, 139-147 (1996).

BURSHTEIN, Z., SHIMONY., Y., LEVY, I., LEJUS, A.M., BENITEZ, J.M. and MOUGEL, F.
Refractive-index studies in $Ca_2 Ga_2 SiO_7$ and $SrLaGa_3O_7$ melilite-type compounds.
J. Opt. Soc. Am. B, 13, 1941-1944 (1996).

CELLIERS, P., DA SILVA, L.B., HEREDIA, N.J., MAMMINI, B.M., LONDON, R.A. and STRAUSS, M.
Dynamics of laser-induced transients produced by nanosecond duration pulses : Diagnostic and therapeutic cardiovascular intervention VI.
In: Lasers in surgery : advanced characterization, therapeutics and systems VI (San Jose CA, 27-30 Jan., 1996) Proceedings, SPIE 2671, 22-27 (1996).

COHEN, M., EICHENBAUM, A., KLEINMAN, H., CHAIRMAN, D. and GOVER, A.
Single-mode selection and axial mode control in a free-electron maser oscillator using a prebunched electron beam.
Phys. Rev. E, 54, 4178-4187 (1996).

COLOJOARA, C., GABAY, S., VAN DER MEULEN, F.W. and VAN GEMERT, M.J.
Influence of Peak Power in ablation rate of dental hard tissues : mathematical model.
In: Laser applications in medicine and dentistry (Vienna, Austria, 7-10 Sept.1996) Proceedings, SPIE 2922, 243-254 (1996).

DANON, Y., MOORE, M.S., KOEHLER, P.E., LITTLETON, P.E., MILLER, G.G., OTT, M.A., ROWTON, L.J., TAYLOR, W.A., WILHELMY, J.B., YATES, M.A., CARLSON, A.D., HILL, N.W., HARPER, R. and HILKO, R.
Fission cross-section measurements of the odd-odd isotopes ^{232}Pa, ^{238}Np, and ^{236}Np.
Nucl. Sci. Eng. 124, 482-491 (1996).

DAYAN, D. and KIMMEL, G.
Transformations and microstructures in the U-Ta system.
J. Alloys Compd. 243, 161-166 (1996).

DAYAN, U. and KOCH, J.
Ozone concentration profiles in the Los Angeles Basin-a possible similarity in the build-up mechanism of inland surface ozone in Israel.
J. Appl. Meteorol. 35, 1085-1090 (1996).

DUKHAN, A., ZHANG, X.X., KANTROVITCH, I. I. and BAR-ZIV, E.
Evolution of thermal conductivity of char particles burning in regime I up to complete conversion.
In: 26th International Symposium on Combustion (Napoli, Italy, 28 Jul., 1996) Proceedings, (1996).

EISEN, Y., SHOR, A., GILATH, C., TSABARIM, M., CHOURAQUI, P., HELLMAN, C. and LUBIN, N.E.
A gamma camera based on CdTe detectors.
In: Room Temperature Semiconductor X- and -Ray Detectors, Associated Electronics and Applications. 9th International Workshop (Grenoble, France, 18-22 Sept., 1995) Proceedings.
Nucl. Instrum. Methods Phys. Res. A, 380, 474-478 (1996).

EISEN, Y.
Current state-of-the-art industrial and research applications using room-temperature CdTe and CdZnTe solid state detectors.
In: Room Temperature Semiconductor X- and -Ray Detectors, Associated Electronics and Applications. 9th International Workshop (Grenoble, France, 18-22 Sept., 1995) Proceedings.
Nucl. Instrum. Methods Phys. Res. A, 80, 431-439 (1996).

EISENBERG, E., CHARUTZ, D.M., RON, S. and BAER, M.
Toeplitz matrices within discrete variable representation formulation: Application to collinear reactive scattering problems.
J. Chem. Phys., 104, 1886-1892 (1996).

ELIEZER, S.
Guest editor's preface: Laser and particle induced shock waves - a perspective.
Laser Part. Beams 14, 109-11 (1996).

ENGLANDER, A., LAVI, R. and LALLOUZ, R.
Efficient tunable intra-cavity OPO in the mid-IR.
In: Trends in Optics and Photonics on Advanced Solid State Lasers (Memphis, TN, USA, Feb. 1996) Proceedings, p. 155-157 (1996).

ENGLMAN, R.
Maximum entropy principles in fragmentation data analysis
In: High-Pressure Shock Compression of Solids II - Dynamic fracture and fragmentation .
(Springer-Verlag, New York, 1996), p. 264-281.

FABER, K., LORBER, A. and KOWALSKI, B.R.
Extension of analytical figures of merit to multilinear data.
In: International Conference on Chemometric an Analytical Chemistry (CAC 96') (Spain, 25-29 Jun. 1996) Proceedings, p. 86 (1996).

FARAGGI, M., FERRADINI, C. and JAY-GERIN, J.P.
Radiolyse de l'ADN : reactions primaires d'oxydo-reduction.
J. Chimie Phys. 93, 78-92 (1996).

FRAENKEL, M., ZIGLER, A., HOROWITZ, Y., LUDMIRSKY, A., MAMAN, S., MOSHE, E., HENIS, Z. and ELIEZER, S.
Optimal x-ray source development in the spectral range 4-14 Å using a Nd:YAG high power laser.
J. Appl. Phys., 80, 5598-5603 (1996).

FREUD, A.
Implementation of GMP requirements in the radiopharmaceutical industry.
In: 11th International Conference of the Israel Society for Quality (Jerusalem, Israel, 19-21 Nov., 1996) Proceedings, p. 279 (1996).

GABAY, Y., HERER, Y. and KORENFELD, C.
Starting and motivating a committee for improving quality and productivity.
In: 11th International Conference of the Israel Society for Quality ((Jerusalem, Israel, 19-21 Nov., 1996) Proceedings, p. 21-22 (1996).

GABAY, Y., HERER, Y., KORENFELD, C. and BOT, Y.
Failure mode analysis as a driver to safety analysis.
In: 11th International Conference of the Israel Society for Quality (Jerusalem, Israel, 19-21 Nov., 1996) Proceedings, p. 405 (1996).

GENKIN, L., BAER, M. and FALCOVITZ, J.
MOC computation of intermediate-altitude rocket plumes with shock waves.
In: AIAA, 31st Thermophysics Conference (New Orleans, LA, USA, 17-20 June, 1996) Proceedings. AIAA Paper 96-1883 (1996).

GENKIN, L., BAER, M. and FALCOVITZ, J.
Method of characteristics scheme for underexpanded plumes.
In: 36th Israel Annual Conference on Aerospace Sciences (Tel Aviv and Haifa, Israel, 21-22 Feb., 1996) Proceedings, p. 113-119 (1996).

GILATH, I.
Laser-induced spallation and dynamic fracture at ultra high strain rate.
In: High-Pressure Shock Compression of Solids II - Dynamic fracture and fragmentation, New York, Springer-Verlag, p. 90-120 (1996).

GOLDSTEIN, M.
The adjoint Monte Carlo - a viable option for efficient radiotherapy treatment planning.
In: 19th Conference of the Israel Nuclear Societies (Herzlia, Israel, 9-10 Dec., 1996) Proceedings, 11.2 p. 1-4 (1996).

GREEN, A.K., DARVISH, S. and SHAFIR, E.
Practical termination for optical fibers embedded in composites.
In: 3rd International Conference on Smart Structures and Materials (Lyon, France, 3-5 June, 1996) Proceedings, p. 209-212 (1996).

GROF, Y., SCHLESINGER, T. and EVEN, O.
Occupational radiation risks in conveyance of bulk phosphate and potash.
In: 19th Conference of the Israel Nuclear Societies (Herzlia, Israel, 9-10 Dec., 1996) Proceedings, 10.4 p.1-4 (1996).

GROSSMAN, E., LEMPERT, G.D., KULIK, J., MARTON, D., RABALAIS, J.W. and LIFSHITZ, Y.
Role of ion energy in determination of the sp^3 fraction of ion beam deposited carbon films.
Appl. Phys. Lett., 68, 1214-1216 (1996).

HARAN, O., SHAHAM, Y. and ABOUDI, M.
Whole core burnup calculations using MCNP.
In: 19th Conference of the Israel Nuclear Societies (Herzlia, Israel, 9-10 Dec., 1996) Proceedings, 9.3 p. 1-4 (1996).

HARAN, O. and SHVARTS, D.
Transport in stochastic multi dimensional media.
In: 19th Conference of the Israel Nuclear Societies ((Herzlia, Israel, 9-10 Dec., 1996), Proceedings, 1.5 p. 1-4 (1996).

HARARI R., WEISS Y. and BARNEA Y.
Thermohydraulic modeling of dry air PCCS process in the Westinghouse AP-600 ALWR.
In: 19th Conference of the Israel Nuclear Societies (Herzlia, Israel 9-10 Dec., 1996) Proceedings, 7.2 p. 1-4 (1996).

HAREUVENY, R., MARGALIOT, M. and SCHLESINGER, T.
Carcinogenic and other health effects of 50/60 Hz electric and magnetic files; status report.
In: 19th Conference of the Israel Nuclear Societies (Herzlia, Israel, 9-10 Dec., 1996) Proceedings, 2.4 p. 1-5 (1996).

HAREUVENY, R., MARGALIOT, M. and SCHLESINGER, T.
Radiation protection implications related to cellular communications.
In: 19th Conference of the Israel Nuclear Societies (Herzlia, Israel, 9-10 Dec., 1996) Proceedings, 2.5 p. 1-2 (1996).

HAZAK, G.
Lagrangian formalism for the Rayleigh-Taylor instability
Phys. Rev. Lett. 76, 4167-4170 (1996).

HERER, Y , KORENFELD, C., GABAY, Y. and BOT, Y.
Usage of commercial methods for reliability prediction in various industries
In: 11th International Conference of the Israel Society for Quality (Jerusalem, Israel, 19-21 Nov., 1996) Proceedings, p. 342 (1996).

HERRMAN, B., DAHAN, I., SARIEL, J., BIDERMAN, S., BEN-AMAR, G., EINAV, Y., GAZIT, D., HOROWITZ, A. and KIMMEL, G.
Corrosion of molybdenum in sapphire-growth furnaces.
In: 26th Israel Conference on Mechanical Engineering (Haifa, Israel, 21-22 May, 1996) Proceedings, p. 26 (1996).

HOROWITZ, A., BIDERMAN, S., EINAV, Y., AMAR, G. BEN, and GAZIT, D.
Improved control of sapphire crystal growth.
J. Cryst. Growth 167, 183-189 (1996).

ICEKSON, I., PASTEUR, R., DRABKIN, V., LAPIDOT, M., EISENBERG, E., KLINGER, I. and GELMAN, A.
Prolonging shelf-life of carp by combined ionizing radiation and refrigeration.
J. Sci. Food Agric. 72, 353-358 (1996).

IZAK-BIRAN, T. and MOSCOVITCH, M.
Light-induced TL and light-induced fading of TL in alpha :Al_2O_3 :C.
Radiat. Meas. 26, 259-264 (1996).

IZAK-BIRAN, T., MALCHI, S., SHAMAI, Y. and ALFASSI, Z.B.
Low pre- and post-irradiation fading of LiF:Mg,Ti (TLD-100, TLD-600, TLD-700) using a preheat technique.
Radiat. Prot. Dosim. 64, 269-274 (1996).

JACKEL, S., MOSHE, I., KAUFMAN, A., LAVI, R. and LALLOUZ, R.
High energy Nd:Cr:GSGG and Nd:Glass lasers based on phase and polarization conjugated multiple-pass amplifiers.
In: 11th International Symposium on Gas Flow and Chemical Lasers and High Power Laser Conference (Edinburgh, UK, 25-30 Aug., 1996) Proceedings. SPIE 3092, 48-51 (1996).

JENKINS, D., LANDO, M., WINSTON, R. and O'GALLAGHER, J.
A solar-pumped Nd:YAG laser with a record efficiency of 4.7 watt/m^2 of primary mirror area.
Bull. Isr. Phys. Soc. 42, 101 (1996).

JENKINS, D., WINSTON, R., O'GALLAGHER, J., LANDO, M., LEWANDOWSLI, A., BINGHAM, C. and PITTS, R.
Demonstration of new secondary concentration for powering lasers and producing fullerenes.
In: ASES Conference (Asheville, NC, USA) Proceedings, (1996).

KAHANE, S., MOREH, R. and SHAHAL, O.
Rayleigh scattering of E = 465-2842 keV neutron capture gamma -rays from Ta, In and Cu.
Radiat. Phys. Chem. 48, 419-426 (1996).

KALISKY, Y., BEN-AMAR BARANGA, A., SHIMONY, Y., BURSHTEIN, Z., POLLACK, S.A. and KOKTA, M.R.
Cr^{4+} doped garnets: their properties as non-linear absorbers.
Opt. Mater. 6, 275-80 (1996).

KALISKY, Y., BEN-AMAR BARANGA, A., SHIMONY, Y., BURSHTEIN, Z.,POLLACK, S.A. and KOKTA, M.R.
Cr^{4+} doped garnets: their properties as laser materials and non-linear absorbers.
In: Solid State Lasers V (San Jose, CA, USA, 29-30 Jan. 1996) Proceedings, SPIE 2698, 149-56 (1996).

KALISKY, Y., WAICHMAN, K., KAMIN, S. and CHUCHEM, D.
Effect of geometry and preionization conditions on the performance of atmospheric pressure HF chemical laser.
In: Gas and Chemical Lasers (San Jose, CA, USA, 31 Jan.- 1 Feb. 1996) Proceedings, SPIE 2702, 168-178 (1996).

KAPLAN, W.D. and KIMMEL, G.
Ordered $LaGa_4$ and its relation to other structures in the Ga-La binary system.
J. Alloys Compd. 232, 126-132 (1996).

KARPAS, Z.
Operational experience with IMS for process control and environmental monitoring.
In: 5th International Workshop on Ion Mobility (Jackson, Wyoming, USA, 20-22 Aug., 1996) Proceedings, (1996).

KARPAS, Z., HALICZ, L., ROIZ, J., MARKO, R., KATORZA, E., LORBER, A. and GOLDBART, Z.
Inductively coupled plasma mass spectrometry as a simple, rapid and inexpensive method for determination of uranium in urine and fresh water: comparison with LIF.
Health Phys. 71, 879-85 (1996).

KARPAS, Z., LORBER, A. and HALICZ, L.
Direct determination of uranium in urine and blood by Flow Injection - ICPMS.
In: 12th Annual Meeting of the Israel Society for Mass Spectroscopy (ISMS) (Jerusalem, Israel, 19 Feb., 1996) Proceedings, (1996).

KATZ, Y., ALUSH, H. and BUSSIBA, A.
On strain rate enhanced shear localization in light and heavy metals.
In: 4th International Conference on Structures Under Shock and Impact, SUSI 96 (Udine, Italy , July 1996) Proceedings, p. 469-478 (1996).

KIMMEL G., DAYAN D. and YEHESKEL, O.
X ray diffraction broadening effects in ceramic materials.
In: 1st Conference of the Israel Materials Union (Natania, Israel, 29- 30 Apr., 1996), Proceedings, 4.2 p. 4 (1996).

KIMMEL G. and DAYAN, D.
X-ray broadening effect in metallic alloys.
In: 1st Conference of the Israel Materials Union (Natania, Israel, 29-30 Apr., 1996) Proceedings, 4.2 p. 4(I) (1996).

KIMMEL, G., DAYAN, D., SARIEL, J. and ZAMIR G.
Line broadening effect in activated LaN_5.
In: MH96' International Symposium on Metal Hydrogen Systems (Les Dialberets, Switzerland, 25-30 Aug., 1996) Proceedings, (1996).

KOCH, J., DAYAN, U. and GRABER, M.
Complying with the U.N. Framework Convention for Climate Change - Israel as a case study.
Isr. Environ. Bull. 19, (1996).

KOL, R., CANFI, A., DUKHAN, N., PELLED, O., BRIKNER, D., LAICHTER, Y. and GOLD, B.
Acute internal exposure to iodine-125: a case study.
In: 19th Conference of the Israel Nuclear Societies (Herzlia, Israel, 9-10 Dec., 1996) Proceedings, 10.2 p. 1-3 (1996).

KRAVCHIK, T., GHERMAN, U. and LAICHTER, Y.
Aerosol particles sampling in sampling and transport systems.
In: 19th Conference of the Israel Nuclear Societies (Herzlia, Israel, 9-10 Dec., 1996) Proceedings, 5.4 p.1-2 (1996).

KRAVCHIK, T., GHERMAN, U. and LAICHTER, Y.
Aerosol filtration by fibrous and membrane filters.
In: 19th Conference of the Israel Nuclear Societies (Herzlia, Israel, 9-10 Dec., 1996) Proceedings, 7.3 p. 1-2 (1996).

KRUMBEIN, A. D., CANER, M. and SHAPIRA, M.
Calculations of criticality of the AP600 reactor with the KENO V.a code of the SCALE system.
In: 19th Conference of the Israel Nuclear Societies (Herzlia, Israel, 9-10 Dec., 1996), Proceedings, p. 3.1 (1996).

KUZNIETZ, M., PINTO, H. and MELAMUD, M.
Magnetic phase diagrams of the $U(M, M')_2 X_2$ systems (M, M' = Co, Ni, Cu ; X = Si, Ge).
In: 1995 International Conference on Strongly Correlated Electron Systems, SCES'95 (Goa, India, 27-30 Sept. 1995) Proceedings.
Physica B 223-224, 234-236 (1996).

LANDO, M., KAGAN, J., BEN-AMAR BARANGA, A. and ACHIAM, Y.
Development of application oriented solar-pumped lasers.
In: SUN-DAY Symposium on Concentrated Solar Energy (Rehovot, Israel, Apr., 1996) Proceedings, (1996).

LAULICHT, I., POMYALOV, A.V. and BARAK, J.
Low power induced lineshape asymmetry of new ferromagnetic resonance lines in YIG films.
J. Magn. Magn. Mater. 154, L291-L295 (1996).

LAVI, R., ENGLANDER, A. and LALLOUZ, R.
Highly efficient low-threshold tunable all-solid-state intracavity optical parametric oscillator in the mid infrared.
Opt. Lett. 21, 800-802 (1996).

LEPOINTMULLIE, F., DEPAUW, D., LEPOINT, T., SUPIOT, P. and AVNI, R.
Nature of the extreme conditions in single sonoluminescing bubbles.
J. Phys. Chem. 100, 12138-12141 (1996).

LEVINSON, S., GERMAN, U., PELLED, O. and TURGEMAN, S.
A manual low background alpha and beta counting system.
In: 19th Conference of the Israel Nuclear Societies (Herzlia, Israel, 9-10 Dec., 1996) Proceedings, 6.2 p. 1-3 (1996).

LEVINSON S., GERMAN, U., ANKRY, N., ASSIDO, H., SHEMESH, Y. and PELLED, O.
A bar-code reader for an alpha-beta automatic counting system - FAG.
In: 19th Conference of the Israel Nuclear Societies (Herzlia, Israel, 9-10 Dec., 1996) Proceedings, 6.3 p. 1-3 (1996).

LEVINSON, S., GERMAN, U., GILAD, Y., MESSING, M., PELLED, O. and BALLON, I.
Computerized operation of a multidetector spectrometry system.
In: 19th Conference of the Israel Nuclear Societies (Herzlia, Israel, 9-10 Dec., 1996) Proceedings, 6.5 p. 1-7(1996).

LIFSHITZ, Y.
Hydrogen-free amorphous carbon films: correlation between growth conditions and properties.
In: 6th European Conference on Diamond, Diamond -like and Related Materials (Diamond Films '95) (Barcelona, Spain, 10-15 Sept. 1995) Proceedings.
Diam. Relat. Mater. 5, 388-400 (1996).

LORBER, A.
Net analyte signal calculation in multivariate calibration.
In: International Conference on Chemometric and Analytical Chemistry (CAC 96') (Spain, 25-29 Jun., 1996) Proceedings, p. 84 (1996).

LORBER, A., KARPAS, Z. and HALICZ, L.
Flow injection method for determination of uranium in urine and serum by inductively coupled plasma mass spectrometry.
Anal. Chim. Acta 334, 295-301 (1996).

LYUBIN, V., KLEBANOV, M., BAR, I., ROSENWAKS, S., VOLTERRA, V., BOEHM, L. and VAGISH, V.
Laser-induced phenomena in chalcogenide glassy films photo-excited processes and applications.
Appl. Surf. Sci. 106, 502-506 (1996).

MARGALIT, M., HAREUVENY, R., RUPPIN, R. and SCHLESINGER, T.
Magnetic vs. electric fields in RF safety standards; the physical origin of difference and the practical implications.
In: 19th Conference of the Israel Nuclear Societies (Herzlia, Israel, 9-10 Dec., 1996) Proceedings, 2.3 p.1-7 (1996).

MARTIN, L.P., DADON, D. and ROSEN, M.
Evaluation of ultrasonically determined elasticity-porosity relations in zinc-oxide.
J. Amer. Ceram. Soc. 79, 1281-1289 (1996).

MARTINEZ-VAL, J.M., ELIEZER, S., PIERA, M. and VELARDE, G.
Fusion burning waves in proton-boron 11 plasmas.
Phys. Lett. A 216, 142-152 (1996).

MEIMON, Y., GRUNTMAN, S., TARAGAN, E., DANINO, M., WEISS, S. and AGIE, D.
Volumetric solar receiver-mechanical and thermal design.
In: 26th Israel Conference on Mechanical Engineering (21-22 May, 1996, Haifa, Israel) Proceedings, p. 452-454 (1996).

MITCHELL, D.W., DAS, T.P., POTZEL, W., SCHIESSL, W., KARZEL, H., TEINER, M. , KOEFFERLEIN, M., HILLER, U., KALVIUS, G. M. , MARTIN, A., SCHAEFER, W., WILL, G., HALEVY, I. and GAL, J.
Ab initio electric-field gradients and electron densities at Al^{27}, Fe^{57}, and Zn^{67} in the spinels $ZnAl_2O_4$ and $ZnFe_2O_4$.
Phys. Rev. B, 53, 7684-7698 (1996).

MITNIK, D., MANDELBAUM, P., SCHWOB, J. L., BAR-SHALOM, A., OREG, J. and GOLDSTEIN, W. H.
Excitation-autoionization cross sections and rate coefficients of Cu-like ions.
Phys. Rev. A, 53, 3178-3188 (1996).

MITTLEMAN, D.M., DOUGLASS, D.C., HENIS, Z., WOOD, O.R., FREEMAN, R.R. and MCILRATH, T.J.
High-field harmonic-generation in the tight-focusing limit.
J. Opt. Soc. Am. B, 13, 170-179 (1996).

MONCORGE, R., MANAA, H., DEGHOUL, F., GUYOT, Y., KALISKY, Y., POLLACK, S.A., ZHARIKOV, E.V. and KOKTA, M.
Saturable and excited state absorption measurements in Cr^{4+} :LuAG single crystals.
Opt. Commun. 132, 279-284 (1996).

MOREH, R., FINKELSTEIN, Y. and SHECHTER, H.
NO_2 adsorption on Grafoil between 297 and 12 K.
Phys Rev. B, Condens. Matter 53, 16006-16012 (1996).

MOREH, R., PINTO, H., FINKELSTEIN, Y. and BEGUIN, F.
Tilt of N_2 molecules physintercalated into $C_{24}K$ and C_{24} Rb.
In: 8th International Symposium on Intercalation Compounds (Vancouver, BC, Canada, 28 May- 1 June, 1995) Proceedings.
J. Phys. Chem. Solids 57, 909-913 (1996).

MORENO, D., ADLER, A., SOLOVIOFF, G. and ABRAMOV, E.
The characterization of thermal recrystallization using grain size histograms obtained by image analysis techniques.
In: 1st Conference of the Israel Materials Union (Natania, Israel, 29-30 Apr., 1996) Proceedings, 3.1 p.3 (1996).

MORENO, D., ARKUSH, R., ZALKIND, S. and SHAMIR, N.
Physical discontinuities in the surface microstructure of uranium alloys as preferred sites for hydrogen attack.
J. Nucl. Mater. 230, 181-6 (1996).

MORENO, D. and ELIEZER, D.
He bubble sites in implanted copper alloy.
Scr. Mater. 34, 1851-6 (1996).

MORENO, D., MANWARING, C.A.F. and HARRIS, I.R.
The stability of $LaNi_5$ in a Cu matrix.
J. Mater. Sci. 31, 3259-62 (1996).

MORENO, D. and ELIEZER, D.
Structural changes in a copper alloy due to helium implantation.
Scr. Mater. 35, 1385-9 (1996).

MOSHE, E., DEKEL, E., HENIS, Z. and ELIEZER, S.
Development of an optically recording velocity interferometer system for laser induced shock waves measurements.
Appl. Phys. Lett., 69, 1379-1381 (1996).

MUNITZ, A., ABBACHIAN, R., COTLER, C. and SHACHAM, C.
Liquid phase separation in Cu-Co-Fe and Cu-Fe-Ni-Cr alloys.
High Temp. Mater. Proc. 15, 187-194 (1996).

MUNITZ, A. and ABBASCHIAN, R.
Microstructure of Cu-Co alloys solidified at various supercoolings.
Metall. Mater. Trans. A, Phys. Metall. Mater. Sci. 27A, 4049-4059 (1996).

MURAT, M. and GREST, G.S.
Molecular dynamics study of dendrimer molecules in solvents of varying quality.
Macromolecules 29, 1278-1285 (1996).

MURAT, M. and GREST, G.S.
Molecular dynamics simulations of the force between a polymer brush and an AFM tip.
Macromolecules 29, 8282-8284 (1996).

NIR-EL, Y.
Accurate calibration of a Co-60 Gamma radiographic source.
Mater. Eval. 54, 138-139 (1996).

NIR-EL, Y. and BROSHI, M.
The red ink of the Dead Sea Scrolls.
Archaeometry 38, 97-102 (1996).

NIR-EL, Y. and BROSHI, M.
The black ink of the Qumran Scrolls.
Dead Sea Discoveries 3, 157-167 (1996).

NIR-EL, Y.
An accurate calibration of the detection efficiency of a low-level gamma-ray spectrometry assembly for environmental samples.
In: International Symposium on Harmonization of Health Related Environmental Measurements using Nuclear and Isotopic Techniques (Hyderabad, India, 4-7 Nov., 1996) Proceedings, (1996).

OFER, D., ALON, U., SHVARTS, D., MCCRORY, R. L. and VERDON, C. P.
Modal model for the nonlinear multimode Rayleigh-Taylor instability.
Phys. Plasmas 3, 3073-3090 (1996).

OLSHER, R.H. and EISEN, Y.
A filter technique for optimising the photon energy response of a silicon PIN diode dosimeter.
Radiat. Prot. Dosim. 67, 271-279 (1996).

OREN, Y., ELISH, E., TAMIR, A. and GAVRA, Z.
Dilatometric study of nickel wire electrode electrochemically charged by hydrogen.
J. Alloys Compd. 235, 30-36 (1996).

ORON, M.B., KATZ, M., ZUSSMAN, A. and ROSEMANN, G.
Compact blue lasers based on nonlinear waveguides.
Bull. Isr. Phys. Soc. 42, 99 (1996).

OSOVIZKY, A., BLOCH, J., MINTZ, M. H. and JACOB, I.
Kinetics of hydride formation in massive $LaNi_5$ samples.
J. Alloys Comp. 245, 8-178 (1996).

OSTRAICH, B., KOCHAVI, E., TARAGAN, E., ANTEBY, I. and MEIMON, Y.
Solar receiver quartz window thermomechanical analysis.
In: 26th Israel Conference on Mechanical Engineering (Haifa, Israel, 21-22 May, 1996) Proceedings, p. 458-460 (1996).

PAISS, I. , FASTIG, S. and LAVI, R.
Narrow-linewidth optical parametric oscillator with an intracavity laser gain element.
Opt. Lett. 21, 1652-1654 (1996).

PELLED, O., GERMAN, U., KOL, R., LEVINSON, S., WEINSTEIN, M., LAICHTER, Y. and ALPHASY, Z.
Limitations of absolute activity determination of I-125 sources.
In: 19th Conference of the Israel Nuclear Societies (Herzlia, Israel, 9-10 Dec.,1996) Proceedings, 8.2 p.1-3 (1996).

PERELMUTTER, L., GOLDENBERG, C., SUDAI, M., ALIMI, R., FURMAN, M., KIMHE, D., KAPLAN, Z., ARIE, S., ZEEVI, Z. and MELNIK, D.
A technique for temperature compensation by controlled ignition power in SPETC guns.
In: 16th International Symposium on Ballistics (San Francisco, CA, USA, Sept. 1996) Proceedings, Vol. 1, p. 147-152.

PERRY, T.S. , SPRINGER, P.T. , FIELDS, D.F. , BACH, D.R. , SERDUKE, F.J.D., IGLESIAS, C.A., ROGERS, F.J., NASH, J. K. ,CHEN, M.H., WILSON, B.G., GOLDSTEIN, W.H., ROZSYNAI, B., WARD, R.A., KILKENNY, J.D., DOYAS, R., DA SILVA, L. B., BACK, C.A., CAUBLE, R., DAVIDSON, S.J., FOSTER, J.M., SMITH, C.C., BAR-SHALOM, A. and LEE, R.W.
Absorption experiments on x-ray-heated mid-Z constrained samples.
Phys. Rev. E, 54, 5617-5631 (1996).

PLATZNER I.
Isotope ratio mass spectrometry of lead.
In: 12th Annual Meeting of the Israel Society for Mass Spectrometry (ISMS) (Jerusalem, Israel, 19 Feb., 1996) Proceedings, (1996).

POKRYVAILO, A., KANTER, M. and SHAKED, N.
A two-stage opening switch for inductive energy storage systems.
In: 22nd International Power Modulator Symposium (Boca Raton, FL, USA, 25-27 June, 1996) Proceedings, p. 228-31 (1996).

POKRYVAILO, A., KANTER, M. and SHAKED, N.
Discharge efficiency of cylindrical storage coils.
IEEE Trans. Magn. 32, 497-504 (1996).

PRAWER, S., NUGENT, K.W., LIFSHITZ, Y., LEMPERT, G.D., GROSSMAN, E. KULIK, J., AVIGAL, I. and KALISH, R.
Systematic variation of the Raman spectra of DLC films as a function of sp^2-sp^3 composition.
Diam. Relat. Mater. 5, 433-438 (1996).

RAITSES, Y., ASHKENAZY, J. and GUELMAN, M.
Hall thruster operation in a variable thrust mode.
In: 36th Israel Annual Conference on Aerospace Sciences, (Tel Aviv and Haifa, Israel, 21-22 Feb., 1996) Proceedings, p. 446-454 (1996).

RAITSES, Y., ASHKENAZY, J. and GUELMAN, M.
Propellant utilization in Hall thrusters.
In: AIAA, ASME, SAE, and ASEE, 32nd Joint Propulsion Conference and Exhibit (Lake Buena Vista, FL, USA, 1-3 July, 1996) Proceedings. AIAA Paper 96-3193. (1996).

RAITSES, Y. and ASHKENAZY, J.
Discharge characteristics of Hall current accelerators.
In: ISDEIV. 17th International Symposium on Discharges and Electrical Insulation in Vacuum (Berkeley, CA, USA, 21-26 July 1996) Proceedings, Vol. 1, p. 492-6 (1996).

RAIZMAN, A., SHER, A. and CINADER, G.
X-ray measurements of strains in MOCVD grown thin cap layers of CdTe.
In: 7th International Conference II-VI Compounds and Devices (Edinburgh, UK, 13-18 Aug., 1995) Proceedings.
J. Cryst. Growth 159, 126-9 (1996).

RAVEH, A., ARKUSH, R., ZALKIND, S. and BRILL, M.
Passivation of uranium metal by radio-frequency plasma nitriding against gas phase (H_2 , H_2O) corrosion.
Surf. Coat. Techol. 82, 38-41 (1996).

ROSENFELD, Y.
Short-range screening potentials for classical Coulomb fluids: Reanalysis of Monte Carlo sampling and cluster model studies.
Phys. Rev. E, 53, 2000-2007 (1996).

ROSENMAN, E., PERSKY, A. and BAER, M.
The effect of a potential well in the quasi-asymptotic region of a potential energy surface on the dynamics of the $F+H_2$ reaction.
Chem. Phys. Lett. 258, 639-643 (1996).

ROSENMAN, E., HOCHMANKOWAL, S., PERSKY, A. and BAER, M.
A three dimensional quantum mechanical study of the $F+H_2$/D2 reactions on a new potential energy surface.
Chem. Phys. Lett. 257, 421-428 (1996).

ROSENMAN, G., SKLIAR, A., LAREAH, Y , ANGERT, N., TSEITLIN, M., ROTH, M., ORON, M. and KATZ, M.
Asymmetric secondary electron emission flux in ferroelectric $KTiOPO_4$ crystal.
J. Appl. Phys., 80, 7166-7168 (1996).

ROTTER, S.
A novel surface treatment for enhanced nucleation of diamond on foreign substrates and non-planar structures.
In: 1st Israel-Japan binational workshop on diamond science and technology (Osaka, Japan, 11-12 Mar., 1996) Proceedings.
Diam. Films Technol. 6, 331-6 (1996).

RUPPIN, R.
Plasmon frequencies of cube shaped metal clusters.
J. Phys. D, 36, 69-71 (1996).

SAGIE, D., GRUNTMAN, S., TARAGAN, E., DANONO, M., WEISS, S. MEIMON, Y. and OSTRAICH, B.
Volumetric solar thermal receiver principles and technological approach.
In: 26th Israel Conference on Mechanical Engineering (Haifa, Israel, 21-22 May, 1996) Proceedings, p. 449-451 (1996).

SAPHIER, D. and RAYMOND, P.
Design of highly moderated pressurized water reactor based on critical heat flux conditions.
Nucl. Eng. Des. 163, 263-271 (1996).

SAPHIER, D., GORELIC, Z. and SHAPIRA, M.
The importance of proper feedback modeling in HWR.
In: 5th International Conference on Simulation Methods in Nuclear Engineering (Montreal, Canada, 8-11 Sept., 1996) Proceedings, Session 5A, pt. 2 (1996).

SCHIESSL, W., POTZEL, W., KARZEL, H., STEINER, M., KALVIUS, G.M., MARTIN, A., KRAUSE, M.K., HALEVY, I. , GAL, J., SCHAEFER, W., WILL, G., HILLBERG, M. and WAEPPLING, R.
Magnetic properties of the $ZnFe_2O_4$ spinel.
Phys. Rev. B 53, 9143-9152 (1996).

SCHLESINGER, T., BEN SHLOMO, A. and GINZBURG, G.M.
An economic evaluation of the rare-earth screens to reduce the radiation dose from diagnostic x-ray procedures in Israel.
In: 19th Conference of the Israel Nuclear Societies (Herzlia, Israel, 9-10 Dec., 1996) Proceedings, 4.2 p. 1-9 (1996).

SCHLESINGER, T., SILVERMAN, I. and SHAPIRA, M.
Revised dose limits and a new respiratory tract model and their implications for the annual limits of intake of radioactive materials - a review of recent ICRP publications.
In: 19th Conference of the Israel Nuclear Societies (Herzlia, Israel, 9-10 Dec., 1996) Proceedings, 2.1 p. 1-8 (1996).

SCHLESINGER, T., HAREUVENY, R. and MARGALIOT, M.
Limitations on the concentration of radioactive substances (natural or enhanced by human activity) in building materials; a draft proposal for Israeli regulations.
In: 19th Conference of the Israel Nuclear Societies (Herzlia, Israel, 9-10 Dec., 1996) Proceedings, 10.3 p. 1-5 (1996).

SHALEV, S., GALIE, T., GREEN, A.K., TUR, M. and SHAFIR, E.
Health monitoring of a smart composite structure achieved by embedded optical fiber sensors.
In: International Conference on Aeronautic Sciences (Milan, Italy, Sept. 1996) Proceedings, (1996).

SHILOH, K., ELIAHU, A., ROSENBERG, A., ZILBER, R. and BUCHMAN, A.
Aging characterization of adhesives and bonded joints by non-destructive damping measurements.
In: Nondestructive evaluation of materials and composites (Scottsdale, AZ, USA, 3-5 Dec, 1996) Proceedings, SPIE 2944, 30-36 (1996).

SHIMONY, Y., BURSHTEIN, Z., BEN-AMAR BARANGA, A., KALISKY, Y. and STRAUSS, M.
Repetitive Q-switching of a CW Nd:YAG laser using Cr^{4+} :YAG saturable absorbers.
IEEE J. Quantum Electron. 32, 305-10 (1996).

SHIMONY, Y., BURSHTEIN, Z., KALISKY, Y., BEN-AMAR BARANGA, A. and STRAUSS, M.
Progress in Q-switching of Nd:YAG lasers using Cr^{4+} :YAG saturable absorber.
In: 4th French Israeli Symposium on Nonlinear and Quantum Optics - FRISNO 4 (Les Arces, France, 21-25 Jan., 1996) Proceedings.
J. Nonlinear Opt. Phys. Mater. 5, 495-504 (1996).

SHIMONY, Y., RAZ, O. and DARIEL, M.
$ZnGeP_2$: A promising nonlinear crystal for frequency conversion into mid-IR.
In: Meeting of the Israeli Association for Crystal Growth (Jerusalem, Israel, 3 Dec., 1996) Proceedings, (1996).

SILVERMAN, I., SHAPIRA, M., CANER, M. and SAPHIER, D.
A computerized energy systems code and information library at Soreq.
In: 19th Conference of the Israel Nuclear Societies (Herzlia, Israel, 9-10 Dec., 1996) Proceedings, 3.2 (1996).

SILVERMAN, I., SHAPIRA, M. and SAPHIER, D.
Recent advances in DSNP - A simulation language for dynamic simulation of nuclear power-plant.
In: 5th International Conference on Simulation Methods in Nuclear Engineering (Montreal, Canada, 8-11 Sept., 1996) Proceedings, Session 4A, pt. 2 (1996).

SILVERMAN, I., SHAPIRA, M. and SAPHIER, D.
A new thermal-hydraulic core module based on the drift-flux model for the DSNP.
In: 19th Conference of the Israel Nuclear Societies (Herzlia, Israel, 9-10 Dec., 1996) Proceedings, 7.1 (1996).

SMILANSKI, I.
Plasma parameters of metal vapour lasers.
In: Pulsed Metal Vapour Lasers. NATO Advanced Research Workshop on Pulsed Metal Vapour Lasers - Physics and Emerging Applications in Industry, Medicine and Science (St. Andrews, UK, 6-10 Aug. 1995) Proceedings, p. 87-99 (1996).

STEINITZ, G.,VULKAN, U. and LANG, B.
Monitoring of the tectonically related radon flux in Israel.
In: Current Research - Geological Survey of Israel, 10, 148-153 (1996).

STEINITZ, G., LANG, B., VULKAN, U. and AVNI, Y.
Radon flux in syenitic rocks along the Ramon Fault, Makhtesh Ramon
In: Israel Geological Society Annual Meeting (Eilat, Israel, 18-21 Mar., 1996) Proceedings, p. 90 (1996).

STRAUSS, M., AMENDT, P., LONDON, R.A., MAITLAND, D.J., GLINSKI, M.E., CELLIERS, P., BAILEY, D.S. and YOUNG, D.A.
Computational modeling of laser thrombolysis for stroke treatment: Diagnostic and therapeutic cardiovascular intervention VI.
In: Lasers in surgery : advanced characterization, therapeutics, and systems VI (San Jose, CA, USA, 27-30 Jan., 1996) Proceedings, SPIE 2671, p. 11-21 (1996).

SZICHMAN, H. and BAER, M.
A 3-dimensional quantum-mechanical study of the NH+NO reactions.
J. Chem. Phys. 105, 10380-10386 (1996).

TAMBOUR, Y., GREENBERG, J.B. and SILVERMAN, I.
Far-field coalescence effects in polydisperse spray diffusion flames
In: Recent advances in spray combustion: Spray atomization and drop burning phenomena. Vol. 1. Reston, VA, American Institute of Aeronautics and Astronautics (Progress in Astronautics and Aeronautics.
Vol. 166), p. 399-410 (1996).

TING, A., FISCHER, R., FISHER, A., MOORE, C.I., HAFIZI, B., ELTON, R., KRUSHELNICK, K., BURRIS, R., JACKEL, S., EVANS, K., WEAVER, J.N., SPRANGLE, P., ESAREY, E., BAINE, M. and RIDE, S.
Demonstration experiment of a laser synchrotron source for tunable, monochromatic x-rays at 500-ev.
Nucl. Instrum. Methods Phys. Res. A, 375, abs 68-70 (1996).

TUGENDHAFT, I., BORNSTEIN, A., WEISSMAN, Y. and HARDY, A.
Coupling efficiency of directional fiber couplers in the mid-infrared.
Appl. Spectrosc. 50, 906-9 (1996).

VENKERT, A., AIZENSHTEIN, M., ARKUSH, R. and SHAMIR, N.
Stress induced preferential oxidation at the uranium-uranium carbide interface.
J. Nucl. Mater. 231, 254-256 (1996).

VULKAN, U., LANG, B. and STEINITZ, G.
Electronic monitoring of radon at the northwestern Dead Sea, first results.
In: Israel Geological Society Annual Meeting (Eilat, Israel, 18-21 Mar., 1996) Proceedings, p. 94 (1996).

WAICHMAN, K.
Kinetic study of the effects of boundary geometry on rarefied vapor flow.
Phys. Fluids 8, 1321-1329 (1996).

WAICHMAN, K., CHUCHEM, D. and KALISKY, Y.
The effect of the geometry of the active medium on the performance of (SF_6 + H_2) pumped HF laser.
IEEE J. Quantum Electron. 32, 357-363 (1996).

WALACH, N. and GUR, Y.
Leukocyte alkaline-phosphatase and serum alkaline-phosphatase in patients with metastatic breast and colon-cancer.
Neoplasma 43, 297-300 (1996).

WEISS, S., DANINO, M., MEIMON, Y., SAGIE, D. and TARAGAN, E.
Solar receiver system compound parabolic concentrator.
In: 26th Israel Conference on Mechanical Engineering (Haifa, Israel, 21-22 May, 1996) Proceedings, p. 455-457 (1996).

WEISS Y., LAHAV Y., SZANTO M. and SHAI, I.,
Heat transfer characteristics of induced mixed convection (IMC).
In: 26th Israel Conference on Mechanical Engineering (Haifa, Israel, 21-22 May, 1996) Proceedings, p. 300-302 (1996).

WEISSMAN, Y.
Optical noise coherence effects in a Mach-Zehnder system.
J. Lightwave Technol. 14, 888-93 (1996).

WERDIGER, M., ARAD, B., HENIS, Z., HOROWITZ, Y., MOSHE, E., MAMAN, S., LUDMIRSKY, A. and ELIEZER, S.
Asymptotic measurements of free surface instabilities in laser-induced shock waves.
Laser Part. Beams 14, 133-47 (1996).

WINHART, G. , EIDMANN, K. , IGLESIAS, C. A.and BAR-SHALOM, A.
Measurements of extreme uv opacities in hot dense Al, Fe, and Ho.
Phys. Rev. E, 53, R1332-1335 (1996).

WOLF, A., PAAR, V. and BRANT, S.
Theoretical and experimental investigation of shape coexistence in N=59 Isotones.
In: 9th International Symposium on Capture Gamma-Ray Spectroscopy and Related Topics (Budapest, Hungary, Oct., 1996) Proceedings, (1996).

WOLF, A. and GINOCCHIO, J.N.
Analytical determination of proton, neutron deformations and F-spin admixtures in even-even isotopes.
In: 9th International Symposium on Capture Gamma-Ray Spectroscopy and Related Topics (Budapest, Hungary, Oct., 1996) Proceedings, (1996).

WOLF, A.
Proton-neutron symmetry in even-even nuclei.
In: 5th International Conference on Applications for Nuclear Techniques. Neutrons in Research and Industry (Crete, June, 1996) Proceedings, (1996).

WOLF, D., SEMBIRA, A.N., POST, R.G. and WHITE, D.H.
Extruder-melter process concept for vitrification of high level wastes.
In: WM'96 (25-29 Feb., 1996, Tucson, Arizona, USA) Proceedings, (1996).

YANIV, Z. and ROTTER, S.
Highly controlled and localized spacer fabrication technology for LCDs.
In: International Workshop on Active-Matrix Liquid Crystal Displays (Kobe, Japan, 27-29 Nov., 1996) Proceedings, Vol. 1, p. 395-396 (1996).

YEHESKEL, O.
Sound velocity as a research tool in materials science.
In: 1st Conference of the Israel Materials Union (29-30 Apr., 1996, Natania, Israel) Proceedings, 3.1 p. 4 (1996).

YOGEV, A., APPELBAUM, J., ORON, M. and YEHEZKEL, N.
Concentrating and splitting of solar radiation for laser pumping and photovoltaic conversion.
J. Propuls. Power 12, 405-409 (1996).

ZHANG, X.X. and BAR-ZIV, E.
A 3-D position controller for a charged particle suspended in a modified electrodynamic chamber.
Rev. Sci. Instr. 67, 3483-3490 (1996).

ZHANG, X., DUKHAN, A., KANTOROVICH, I.I. and BAR-ZIV, E.
Fragmentation of highly porous char particles burning in regime I.
Combust. Flame 106, 203-206 (1996).

ZHANG, X. and BAR-ZIV, E.
Direct determination of 3D forces applied on a particle suspended in an electrodynamic chamber.
Meas. Sci. Technol. 7, 1713-1720 (1996).

ZOLER, D., KAPLAN, Z. and ASHKENAZY, J.
Analysis of powder particle acceleration and heating processes in a ischarge capillary-ablative pipe device.
Plasma Sources Sci. Technol. 5, 588-601 (1996).

ZOLER, D., ALIMI, R., PERELMUTTER, L., GOLDENBERG, C. and MELNIK, D.
A solid phase model for solid propellant ignition with plasma.
In: 4th International Symposium on Chemical Propulsion (Stockholm, Sweden, May, 1996) Proceedings. (1996).